CHARACTERIZATION AND ALTERNATIVE USE STUDY OF FLY ASH

IBRAHEEM ADETUNJI ADEOTI

CHARACTERIZATION AND ALTERNATIVE USE STUDY OF FLY ASH

BY

Adeoti Ibraheem Adetunji©

A thesis submitted to the

School of Graduate Studies

In partial fulfillment of the

Requirements for the degree of

Masters of Engineering

Faculty of Engineering and Applied Science

Memorial University of Newfoundland

July 2011

St. John's Newfound Canada

ABSTRACT

In the generation of power from fossil fuels and biomass, fly ash (FA) is produced and represents both an environmental and economic cost with respect to disposal. However, it also represents a re-use opportunity. Increasing solid waste disposal costs and a focus on sustainable processing necessitates research in alternative uses for fly ash. In this thesis, two ash samples, hog-boiler precipitate ash sample (HBP) and mixed ash pond sample (MAP) from the AV-cell pulp and paper plant were examined for their chemical, physical, thermal, and mineralogical properties. Other physio-chemical properties like density, pH and buffering power were also determined.

Characterization results were used to determine and test alternative uses for FA. Result shows that the samples are rich source of aluminosilicate, SiO_2, CaO, and Al_2O_3 which are feedstock for adsorption and zeolite synthesis. The concentration of SiO_2 to Al_2O_3 is greater than 1.5 therefore indicating good potential for zeolite synthesis. The FAs pH was between 10.0 and 13.0 with buffering power ranges from 0.5 to 4.9 mmol/pH, as such, were tested for acid mine drainage (AMD) neutralization. Treated effluent water final pH was between 9.0 and 12.2 with contaminant removal efficiency of 85%. Neutralization residue was treated hydrothermally and resulted in an increased adsorption properties zeolite, tested for AMD treatment and yielded above 90% contaminant removal efficiency. The total chemical species (SiO_2 + Al_2O_3 + $CaCO_3$ + CaO + Na_2O + K_2O + MgO Fe_2O_3) is greater than 90 wt.% hence, the FAs were tested for permeable reactive barriers (PRB) application and its contaminant removal efficiency was also greater than 90% with final treated effluent water pH ranges between 8.4 and 12.2.

Overall, AMD treatment with FA provides a low cost, environmentally safe and beneficial use of what would be considered a waste.

ACKNOWLEDGEMENTS

Glory be to Allah (SWT) who from His infinitesimal mercy showers His bless and mercy on me, protect and guide me from the beginning of this project till the very end.

My profound and sincere gratitude goes to my able supervisors, Dr. Kelly Hawboldt and Dr. Abdul Iliyas for their perpetual support, guidance and encouragement throughout the course of this research work. Their effort and kindness is highly reckoned and appreciated.

Extensive thanks go to all professors and staff in the Faculty of Engineering and Applied Science who's their contribution to the fulfillment of two years program is invaluable. I would like to also give special thanks to Dr. Johansen Thormod, Dr. Kelly Hawboldt and Dr. Abdul Iliyas for the knowledge impacted on me from various discipline during the program. This was also extended to all my course mates including but not limited to Justin Skinner, Tajudeen Bello and Sameena Trina. Their input can neither be belittled nor over emphasized.

I am also indebted to the CREAIT network group, Memorial University of Newfoundland for their patience and endless understanding while using their instrument for this research work. I would like to give thanks to Brent Myron (C-CART), Lakmali Hewa (Earth Science), Micheal Shaffer, David Grant and Nancy Leawood (MAF-IIC), their contribution means a lot to me.

I also acknowledge the MITACS and AV Cell financial support and contribution for the MITACS ACCELERATE programs. The generosity and support of Jason Foran AVCell (Effluent Department) during my internship program cannot be forgotten, your effort and guidance was highly appreciated.

Finally, I am indebted to my beloved parents, Mr. and Mrs. Imran Oluwalogbon for their perpetual support, encouragement and love.

TABLE OF CONTENTS

LIST OF ABBREVIATIONS

ACAA	American Coal Ash Association
Al	Aluminum
AMD	Acid mine drainage
Al_2O_3	Aluminum Oxides
As	Arsenic
ASTM	American Society for Testing and Materials
ATPF	Agglomerated Tailings Paste Fill
BET	Brunauer Emmett Teller
B	Boron
Ca	Calcium
$CaCO_3$	Calcium Carbonate (calcite)
CaO	Calcium Oxide (quick lime)
$Ca(OH)_2$	Calcium hydroxide(slaked lime)
$CaSO_4$	Calcium sulphate
CCME	Canadian Council of Ministers of the Environment
Cd	Cadmium
CEPA	Canadian Environmental Protection Act
CIRCA	Association of Canadian Industries Recycling Coal Ash
Co	Cobalt
CO_2	Carbonate dioxide
Cu	Copper
EDX	Energy Dispersive X-ray

FA	Fly Ash
Fe	Iron
$FeCO_3$	Iron carbonate
GHG	Greenhouse Gas
GC	Gas Chromatographic
HBP	Hog boiler precipitate ash sample
HBP FA	Hog boiler precipitates Fly Ash
HCl	Hydrochloric acid
HF	Hydrofloric acid
HNO_3	Nitric acid
H_2O	Water
ICP-MS	Inductively Coupled Plasma Mass Spectrometer
ICP-OES Spectroscopy	Inductively Coupled Plasma-Optical Emission
JCFA-1	Japanese Coal Fly Ash- 1 grade
K	Potassium
K_2O	Potassium Oxide
LOI	Loss on Ignition
MAP	Mixed Ash Pond ash samples
MAP FA	Mixed Ash Pond Fly Ash
MAP-1	MAP particle size range of <75µm to >125µm particle size
MAP-2	MAP particle size range of >180µm to>300µm particle size
MAP-3 size	MAP particle size range of >500µm and above particle

Mg	Magnesium
MgO	Magnesium Oxide
mg/L	Miligrams per liter
mg/kg	Miligram/kilogram
mL	Mililiter
mmol/pH	Millimole per unit pH
MLA	Mineral Liberation Analysis
MSW	Municipal Solid Wastes
Mt	Metric tonnes
Na	Sodium
Na_2CO_3	Sodium carbonate (Caustic)
Na_2O	Sodium oxide
NaOH	Sodium hydroxide (Caustic)
P	Phosphorus
P_2O_5	Phosphorus Oxide
PRB	Permeable Reactive barriers
RENEL	Romanian Energy and Electricity Authority
RL	Less than reportable limit
Si	Silicon
SiO_2	Silicon Oxide (quartz)
SEM	Scanning electron Micro Analyzer
SO_4	Sulphate

TCD	Thermal Conductivity meter
TCLP	Toxicity Characteristics Leaching Procedure
TGA	Thermo-Gravimetric Analysis
Ti,	Titanium
TiO_2	Titanium Oxide (Rutile)
TOC	Total Organic Carbon
U	Uranium
US EPA	United States Environmental Protection Agency
µm	Micro meter
wt.%	Percentage by weight
XRD	X-Ray Diffraction
XRF	X-Ray Fluorescence Spectroscopy
Zn	Zinc

LIST OF TABLES

LIST OF FIGURES

CHAPTER ONE

Introduction

1.1 Background

Fly ash (FA) is the by-product generated from combustion of fossil fuels, forest residues, sawmill residues, wood and biomass. Fly and boiler ash is a more general name given to many types of ash produced by the burning of various carbon materials. The common and more general types are; wood ash, coal ash, tire ash and incinerator ash, with each type having its specific chemical and physical characteristics.

In Canada, power generation through thermal combustion of coal alone was estimated to be around 19% with coal power generating plants using roughly 93% of total coal resources produced in Canada. This result in 5 million tonnes fly ash every year from coal and less than 32% was recycled while the remainder was land-filled (Muluken et al., 2009). Other industries produce FA such as power, steam plants, pulp and paper etc..., take for instance, 16.1 million tonnes of boiler ash were generated in 1996 in Europe by the utility industry.

The disposal practice is commonly land filling however, the resulting leachate is possibly toxic and may infiltrate into surrounding ground water or surface water. Furthermore, available land mass for landfills is decreasing. As such, identifying and developing applications for FA is critical. The increasing world population results in an increasing and higher demand for electricity (Feuerborn, 2005). Meanwhile, electricity and power

generation plants has discovered most interest in coal combustion and biomass, which also suggested a likely continuity in an increasing FA generation. Throughout the world, fly ash and boiler ash are mostly disposed of in landfills.

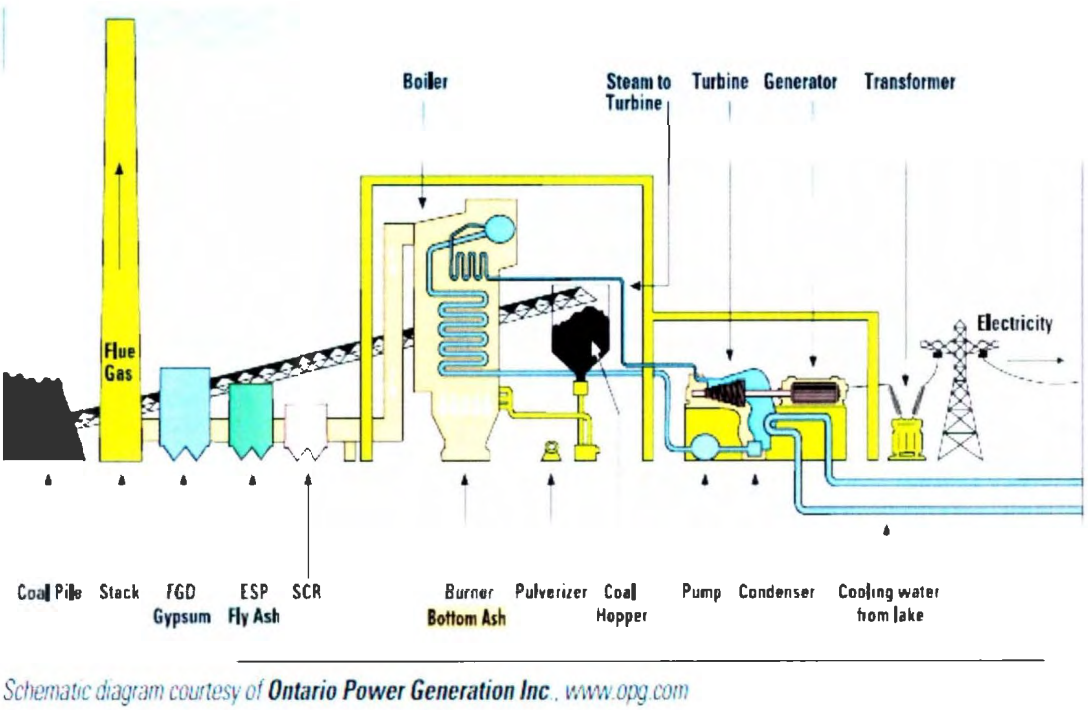

Schematic diagram courtesy of ***Ontario Power Generation Inc.***, *www.opg.com*

Figure 1.1: Utility Plant (Ontario Power Generation Inc.) generating Boiler and Fly Ash. (Modified from Association of Canadian Industries Recycling Coal Ash CIRCA, 2010)

The management of acid mine drainage (AMD) is one possible use for FA. AMD is acidic waste water formed from oxidation of sulphide compounds in mine waste water and drainage. The effect is the generation of sulphuric acid with resulting low pH. The low pH is toxic to water borne organisms and also results in the bioavailability of heavy metals (Kumar et al., 2008, Somerset et al., 2005, Misra et al., 1996.).

In recent years, researchers have proposed various ways of AMD abatement and mitigation. Neutralization using chemical precipitation (using lime/limestone) and agglomeration is the most common method (Bably and Roberts, 2010). The average cost of limestone use at a mine site per annum is approximately $225,000 (Hewitt, 2006), and that of hydrated lime is approximately $371,888 (Hewitt, 2006), therefore using these chemicals to manage AMD can be costly.

Application of FA to replace lime and other chemicals in the management of AMD and reactive mine tailings has been suggested by Kumar et al., (2008), Somerset et al., (2005) and Misra et al., (1996). The potential of FA to neutralize AMD is based on the presence of alkaline minerals/chemicals in significant quantity such as CaO, MgO, K_2O, $CaCO_3$, $Ca(OH)_2$, etc... (Somerset et al., 2005). Precipitation of metal hydroxides occurs at certain pH ranges therefore controlling AMD pH enhances metal removal (Aube, 2004).

1.2 Research Objective and Scope

Coal and wood fired utility generation companies/stations require FA management to control costs. FAs contain large amount of heavy metals that may leach into the ground water in amounts exceeding provincial and/or federal regulatory levels for safety, thereby posing an environmental risk. Recycling FA and boiler ash through its usage for various application purposes would significantly reduce its environmental impact and cost of disposal.

The objectives of this research are to investigate and determine the feasibility and options for fly and boiler ash, including:

- Characterization of FA samples collected from AV-Cell Pulp and Paper Industry (Atholville, New Brunswick) in terms of chemical composition, mineralogical composition, elemental composition, amorphous and crystallinity, thermal properties, surface area and textural properties, morphology, physcio-chemical and other physical properties.
- Application of FA as low cost lime replacement in AMD treatment.
- Application of FA as permeable reactive barrier membrane (PRB) in AMD treatment.
- Investigate the conversion of "spent" FA during AMD neutralization to zeolite for adsorption applications.

1.3 Thesis Organization

The thesis is organized into several chapters. This chapter, one, includes brief background description, which introduces the basic content and subject matter of the research work, the scope and objectives of the research. Chapter two reviews the literature. Chapter three describe the experimental work including characterization of raw fly ash (chemical, thermal, mineralogical, morphology, surface area, crystallinity, physcio-chemical, and other physical characterization), FA: AMD neutralization, Zeolite Synthesis, AMD generation through weathering test and Permeable Reactive Membrane

experiments (PRB) experiments. The results and analyses are presented in chapter four. Chapter five comprises brief of the summary of conclusions and recommendation.

CHAPTER TWO

Literature Review

2.1 Fly Ash Review

Increasing demands in energy require better energy management in thermal power plants, utility and steam plants. Low cost fuel sources such as coal and lignite, heavy oils, forestry residue (fossil fuels, tree barks, saw dust, wood chips), and other plant biomass are burned in furnaces to produce heat to drive steam turbines. Combustion by-products includes solid residues, which become entrained in the exhaust gases; removed in the post–combustion, are referred to as fly ash (FA). The heavy fraction that are not entrained are collected in a hopper containing water located at the bottom of the furnace and is mostly referred to as the Boiler ash. The boiler ash is disposed in a pond using high-pressure water jet. The World Energy Council predicts an increasing rate in energy demand of 1.6% from 2004 to 2030 (Gonzalez et al., 2009).

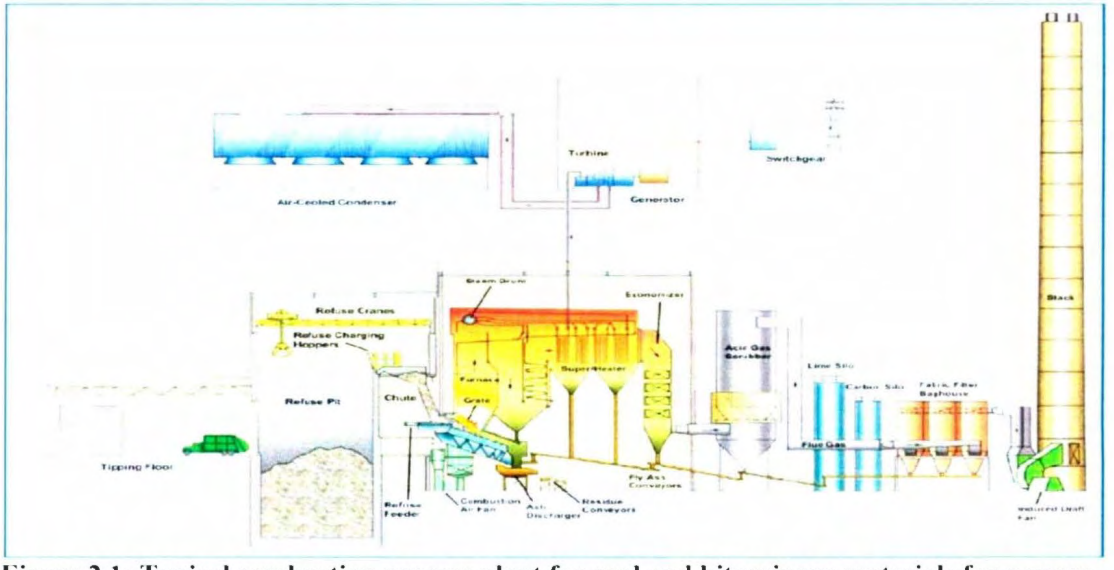

Figure 2.1: Typical combustion process plant for coal and bituminous materials for powers. (Modified from Stantec 2010)

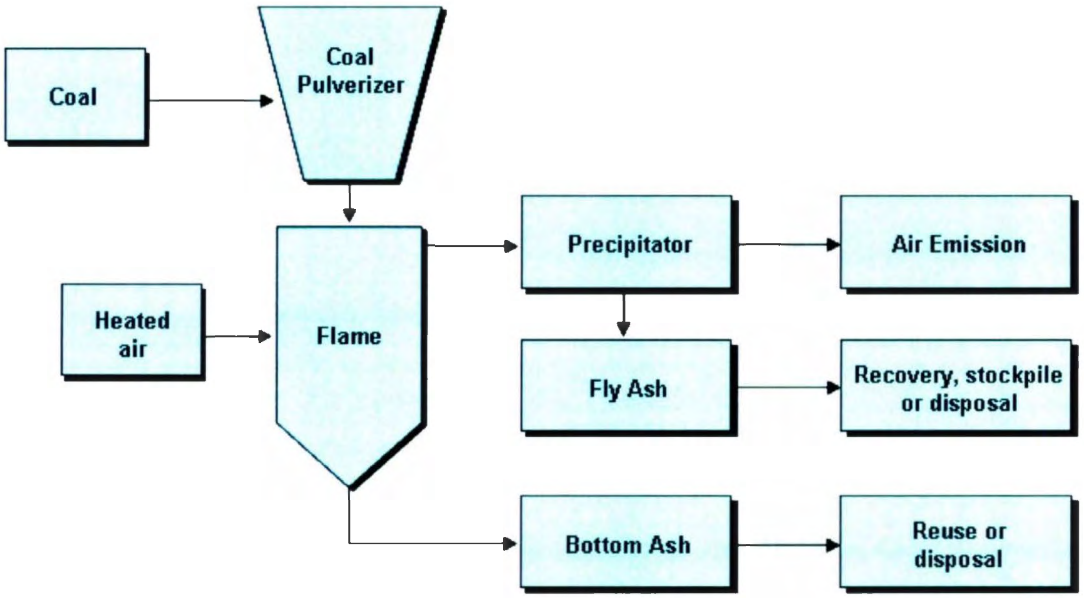

Figure 2.2: Typical flow process for Dry-Bottom Utility Boiler and Production of Coal Ash. (Modified from Sinclair Rob, 2006).

The largest demand growth is in fossil fuels and its allies (coal, biomass, lignite, wood etc…), from about 2772 Mt in 2004 to a projected 4441 Mt in 2030 (Gonzalez et al., 2009). Therefore, fly and boiler ash will be a major challenge with respect to disposal.

2.1.1 Types and Sources of fly Ash

Generally, Boiler Fly Ash is the generic name given to many types of ashes produced by combustion (burning) of various carbonaceous material. Any carbon based fuel or waste material produces ash and the source determines the quantity and quality of the ash produced. The following are the most common ash types reported depending on the material used for combustion.

1. Wood Ash – Generated from wood and woodchips, barks, sawdust and other forest residues are used as heating source for steam turbine. Due to its availability,

low cost and convenience, wood chips and waste pulp liquors, which are produced in chemical pulping processes, are often mixed with fuels and historically preferred for the power boilers (McCubbin, 1983). In addition, wood refuse (wood waste and bark) or hog fuel are common fuels for boilers (McCubbin, 1983).

2. Coal Ash – Coal powered electrical generating plants utilize pulverised coal and produce coal fly ash as a waste product. Coal fly ash includes organic and inorganic matter released during coal combustion process which solidifies while suspended in exhaust gases and collected through electrostatic precipitators (Wang et al., 2006).
3. Tire Ash – An alternate disposal method for used tires is to grind and burn for fuel. Combustion or pyrolysis of waste tires results in tire ash residue the chemical nature of tires gives rise to toxic and metal rich ash residue generated from tires.
4. Incinerator Ash – This is produced from burning garbage and municipal solid wastes (MSW). It is an alternate to solid waste disposal method.

2.2 Characteristics of FA

2.2.1 Morphology

The common nature of FA particles produced from utility and power plants consists amorphous particles ranging from 0.01 – 100 μm diameter (glass-like and/or crystalline). Spherical-shaped particles are the major constituent of FA and may be either hollow

spheres called **cenospheres**, or broad spherical particles filled with smaller particles and crystals called the **plerospheres** (Zhou and Haynes, 2010, and Gonzalez, 2009).

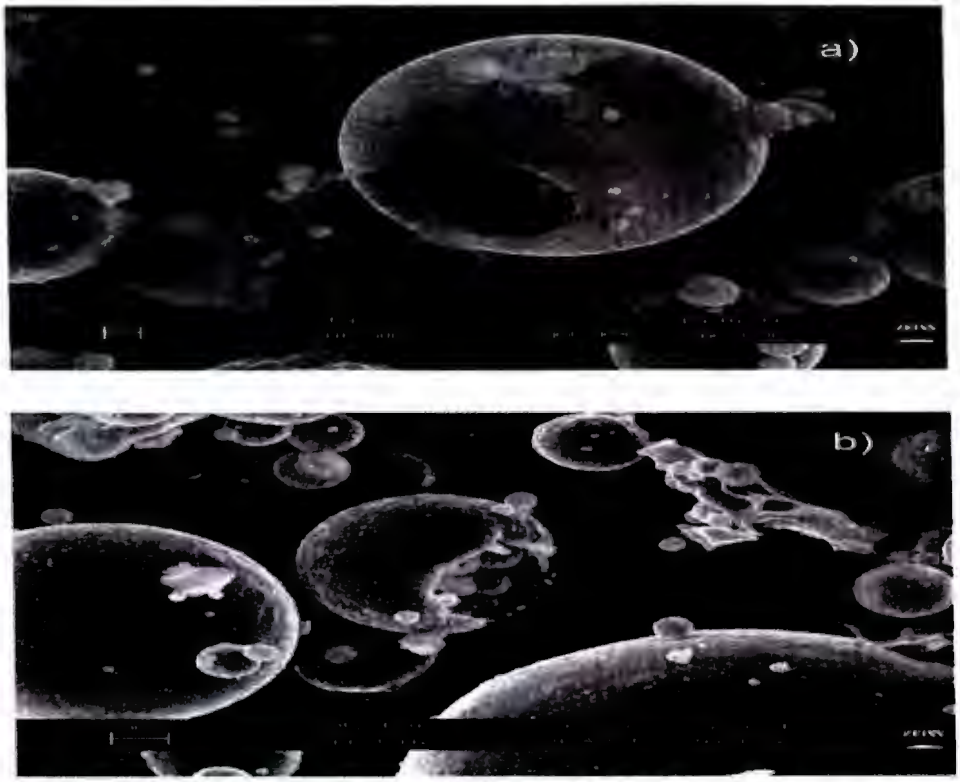

Figure 2.3: (a) Cenospheres (b) Plerospheres (Modified from Claudia et al., 2009)

2.2.2 Chemistry and chemical composition of Flay Ash

Generally, the physicochemical and mineralogical characteristics of fly ash vary and depend on source and type of feedstock (coal, lignite, wood etc…), conditions of combustion, particle size, weathering extent and age of fly ash (Ram and Masto, 2010, Zhou and Haynes, 2010). Most fly ash consists of major, minor, trace and micro-element as its constituents. Chemically, 90 – 99% of the FAs consists of Si, Al, Fe, Ca, Mg, Na and K. The major elements present are Si, Al, Fe and Ca while the minor elements are Mg, Ti, and K. (Ram and Masto, 2010). Although typical chemical content of FA is

usually expressed as oxides e.g SiO_2, Al_2O_3, Fe_2O_3, CaO, Na_2O, TiO_2, MgO, K_2O etc… major and micronutrients of FA include P, B, Cu, Zn and Mn and some trace elements and radioisotopes. Naturally occuring radionuclides in the FAs are reported to be from U, and Th series, as well as ^{40}K (Ram and Masto, 2010).

Table 2.1: Typical Ranges in chemical copositition of various coal generated FA (Modified from Behera, 2010)

Component	Bituminous	Sub-bituminous	Lignite
SiO_2 (%)	20-60	40-60	15-45
Al_2O_3 (%)	5-35	20-30	20-25
Fe_2O_3 (%)	10-40	4-10	4-15
CaO (%)	1-12	5-30	15-40
LOI (%)	0-15	0-3	0-5

Table 2.2: Typical Chemical composition of FA (Modified from Kumar et al., 2008)

Major Oxides	Concentration(%w/w)	Trace element	Concentration (mg/kg)
SiO_2	51.5	As	12
TiO_2	1.4	Cu	43
Al_2O_3	26.3	Mo	5
Fe_2O_3	5	Ni	89
MnO	0.1	Pb	47
MgO	2.5	Sr	1385
CaO	7.8	Ba	863
Na_2O	0.8	Cr	178
K_2O	0.7	Zn	61
P_2O_5	0.4	Co	28
H_2O	0.1		
LOI	2.5		
Total	99.1		

2.2.3 Other Physical Characteristics

Generally fly ash is characterized by its light weight, small spherical particles and are greyish to dark grey in colour. FA particles are very fine with density range of 1.97 – 2.89 g/cm^3, specific surface area of 4000 – 10,000 cm^2/g, particle diameter of 1 – 150 µm refractory and pozzolanic characteristics (Behera, 2010). Carette and Malhotra (1986) characterized Canadian FA for their relative performances in concrete application and reported that the physical characteristics of FAs widely varied. Specific gravity for instance ranged from 1.90 for subbituminous ash to 2.96 for iron- rich ash (Carette and Malhotra, 1986). Furthermore, reported FA ranging in surface area from 1300 cm^2/g for bituminous ash to greater than 5810 cm^2/g for lignite ash (Carette and Malhotra, 1986). Although these properties also depend on the combustion conditions and nature of the combustion materials (Behera, 2010), FAs were also characterized by dielectric property with constant of 10^4, therefore can also be applied in electronic areas of application (Behera, 2010).

2.2.4 Classification

ASTM C618 classifies FAs into class C and class F based on the amount of lime present. Class C FAs are those with CaO content greater than 10% while class F FAs are those with content of CaO less than 10% (ASTM C618, Behera, 2010, Ram and Masto, 2010, Roberts et al., 2010, and Muluken et al., 2009). The minimum overall content of SiO_2, Al_2O_3 and Fe_2O_3 is 50% for class C and typically contains a higher lime content greater than 20% (CaO > 20%) while the minimum overall content of SiO_2, Al_2O_3 and Fe_2O_3 is

70% for class F with content of lime (CaO) less than 10% (CaO < 10%) (Zhou and Haynes, 2010).

Table 2.3: Typical Classess of Fly Ash with Compositional ranges (Modified from Behera, 2010)

	Class F		Class C	
Compound	Low-Fe	High-Fe	Low-Ca	High-Ca
SiO_2	46-57	42-54	46-59	25-42
Al_2O_3	18-29	16.5-24	14-22	15-21
Fe_2O_3	6.0-16	16-24	5.0-13	5.0-10
CaO	1.8-5.5	1.3-3.8	8.0-16	17-32
MgO	0.7-2.1	0.3-1.2	3.2-4.9	4.0-12.5
K_2O	1.9-2.8	2.1-2.7	0.6-1.1	0.3-1.6
Na_2O	0.2-1.1	0.2-0.9	1.3-4.2	0.8-6.0
SO3	0.4-2.9	0.5-1.8	0.4-2.5	0.4-5.0
TiO_2	1.0-2.0	1.0-1.5	<1	<1
LOI	0.6-4.8	1.2-5.0	0.1-2.3	0.1-1.0

2.2.5 Mineralogical Composition of FA

The phase and mineral composition of FA comprises of organic, inorganic and fluid constituents with crystalline, liquid, gas and gas – liquid inclusions. Among the mineral phases of FA are the ferro-alluminosilicate glassy materials with variable amount of unburned/free carbon content incorporated with quartz, mullite, magnetite, and hematite as the major mineral phases (Ram and Masto, 2010). FA mainly contains amorphous ferro-alluminosilicate glass (66 – 95%) derived from silicate transformation during combustion and other mineral phases include quartz (SiO_2), mullite ($3Al_2O_3$-2 SiO_2), anorthrite (CaO . Al_2O_3 . $2SiO_2$), gehlenite ($Ca_2Al_2SiO_7$), hamatite (Fe_2O_3), magnetite

(Fe_3O_4), and calcite ($CaCO_3$), depending on the mineralogical nature of the feed materials (Zhou and Haynes, 2010). Wigley and Williamson, (2005) analysed the minerals transformed on fly ash during combustion and categorized as; (1) Clay minerals; kaolinite ($Al_2Si_2O_5(OH)_4$), Illinite ($KAl_3SiO_{10}(OH)_2$), and montmorillonite (like Illinite but with replaceable Ca and Na more abundant than K). (2) Major mineral phase; quartz (SiO_2), pyrite (FeS_2), carbonates; calcite ($CaCO_3$), dolomite ($CaMg(CO_3)_2$), ankerite ($Ca(Mg, Fe, Mn)(CO_3)_2$), and siderite ($FeCO_3$) and (3) Minor mineral phases; apatite ($Ca_5(PO_4)(OH)$), crandallite ($CaAl_3(PO_4)(SO_4)(OH)_6$), feldspar (composition between $NaAlSi_3O_8$ and $CaAl_2Si_2O_8$), garnet ($(Mg, Fe)_3Al_2Si_3O_{12}$) and rutile (TiO_2).

2.2.6 Pozzolanicity of Fly Ash

The ability of fly ash to exhibit its own self-cementing behaviour is referred to as its pozzolanicity. Portland cement production requires a large amount of energy and raw materials therefore has taken energy efficiency alternatives including utilizing fly ash as alternative raw material source (Gonzalez et al., 2009). Class F fly ash is referred to as pozzolanic and class C fly ash known as cementitous materials. In addition, FA has been studied as a binder or cement replacement in concrete (Gonzalez et al., 2009). The high lime content of class C FA allows application as both pozzolanic and cementitous agent whereas class F FA lower lime content restricts it to pozzolanic applications (Tarun, 1993).

2.3 Fly Ash generation and management in Canada

Power from coal accounts for 17% of Canada's total electricity demand resulting in a total coal ash generated in 2004 estimated to be 6.24Mt (Sinclair, 2006). In addition, ash residues are produced yearly in electric power plants, steam boiler plants, and the pulp and paper industry. Its management has been a major problem in Canada and worldwide due to their characteristics and the large amounts generated every year. It was estimated that 553,000 tons of ash residues were generated in Canadian pulp and paper in 1995 (Reid, 1998), 775,000 tons in 2002 (Elliott and Mahmood, 2005) and currently, total of over 5 million tonnes fly ash was reportedly generated every year in Canada (Muluken et al., 2009).

The management practice for 84% of Canadian pulp and paper mills in the past was disposal to landfills. However, the costs associated with tipping fees, the extensive measures required coupled with longer hauling distances have increased substantially in the last decade. In addition there are concerns associated with leaching metals and organic compound and their migration into ground water or nearby surface water. Current recycling rates of fly ashes as estimated by Association of Canadian Industries Recycling Coal Ash (CIRCA, 2010) was valued at 6% bottom ash as at 2007 and therefore, predicted ample room for improvement in future time mostly in concrete and construction areas of application.

Table 2.4: Coal Ash Generation and Usage in Canada (Modified from CIRCA, 2010)

Canada Production and use of Coal Combustion Products (CCPs) 2005 - 2007 Average	
	Bottom Ash
Production	(000 tonnes)
Produced	1624
Disposed/Stored	1421
Removed from disposal	5
Use (Domestic)	
Cement	52
Concrete/Grout	0
Mining Applications	
Road-base/Sub-base	48
Wallboard	0
Others (4)	2
Total Use	102
Use Percentage	6

Table 2.5: Fly ash production and utilization in different countries of the World (Modified from Behera, 2010)

SL NO	Country	Annual FA Production (Mt)(10^6tonnes)	FA Utilization (%)
1	India	112	38
2	China	100	45
3	USA	75	65
4	Germany	40	85
5	UK	15	50
6	Australia	10	85
7	Canada	6	75
8	France	3	85
9	Denmark	2	100
10	Italy	2	100
11	Netherlands	2	100

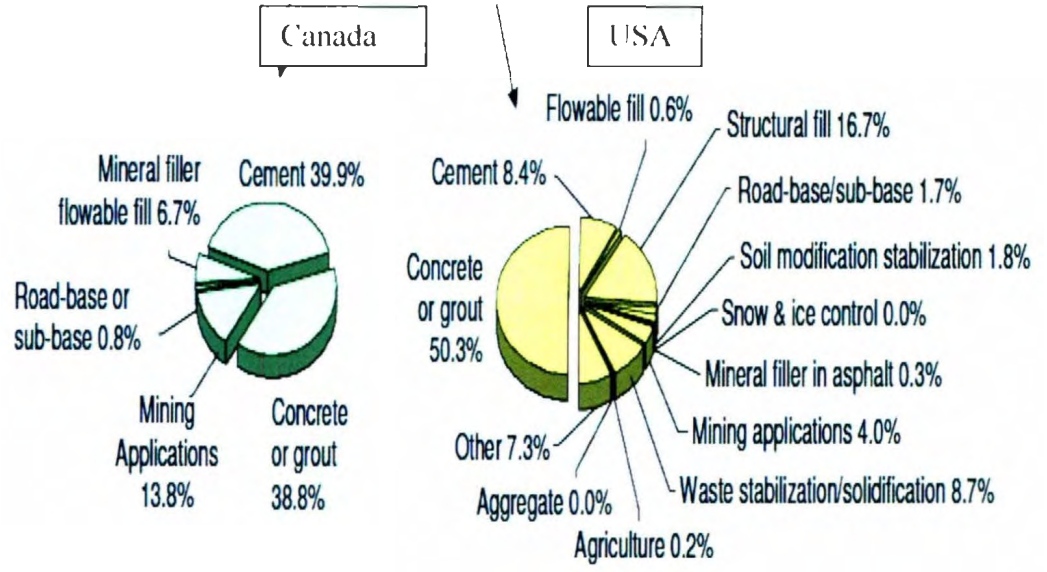

Figure 2.4 Typical FA recycling Options in Canada and USA (Modified from Rob, 2006)

2.3.1 Power Generating Plants

Most power plant boilers use coal, forestry residue, and other fossil fuels therefore, FA is their major by-product. Coal generated FA was estimated to be 349Mt fly ash worldwide in the year 2000 (Wang and Hu, 2006). In Canada, power generation through thermal combustion of coal was estimated to be 19% and resulting in an estimated 5 million tonnes FA per year (Muluken et al., 2009).

2.3.2 Pulp and Paper Industry

The Pulp and paper industry in Canada generate electric power concurrently with steam production for process heat or co-generation. Power boilers utilize forest residue and/or fossil fuels as a heat source. The wood refuse, commonly referred to as hog fuel, consists

of wood wastes such as; saw dust, sticks, wood chips, cutoffs, overs, bark as well as wood harvest residues (McCubbin, 1983). Combustion of these materials generates fly and bottom ash as the major by-products.

2.3.3 Environmental Impacts of Disposal

FA contains fine particles that if not managed properly, become air pollutant (Envis-Newsletter, 2006). In addition, poor management of FA leads to environmental problems which includes loss of usable land, soils and plant contamination, as well as air pollution (Kumar et al., 2008). Landfill practices are generally considered the most economic ways of waste disposal, up to 95% of solid wastes generated worlwide are disposed through this practice (Scott et al., 2005). Landfill is the most common disposal option for FA and pose risks to ground surface water. Disposal of FA will be a challenge in the future as volumes of FA increases and disposal options become more restrictive.

2.3.5 Ash Pond

In the United States, about 52% of the ash is conveyed into the disposal pond (RENEL, 1994). To meet the Resources Conservation and Recovery Act (RCRA) Subtitle D requirements there are two ponds (usually the primary pond and a discharge pond) (RENEL, 1994), and up to 90 percent of the pond water is usually recycled. Ponds are lined with liners and groundwater is monitored to determine and mitigate any leaching (RENEL, 1994).

2.3.6 Government and Provincial Regulations on Fly Ash

Fly ash is categorized as a biosolids therefore all regulations both federal and provincial, that governs biosolids applies to FA (Storm and wastewater, 2003).

Table 2.6: Comparison of different biosolids quality categories (Modified from Storm and Wastewater, 2003)

Parameter	Category 1	Category 2	Category 3
US EPA	Exceptional Quality (EQ)	Class A	Class B
Alberta	(No Classification)		
British Columbia	Class A Compost	Class A	Class B
Ontario	(No Classification)		
Quebec	C1, P1	C2, P2	C3, P3
Pathogen Reduction Requirements	Less than 1000 MPN fecal coliforms per gram of total solids, dry weight or Density of Salmonella less than 3 MPN per grams of total solids, dry weight	Less than 1000 MPN fecal coliforms per gram of total solids, dry weight or Density of Salmonella less than 3 MPN per grams of total solids, dry weight	Less than 2 Million MPN fecal coliforms per gram of total solids, dry weight

2.3.7 USEPA Disposal Standards and Regulations

Table 2.7: Typical USEPA Regulatory Standards for Classes of Biosolids (Modified from Storm and Wastewater, 2003)

Example of Pollutant Limits (mg/kg total solids dry weight)						
	BC Class A Compost	US EPA	Fertilizer Act of Canada	US EPA	BC Class B Biosolids	US EPA
As	13	41	75	75	75	75
Cd	3	39	20	85	20	85
Cr	100	1,200	-	3,000	1,060	3,000
Cu	400	1,500	-	4,300	2,200	4,300
Pb	150	300	500	840	500	840
Hg	2	17	5	57	15	57
Mo	5	(under review)	20	75	(under review)	75
Ni	62	420	180	420	180	420
Se	2	36	14	100	14	100
Zn	500	2,800	1,850	7,500	1,850	7,500

2.4 Mine Tailings and Acid Mine Drainage (AMD)

2.4.1 AMD

Acid mine drainage (AMD) is the acidic water formed from the oxidation of sulphide minerals (Skousen et al., 1997). The environmental impacts and cost of managing AMD in the mineral processing and mining industries is significant. The oxidation of sulphur compounds forms sulphuric acid which would negatively impact ecosystems if released untreated (Bably and Roberts 2010; Kumar et al., 2008, and Somerset et al., 2005).

Figure 2.5: Typical Mine Tailing deposits (Black Hills)
(Modified from Google.com by LeinaDoli)

One of the most well-accepted and most widely used AMD management methods is neutralization with lime (CaO) or limestone ($CaCO_3$) (Bably and Roberts, 2010; Kumar et al., 2008, and Somerset et al., 2005). The limiting factors of neutralising AMD using lime and limestone are the cost involved and diminishing lime reserves; therefore, other treatment options are being explored.

Figure 2.6: Typical Acid Mine Drainage Water Pool
(Modified from Google.com by LeinaDoli)

Outside the application of lime and limestone, chemicals like Na_2CO_3, $Ca(OH)_2$, and NaOH has also been used for AMD neutralization (Somerset et al., 2005). Application of FA to replace lime and other chemicals in the management of AMD and reactive mine tailings is an option due to the chemical make-up of FA. FA is composed of strong alkaline minerals and chemicals with pH (~10.0) capable of bringing the pH of AMD to almost neutral. The potential of FA to neutralize AMD is based on the presence of alkaline minerals/chemicals in significant quantity such as CaO, MgO, K_2O, $CaCO_3$, $Ca(OH)_2$, etc... (Somerset et al., 2005). FA or materials derived from fly ash for AMD treatment could reduce (AMD) management cost due to reduced chemical costs and treatment efficiency. FA and/or FA based zeolite has been also used for AMD treatment (Bably and Roberts, 2010; Kumar et al., 2008; Gitari et al., 2005; Somerset et al., 2005, and Hellier, 1998).

2.4.2 Generation and Chemistry of Acid Mine Drainage from mine wastes

Chemical weathering of sulphide minerals not only reduces pH but also releases contaminants from ore and mine wastes into the water bodies where they become mobile and thus bioavailable (Younger et al., 2002). The fate of AMD depends on the type of mine minerals and the nature of geological surroundings (Paine, 1987). During mining, sulphide minerals such as pyrite (FeS_2) come in contact with oxygen and water thereby resulting in sulphuric acid generation characterized by high acidity (pH 2-4), high sulphate concentration (1-20 g/L) and generally with high concentrations of Fe, Mn, Al, Cu, Zn, Pb and Cd (Kumar et al, 2008). Pyrite is the major contributor to AMD

formation as it is the most common outlined sulphate minerals (Rios et al., 2007 and Skousen et al., 1997). To demonstrate the formation of AMD, the oxidation of Pyrite is outlined below (Rios et al., 2007) :

$$FeS_2 + 3.5O_2 + H_2O \rightarrow Fe^{2+} + 2SO_4^{2-} + 2H^+ \quad (2.1)$$

$$Fe^{2+} + O_2 + 4H^+ \rightarrow 4Fe^{3+} + 2H_2O \quad (2.2)$$

$$4Fe^{3+} + 12H_2O \rightarrow 4Fe(OH)_3(s) + 4H^+ \quad (2.3)$$

$$FeS_2 + 14Fe^{3+} + 8H_2O \rightarrow 15Fe^{2+} + 2SO_4^{2-} + 16H^+ \quad (2.4)$$

Iron is the dominant metal species in AMD from most Canadian mine sites, with concentration ranges from 0.5 – 774 mg/L (Rio, 1997), copper and zinc were also present in significant concentration at most sites and sulphate concentrations reportedly ranged from 950 – 4516 mg/L (Rio, 1997).

2.5 Fly Ash Utilization Options

2.5.1 Zeolitization/Zeolite Synthesis

Zeolites are hydrated aluminosilicate minerals with a three dimensional open structure useful for immobilizing toxic elements (Claudia et al., 2009). FA as a zeolite has been investigated in contaminated water treatment and acid mine drainage (Bably and Roberts, 2010).

Zeolite synthesis from raw FA is accomplished by alkali fusion and hydrothermal treatment of raw FA. Zeolite produced from fly ash is crystalline in nature and due to its high cation exchange capacity; it is very effective in heavy metal removal (Bably and Roberts, 2010). Bably et al., (2010) investigated FA zeolite and found to be effective at

removing contaminant of concern from AMD. Other studies showed similar results including Querol et al., (2002), Gitari et al., (2005), and Solanki et al., (2010).

2.5.2 Neutralization

In typical AMD neutralization lime and/or quicklime is commonly used. These compounds are naturally occuring constituent of FA. Kumar et al., (2008) reported a high percentage of major, minor, trace element and sulphate (SO_4^{2-}) removal by contacting AMD with different doses of raw FA. The contaminants were reportedly removed to minimum bearable (to levels that is less harmful) and the solid residues is suitable as a binder. Rios et al, (2007) investigated removal of heavy metals from AMD using coal FA and synthesized FA zeolites as low-cost sorbents for AMD abatement. Gitari et al., (2010) extended these studies to determine the impact of reaction time and species removal. The effluent water was predicted using geochemical code PHREEQC with WATEQ4 database. The results established that removal of inorganic species depended on the pH regime, and also the SO_4^{2-} removal depends on precipitation of gypsum, barite, celestite and iron-oxyhydroxides at pH greater than 5.5. PHREEQC also predicted iron, aluminum, and manganese-bearing phases precipitation at pH ranges of 5.53 – 9.12.

As part of research contribution to the existing innovations, the current research investigation will be extended to studying the generated solid residues from neutralization process (FA:AMD neutralization) for zeolite synthesis and its subsequent application in waste water management.

2.5.3 Permeable Reactive Barrier (PRB) Application

Permeable reactive barriers (PRB) are used to treat metals and increase the pH of acidic waste water by promoting sulphate reduction and metal sulphide precipitation. Benner et al, (1999) investigated the geochemistry of PRB for AMD treatment in a field of Nickel pond. A dramatic improvement in the water quality was reported with subsequent decrease in contaminants concentrations (SO_4^{2-} was reduced from 3000 to 2000mg/L, Fe decreased from 1300 to 270mg/L, and alkalinity increased from 800 to 2700mg/L). The geochemical modelling indicated supersaturation of the barrier itself with precipitation of Fe, amorphous iron – sulphide, or both. In a study by Komnitsas et al., (2004), lignite FA was used as a PRB for metal ions removal (Fe, Mn, Zn, Ni, Cd, Co, Al and Cu) AMD. It was reported that almost all inorganic contaminants were removed almost completely after several days.

The contaminant removal mechanism proposed was hydroxide-oxidations, precipitation, and co-precipitations with subsequent adsorption onto the barrier surface. Muluken et al, (2010) studied the feasibility of using coal FA and FA – bentonite mixtures as a barrier materials for mine waste. The overall results showed that heavy metals were removed from the AMD effluent well below the leachate criteria set by the Ontario Government.

2.5.4 Tailing waste Agglomeration and Backfilling Application

Figure 2.7: Typical Tailing Agglomeration (Modified from Golder Paste Technology LTD) (PASTEC)

Traditionally, coarse fractions of mine tailings are used for backfill excluding the fine fractions by a classification process. Agglomeration has been one of the most effective methods of dealing with reactive fine fractions of mine tailings with the use of binders. Fly ash is now widely used in this application area (fig.2.7, agglomeration and paste), as binder in replacement of Portland cement to immobilize the reactive components of mine tailings. The use of this technology provides an attractive recycling option for minimizing engineering and environmental constraints commonly associated with fine mineral wastes disposal. Misra et al. (1996) investigated the use of FA to agglomerate mine tailings from two Canadian fields (Noranda, Quebec, Canada and Cyprus Thompson Creek, Clayton, Idaho). It was reported that FA significantly reduced cement requirement without decrease in strength and immobilization effect. Misra et al., (1996) also used toxicity characteristics leaching procedure (TCLP) tests on the Noranda mine tailings.

using a FA – cement mixture as a binder. Extractable contaminant concentration were lowered in the resulting leachate and below the regulated level than pastes prepared from using fly ash or cement alone.

Amaratunga, and Yaschyshyn, (1997) studied the effect of various binder dosages, curing periods and combination of pellets to tailing ratios on fine gold mill tailings. Compressive strengths of the paste were enhanced while the modulus of elasticity was trippled with pozzolanic binders. The results suggested that agglomerated tailings paste fill (ATPF) minimizes fine tailings surface disposal and maximizes utilizing fine tailing pastes for backfill applications. Jang and Kim, (2000) reported that highest strength was obtained with optimum mixing ratio of 85% cement, 5% tailing waste and 10% fly ash.

Figure 2.8: Typical Tailing Agglomeration (Modified from Golder Paste Technology LTD) (PASTEC)

2.5.5 Light concrete and Cement Application

Siliceous by-products with good pozzolanic characteristics have the potential of making any structure more durable (Piyush and Raj, 2002). This is due to dense microstructure formed during pozzolanic reactions; the significant reduction in attacks from environment is through interconnected microspores (Piyush and Raj, 2002). Piyush and Raj, (2002) used mixed pond ash from an integrated steel plant to manufacture bricks which was reportedly cost effective with superior stregth and structural quality. Piyush and Raj, (2002) established that the mixed pond ash used was within the range of 45 – 50% and gives the optimum ratio.

Figure 2.9: Light concrete Plant (Modified from Sinclair Rob, 2006)

In 2006, a survey by the American Coal Ash Association (ACAA) indicated that annual generation of fly ash in the US was estimated to be 72.4 million tons and 45% of the total was re-used. Furthermore, 59% of the utilized ash was used in cement and concrete

(Karthik, 2009). As such, currently concrete is the largest market for FA, greater than 30% of total cementing materials require ash content in concrete application, (Karthik, 2009). In block manufacturing, addition of fly ash enhanced; strength, plasticity, improved finishing and textures, better mould life, reduced shrinkage and increased durability (Headwaters Resources, 2005).

2.5.6 CO_2 capture and sequestration

The capture and control of CO_2 is estimated to be approximately $60 to $500 per tonne of CO_2 captured (Phelps et al., 2004). Phelps et al., (2004) investigated the utilization of metal-rich fly ash to sequester CO_2 and metals. The process involved microbial conversion of CO_2 (biogeochemical carbonation) into sparingly soluble carbonaceous material (e.g $CaCO_3$ and $FeCO_3$) using metal-reducing bacterial on metal-rich fly ash and lime. The precipitation of the resulting mixture showed carbonate formation indicating CO_2 capture. Muduli et al.(2009) used gypsum (calcium bearing material) and silica-aluminum rich FA mixture for CO_2 capture. This combination caused mineral carbonation and was proposed for long term CO_2 storage under ambient atmospheric condition. Arenillas et al., (2005) utilized FA material as a sorbent for CO_2 capture. The absorption capacity of the sorbent was enhanced by the addition of organic bases (polyethylenimine with polyethylene).

2.5.7 Effluent gas stream adsorption

Steam hydration (hydrothermal activation) of pozzolanic fly ash produces a calcium-aluminum silicate-hydrate ($Ca_2(Si_6Al_3)O_{24}.8H_2O$) and calcium carbonate ($CaCO_3$) which

can be used in SO_2 removal (Teong et al., 2003). Previous research has established that calcium-aluminum silicate-hydrate converts SO_2 to aluminum silicate-hydrate and calcium carbonate to calcium sulphate ($CaSO_4$) (Teong et al., 2003). Davini, (1996) investigated utilizing FA – $Ca(OH)_2$ to synthesize a SO_2 sorbent and established that the produced sorbent was pozzolanic in nature with a better reactivity towards SO_2 than use of $Ca(OH)_2$ alone. This behaviour was attributed to improved surface area of the sorbent synthesized.

2.5.8 Contaminated site remediation

Sorbent capability of pozzolanic fly ashes with respect to major/heavy metals such as lead, copper, zinc iron, cadmium etc... and that of cementitious fly ash with respect to minor and traced metals such as manganese, magnesium, etc... Antonio and Ayuso, (2008) studied the sorbent ability as applicated to soil remediation. Tests were performed with 4% of FA sorbents in laboratory column tests. More than 50% reduction in all metal contaminants was reported. Matsi and Keramidas, (1999) investigated alkaline fly ash application for contaminated soil (acid soils) amendment by growing Ryegrass (*Lolium perenne L.)* on pots containing fly ash – sand mixtures for 300days in order to analyse effectivity of fly ash to remediate acid soils. A significant increase in dry biomass yeild of ryegrass was reported with fly ash application and cumulative uptake of boron and phosphorus increased with fly ash application.

CHAPTER THREE: EXPERIMENTAL METHODS

3.1 Sample Collection

The ashes analyzed in this characterization study were collected from AVCell Pulp and Paper plant located at 175 Mill Road, Campbellton, New-Brunswick, Canada. The ash originated from two different sources; (i) the Hog-Boiler Precipitate ash sample (HBP) (fig.3.1a) collected from the hog-precipitator is the lighter and finer fraction called the fly ash (FA) and (ii) the Mixed Ash Pond sample (MAP) (fig.3.1a) or the bottom/boiler ash collected at the bottom of the boiler is the heavier fraction of the combustion residue. Standard proximate analysis of the fly ash samples were carried out according to procedures of the American Society for Testing and Materials (ASTM) standards.

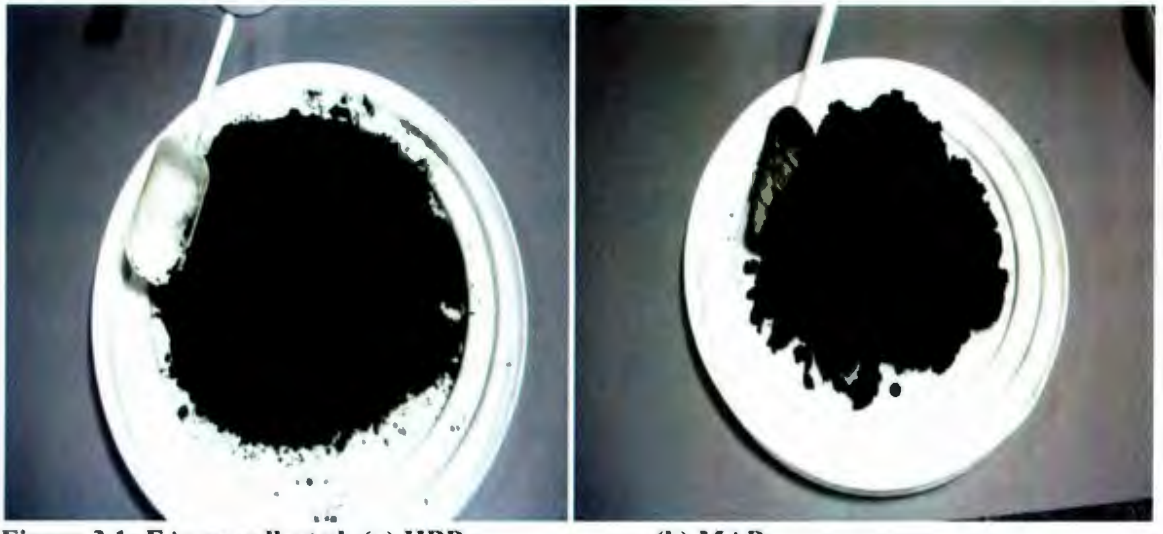

Figure 3.1: FAs as collected. (a) HBP (b) MAP

3.2 Characterization of Fly Ash

3.2.1 Chemistry and Elemental analysis of Fly ash

The concentrations of various elements in the ash samples were analysed using Inductively Coupled Plasma Mass Spectrometer (ICP-MS, fig.3.2) and Inductively Coupled Plasma-Optical Emission Spectroscopy (ICP-OES). The samples were first digested by mixing approximately 1.0 g of each sample with 2 mL nitric acid (8N HNO_3) and 1.0 mL of hydrofluoric acid (HF) in a Teflon bottle. The mixture was covered and heated to 70°C for 48 hours. The heated sample was rinsed with nitric acid (8N – HNO_3) after 48 hours and dried at 100 °C. Aqua Regia (3:1 conc. HCl: HNO_3) was added and the samples were heated to 70°C for another 48 hours then allowed to evaporate to dryness after addition of 2mL 8N – HNO_3. The samples were then rinsed with nano pure water and filtered using 0.45µm micropore membranes. The filtrate (a clear liquid) was diluted with 2%HNO_3 and analysed using ELAN-DRC-II (fig.3.2, ICP-MS) with power of 12kW, pulse stage volt of 1kV and 1.05L/min nebulizer gas flow rates. A Perkin Elmer Optima 5300DV dual view (ICP-OES) was used to compare and confirm the ICP-MS results.

Figure 3.2 ELAN-DRC-II (ICP – MS)

3.2.2 Chemical Composition of Fly ash: Mineral liberation ablation (MLA)

Screening and Refluxing:

Dry ash samples were screened into different particle sizes using ROTAP-W.S. Tyler 8570(2005) shaker with U.S.A standard testing sieves (ASTM E-11 specification). Sieves sizes were arranged from the bottom in ascending order; <45μm, >75μm, >125μm, >180μm, >225μm, >300μm and 500μm. Samples were fetched into the 500μm sieve and coupled into the Tyler set up with other sieves. The machine was turned on for 15 minutes thereby separating ash particles into different sizes. The screened samples were classified into three groups according to particle size range. The first group (MAP-1) was

represented by size fractions from <75 µm up to >125µm, second group (MAP-2) was represented by size fractions from >180µm up to > 300µm and the third group (MAP-3) was represented by size fractions >500 µm for refluxing. Quanta-chrome Rotary-Micro-Riffler (fig.3.3a) was used for sample sizing each size group was divided into eight equal amounts. Approximately 1.0g of each sample was then mounted onto Epofix-Resin polymer (proxy) which evenly distributed the sample particles onto its surface for grinding and polishing. The polished samples were then taken to an FEI Quanta 400 scanning electron micro analyzer (SEM-EDX, fig. 3.3d), operated with the typical accelerating voltage of 12kV equipped with energy dispersive x-ray (EDX) spectrometer. The SEM is coupled with MLA software which provides quantitative estimates of mineral weight percentages with respect to area and size of grains. The samples chemical composition were identified by matching optically taken spectrums with data base.

Figure 3.3a: Quanta-chrome Rotary-Micro-Riffler

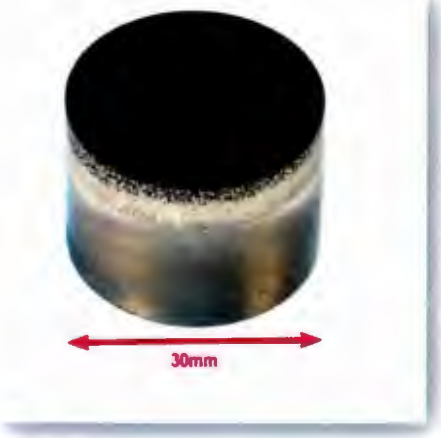

Figure 3.3b: Sample mounted on Epofix polymer **Figure3.3c:Struers Polisher**

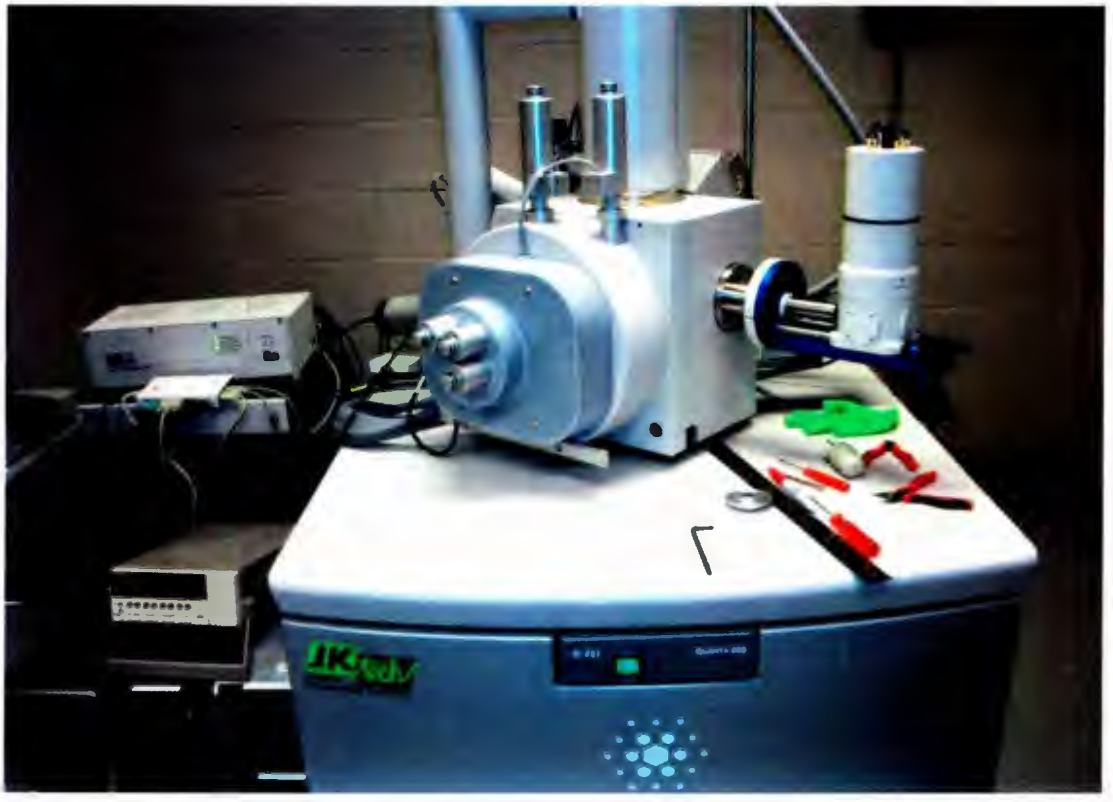

Figure 3.3d: Quanta 400 scanning electron micro analyzer (SEM-EDX)

3.2.3 Morphology: Scanning electron microscope (SEM)

The morphology and micro-structure of the samples were taken using FEI Quanta 400 scanning electron micro analyzer (SEM-EDX, fig.3.3d) operated with the typical accelerating voltage of 12kV. The same instrument used for MLA processing was required for this analysis which includes the mineral identification of the samples based on the optical quantitative and estimates based on proportions, sizes and shapes of the grains in the proxy mounts taken in an automated fashion by the instrument (SEM).

3.2.4 Crystallinity and Mineralogical composition: *X-ray diffraction (XRD)*

Mineral phases and crystalline minerals present in the ash residues were identified using XRD in a Rigaku Ultima-IV (fig.3.4). A small amount of sample (about 0.20g) was mounted on the aluminum plate trough and irradiated with a Cu-Kα radiation energy source. The instrument uses an accelerating voltage of 40kV and current of 44mA with 0.03° step. The best peak definition and the lowest background was produced at a rate of 2-theta/min. Data were digitally recorded and peak matching with JCPDS database (as a source of reference data) was done using Jade software.

Figure 3.4: Rigaku Ultima-IV

3.2.5 Thermal properties and Loss on Ignition

3.2.6 Thermal Analysis

Thermal-properties of the samples were obtained using Thermo-Gravimetric Analysis instrument, TGA Q5000 series (fig.3.6). Total loss on ignition (LOI) and the total organic carbon (TOC) of the samples were determined using a modified step-wise isothermal technique with the TA instrument customized and set to Hi-Resolution of 4.2, sensitivity of 1.2, and ramping rate of 20 °C/min under inert (N_2) and reactive (O_2) atmospheres at 75mL/min gas flow. A series of step-wise TGA under reactive and/or inert atmospheres was carried out. Approximately 0.35mg of sample was weighed into platinum pan and

loaded into tared equipment under programmed steps as described above. This experiment was repeated at different resolutions, sensitivities and ramping rates in order to obtain the best reproducibity. The TGA steps are briefly described as follow:

Heating the sample from 35 ºC to 100ºC at 20ºC /min in N_2 atmosphere at 75mL/min gas flow and holding isothermally for 15minutes at 100ºC. The process was heated afterwards to 1000ºC at the same condition of heating rate and gas flow in N_2 (inert) atmosphere. It was then cooled from 1000ºC to 100ºC with 20ºC /min cooling rate under N_2 at 75mL/min gas flow and gas was switched from inert to reactive (N_2 to air) then heating from 100-1000ºC with heating rate of 20ºC /min in air at 75mL/min gas flow.

The inorganic carbon from the ash samples was removed by acid treatment where the samples' carbonates were converted to CO_2. The same TGA procedure as described above was followed except that heating to 1000ºC under N_2 atmosphere was eliminated (not required because carbonates/inorganic carbons were removed by acid treatment prior to TGA). Any decomposition measured with the TGA could then be attributed strictly to loss of moisture content, dehydration of hydrated limes under N_2 atmosphere and organic carbon oxidation under reactive (O_2) atmosphere. Oxidation that occurred between regions of 550ºC to 900ºC approximates TOC since the inorganic carbon contents in form of carbonates have been removed prior to TGA process.

transferred the sample to oxidation reactor (at 1050°C), the product gas mixture then passed through oxidation catalyst, (CrO_3) which ensured complete combustion of the sample. Cobaltic oxide removed halides and SO_2 followed by reduction of the sample stream in a reactor (at 650°C) where excess O_2 was absorbed with reduction of NO_2 to N_2. The resulting N_2 and CO_2 peaks were used to determine the percentage weight of carbon.

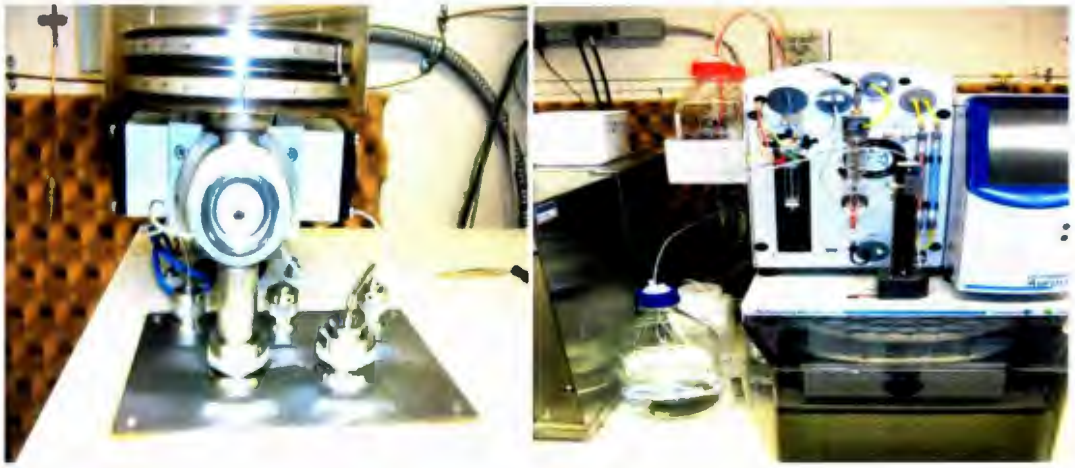

Figure 3.6a: components of Erba NA1500 Elemental Analyzer (EA)

Figure 3.6b: Erba NA1500 Elemental Analyzer (EA)

Total Organic Carbon (TOC) Content

The inorganic carbon of the ash samples were removed prior to the above described process by acid treatment which removes carbonates (CO_3) from the calcium carbonate present in the samples. Hence, the carbon content detected by the TCD represents the TOC content of the sample. The inorganic carbon content of the samples was determined by carefully weighed approximately 1.0g of each ash sample into different Teflon bottle and mixed with 20% nitric acid (20% HNO_3 by volume) and stirred for 5 to 10 minutes until all bubbling (CO_2 liberation) stopped. It was then rinsed with deionised water (nano pure) and heated to dryness at 105 °C for 48 hours on a hot plate. The same procedure as described for total carbon content then followed.

3.2.8 Surface area and pore volume determination (Specific surface area determination (BET) method)

The samples were sent to materials surface characterization laboratory, at the Chemical Engineering Department, University of New Brunswick for specific surface area determination. Nitrogen isotherms were measured at -196 °C (77K) using BEL-sorp MAX (BEL Japan Inc.). Prior to each measurement, the samples were de-gassed to 10^{-4} Torr at 120 °C (393K) with sample mass ranges from 0.339 to 1.60g. The specific surface area of each sample was calculated using BET correlation and Nitrogen adsorption-desorption data.

3.2.9 Buffering power

The sample buffer capacity was determined by titrating the sample with 1 M hydrochloric acid in a 250ml capacity conical flask against 0.33 gem^{-3} mass concentration ash sample. The volume of acid used for each unit pH change was recorded and used to compute the buffering power of each ash sample in millimole per unit pH (mmol/pH).

3.2.10 Porosity and Density

Porosity

For the porosity measurement a 200ml capacity measuring cylinder was used. Distilled water at room temperature was poured into the cylinder up to the 200ml mark and then transferred to a conical flask. The glass cylinder was dried and fly ash sample was filled into the measuring cylinder (with constant shaking for good compaction) up to the 200ml mark. Initially measured water from conical flask was then gently poured into the sample in the measuring cylinder until it saturated the ash sample up to 200ml mark. The volume of water used that saturated the sample up to the 200ml mark represents the pore volume of the ash (represented by V_1). It was determined by taking the volume of water remained in the flask (represented by V_2) from total volume (represented by V_1 −200ml = bulk volume). Hence porosity of each sample was determined from the relationship as given below;

$$\text{Porosity } (\emptyset) = \frac{\text{pore Volume}}{\text{Bulk Volume}} = V_1/V_1 \qquad (3.1)$$

Density (True Density)

The densities of the samples were measured in a similar way to porosity measurement. A 500ml measuring glass cylinder was filled with water up to 200ml mark (represented by V_1). Dry ash sample was carefully weighed using micrometer digital balance and recorded (M_S). This known mass of ash sample was then filled into the 200ml of water in the measuring cylinder thereby displacing some volume of water. The final volume of water was noted (represented by V_2) and the true volume of the sample (represented by V_S) was determined taking the initial volume V_1 from the final volume V_2 (i.e. $V_S = V_2 - V_1$) and each samples' density was determined using the simple correlation;

$$\text{Density } (\rho) = \frac{\text{Mass of sample}}{\text{Volume of sample}} = M_S / V_S \qquad (3.2)$$

3.2.11 FA pH measurement

A bench pH/ion meter (Oakton pH 2100 series) was used to determine the pH values of the samples. Nano pure water was used to dilute approximately 4.0g of each sample in a conical flask. The mixture was thoroughly mixed and shaken for 30 to 40 minutes in a VWR OS – 500 series shaker and pH meters' electrode was dipped into the mixture at the end of mixing. The digital numeration displayed on the meter was allowed to stable and the reading was taken for the samples.

3.3 Mine tailings Characterization

Mine tailings samples used in this research studies were collected from Vale Sadbury mining site in Ontario, Canada.

3.3.1 Chemical and Mineralogical composition: *Mineral Liberation Ablation (MLA)*

Approximately 1.0g dry mine tailing was mounted into Epofix-Resin polymer (proxy) which held and evenly distributed the sample particles on to its surface (Ref. fig.3.3b). The polished samples were then taken to an FEI Quanta 400 scanning electron micro analyzer (SEM-EDX, fig. 3.3d), operated with the typical accelerating voltage of 12kV equipped with energy dispersive x-ray (EDX) spectrometer coupled with MLA software. The MLA provides quantitative estimates of mineral abundances with respect to area and size of grains rather than point counting of the grains. The samples chemical composition was identified by matching optically taken spectrums with data base.

3.3.2 Crystallinity via X-Ray Diffraction

Mineral phases and crystalline minerals of the tailing residues were identified using XRD in a Rigaku Ultima-IV(fig.3.5). A small amount of dry powdery tailing (about 0.20g) was mounted on the aluminum plate trough and irradiated with a Cu-Kα radiation energy source. The instrument uses an accelerating voltage of 40kV and current of 44mA with 0.03° step. The best peak definition and the lowest background was produced at a rate of

2-theta/min. Data were digitally recorded and peak matching with JCPDS database (as a source of reference data) was acquired using Jade software.

3.3.3 Mine Tailings Chemistry via Digestion and ICP-MS

The digestion process required here is different from that of the fly ash. A 0.22g (or slightly above) of dry tailing sample was weighed into an empty clean jar and 2ml of pure distilled water and 10ml 16Molar concentrated nitric (HNO_3) acid were added. A 1ml of bromine was pipetted into the mixture and heated to 100°C for 30 – 35 minutes. Then 5ml of deionized water was added to the heated sample after 40 minutes followed by the addition of 12Molar concentrated hydrochloric acid (HCl). The sample was then heated to 120 °C for another 30 minutes after which it was allowed to cool at room temperature and 50ml of deionized water was added. The samples were filtered using 0.45µm micropore membranes and the filtrate was mixed with 2%HNO_3 and analysed. The analysis was performed with an ELAN-DRC-II (ICP-MS, fig.3.2a) with ICP RF-power of 12kW, pulse stage volt of 1kV and 1.05L/min nebulizer gas flow rates. A Perkin Elmer Optima 5300DV dual view (ICP-OES, fig.3.2b) was used to compare and confirm ICP-MS results.

3.3.4 AMD Generation via Weathering - humidity Test Cell

Mine tailings as collected are used to generate AMD using a humidity test cell. The humidity test cell used was constructed of cylindrical Plexiglas with inside diameter of

12cm and 35cm long. It also consists of chambers that provided for air input and output openings. Approximately 1.5kg of mine tailings was filled into the cell at 50% degree of water saturation and was allowed to be seated on a perforated plate sitting at the base of the Plexiglas-column which was covered with geotextile filter with a grade 4 whatman filter paper for retention of solid residues while allowing the leachate to drain. Using the pressure and vacuum pump, dry air fluxes were passed into the column through the top of the cell for three days followed by switching into wet air (using humidifier) also for three days, all at room temperature. On the seventh day, 750ml deionised water with pH of 7.5 was used to soak the oxidized sample in the humidity cell for 3 – 4 hours before it was drained and collected in a 500ml capacity conical flask through the outlet chamber at the base of the column. The leachate was filtered through 0.45µm micropore membranes and was then taken for ICP-MS and ICP-OES to test for trace, minor and major. The weathering test on the tailings continues every week with 3 days of dry air cycle, 3 days of humid air cycle and effluent drainage at the 7^{th} day. Leachate collected from humidity test cell represented the required acid mine drainage (AMD) with pH ranges from 1.8 – 3.46 was each time taken to ICP-MS and ICP-OES for analysis.

Figure 3.7a: Humidity Test Cell

Figure 3.7b: Raw Acid Mine Drainge (AMD)

3.3.5 AMD Characterization (ICP-MS and ICP-OES)

The composition of various elements in the collected AMD water was analyzed using inductively coupled plasma atomic spectroscopy (ICP-MS, fig.3.2a) and Inductively Coupled Plasma-Optical Emission Spectroscopy (ICP-OES, fig.3.2b). These instruments analyzed the traced, minor, major and sulphate contents of the AMD. The filtered leachate from the weathering test was diluted with 2%HNO_3 and analyzed using ELAN-DRC-II (ICP-MS) with ICP RF- power of 12kW, pulse stage volt of 1kV and 1.05L/min nebulizer gas flow rates and Perkin Elmer Optima 5300DV dual view (ICP-OES).

3.3.6 AMD: FA Neutralization: (Neutralization reaction between FA: AMD)

Neutralization includes a laboratory scaled batch-wise experiment at room temperature using an open pyrex glass beaker. A 50mL of AMD was treated with different doses of each ash samples (ranges from 10g/L to 500g/L) followed by vigorous mixing using VWR-OS – 500 series shaker for 4 hours. A pH meter, OAKTON 2100 series was used to measure the pH and electrical conductivity (EC) of the mixture at a regular time interval of 30 minutes. After 4 hours of reaction, the mixture was allowed to settle and then filtered using 0.45µm micropore membranes and the clear filtrate analysed using ELAN-DRC-II (ICP-MS, fig.3.2a) and Perkin Elmer Optima 5300DV dual view (ICP-OES).

3.4 Zeolitization

Solid residue recovered from neutralization was dried in oven at 70°C (fig.3.8a) and milled/crushed to a fine powder of even particle to approximately 5µm grain size in readiness for the zeolite application. The particles were mixed with NaOH in the ratio of 1: 1.2 (SR: NaOH) and homogenized by grinding with an agate mortar and pestle then fused in an oven at 550°C – 600°C for 1 – 2 hrs. The fused product was then cooled at room temperature, grounded into a powder and then mixed thoroughly with distilled water. The slurry was aged for 9 – 12 hrs at room temperature with constant stirring. The aged slurry was allowed to nucleate and crystallize at a temperature range of 30 – 60°C for 72 hours (fig.3.8b). The crystals were filtered and washed with de-ionized water until pH of 10 – 11 was obtained after which it was dried in an economy oven series model

its crystallinity and mineralogy, MLA to determine its chemical composition, SEM technique for its morphological characteristics and its surface area determination using BET technique, some samples were sent to materials surface characterization laboratory, at the Chemical Engineering department, University of New Brunswick, Fredericton, Canada.

Zeolite synthesis steps:

i) Co-disposal solid residue dried in oven at 70 °C (degree Celsius).

NB: (HBP dose of 100g/l, and MAP dose of 250g/l) was used as the optimum amount of ash for zeolite synthesis.

Figure 3.8a: Co-disposal solid residue dried in oven at 70 °C

ii) Fusion of dried co-disposed solid residue with sodium hydroxide pellets in an oven at 550–600 °C for 1-2hrs, (HBP: NaOH ratio of 1: 1.2 and MAP : NaOH ratio of 1 : 1.5 %wt/wt).

iii) Milling to fine powder

iv) Mixing with de-ionized water at room temperature and aging for 12 hours.

v) Crystallization at 60 – 90 °C for 72 hrs.

Figure 3.8b: Crystallization at 30 – 60 °C for 72 hrs

vi) Filtration and washing at room temperature, then drying at 70 – 80 °C for 10 hrs

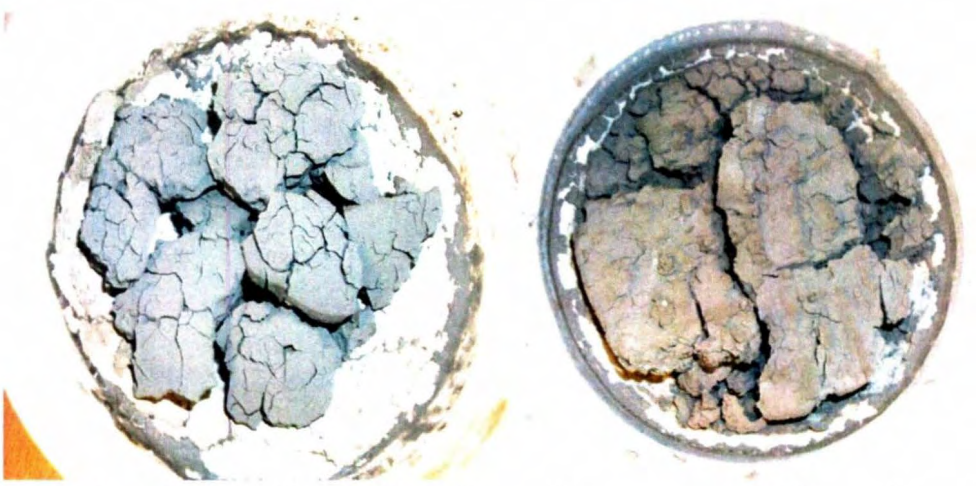

Figure 3.8c: Dried at 70 – 80 °C HBP sample **MAP sample**

These are the final products (synthesized zeolite) for each sample which later grounded into powder form.

Zeolite Characterization

3.4.1 Chemical composition

The chemical composition of the synthesized zeolite materials was determined using the same instrument and procedure as described in section 3.2.2.

3.4.2 Crystallinity and Mineral composition Using X-Ray Diffraction

Mineral phases and crystalline minerals of the synthesized zeolite samples were identified using XRD in a Rigaku Ultima-IV. The same procedure was also used as the one described in section 3.2.4.

3.4.3 Morphology: Scanning electron microscope (SEM)

The morphology and micro-structure of the zeolite samples were analyzed with FEI Quanta 400 scanning electron micro analyzer (SEM-EDX, fig.3.3d) operated with the typical accelerating voltage of 12kV. The sample preparation is the same as described in section 3.2.2 and the mounted samples analyzed using the same instrumental set up as stated above.

3.4.4 Surface area and Adsorption Isotherms

The Zeolite powder samples were sent to the same laboratory described earlier in section 3.2.8 for the specific surface area determination. The same procedures and instrumentals were also required as those described in the section stated.

3.4.5 Zeolite –AMD neutralization/Adsorptions

Neutralization/adsorption of AMD contaminants includes laboratory scaled batch-wise experiment conducted at room temperature using an open Pyrex glass beaker. 50mL of

AMD was reacted with 5g (equivalent to 100g/L) of HBP-Zeolite in one beaker and 10g (equivalent to 200g/L) of MAP-Zeolite in a separate beaker, followed by vigorous stirring for 4hours on VWR-OS-500 series shaker. The rest procedure is the same as described in section 3.3.6.

3.5 Permeate Reactive Barrier (PRB) Application

The setup consists of a laboratory scaled reactive column under continuous flow of the acid mine drainage water (AMD) through reactive barrier consisted of FA and silica sand (1:1 FA: Silica sand proportion, Ref. Fig. 3.9a).

Two column used were made up of 6.50cm inner diameter and 28cm long Plexiglas connected to each other. Each column has two openings (top and bottom) that allowed for inlet and outlet of liquid. Both ashes are strong alkaline in nature with pH greater than 11 and total percentage by weight of SiO_2 + Al_2O_3 + CaO greater than 60%. MLA and XRD techniques confirms the presence of cementing agent/material such as hydrated lime, quicklime, gypsum and clay in both samples therefore they are pozzolanic and possess cementitous properties. The samples were homogenized with silica sand in ratio 50% w/w to prevent clogging at some point in the experiment. The silica sand of size ranges of 20-30 mesh (0.60-0.84mm) and density of 1.40g/ml was used and the FA-silica sand mixture was placed in the middle section of each column in between 3cm pure silica sand layer at the top and 5cm silica sand layer at the bottom (fig.3.9a). Significance of this arrangement is to minimize or eliminate potential clogging and cementation problem during the later stages of the process.

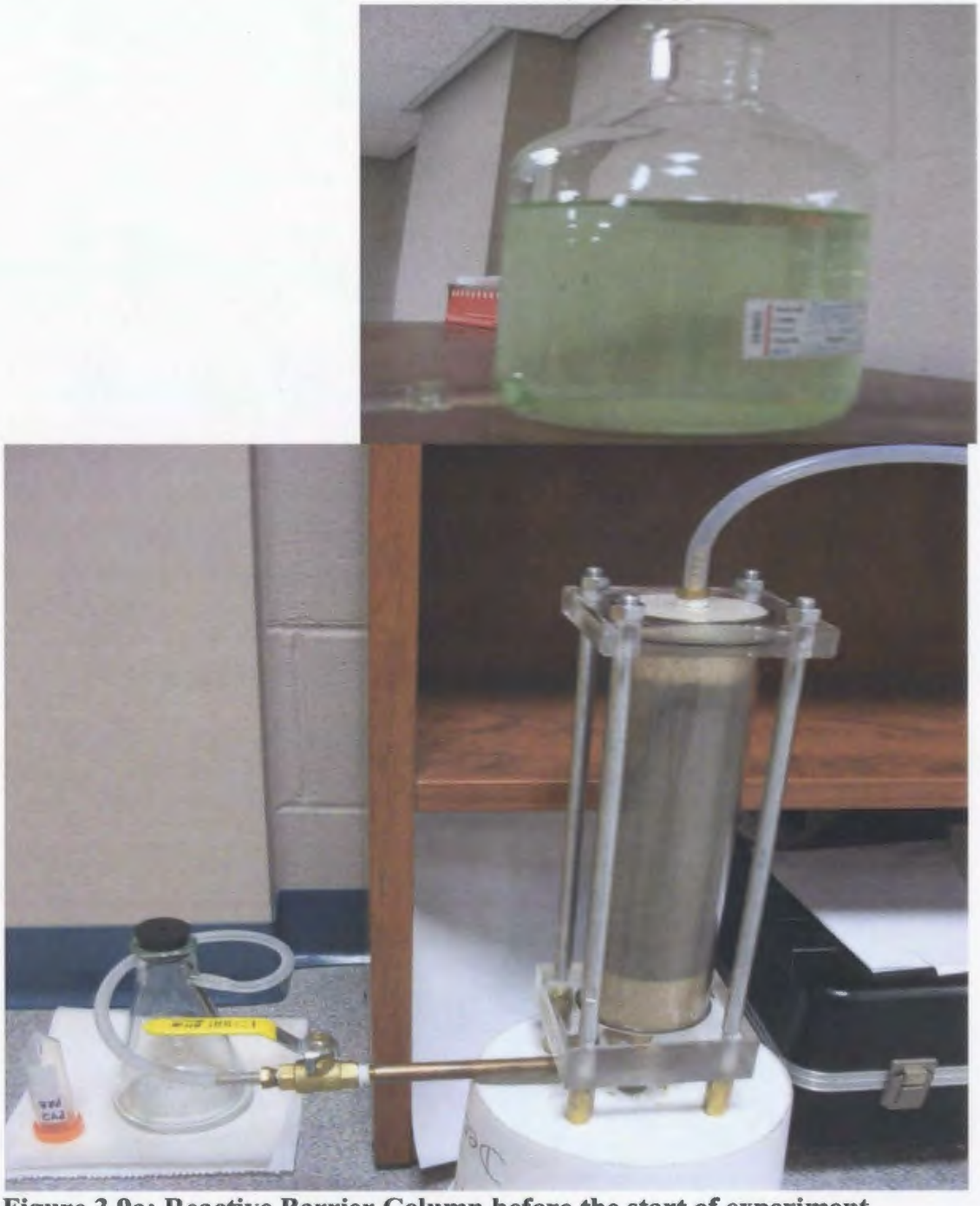

Figure 3.9a: Reactive Barrier Column before the start of experiment

Figure 3.9b: Reactive Barrier Column at the start of experiment

CHAPTER FOUR: PRESENTATION AND DISCUSSION OF RESULTS

4.1 Characteristics of Fly Ash

4.1.1 Trace, Minor and Major element

The metals analyzed are outlined in table 4.1. The most abundant metals present in both samples are silicon (Si), phosphorus (P), potassium (K), sodium (Na), calcium (Ca), iron (Fe), manganese (Mn), magnesium (Mg), aluminum (Al) and zinc (Zn). Additionally, metals such as copper (Cu), titanium (Ti), nickel (Ni), vanadium (V) and chromium (Cr) were present. Metals at trace levels include cobalt (Co), arsenic (As), molybdenum (Mo), selenium (Se), cadmium (Cd) as well as silver (Ag). mercury (Hg) was not detectable in the HBP sample and MAP-3 but trace quantities were measured in MAP-1 and MAP-2. Metals such as Ti, As, Mo, Se, Pb, Hg, Cd, and Ag not detectable by ICP-OES, therefore were analyzed using ICP-MS. Also metals like Si, P, Na and K were analyzed using SEM-EDX, this is due to the fact that the calibration reference used (JCFA-1) for other metals was not suitable for calibration of these (Si, P, Na and K) metals. There is little difference in concentrations among the grouped size fractions of the MAP samples analyzed except in the case of two metals (Na and K) with higher concentration in the two largest size fractions, MAP-2 and MAP-3.

Table 4.1: Elemental composition of the ash samples

Element	HBP	MAP-1	MAP-2	MAP-3
	mg/kg	mg/kg	mg/kg	mg/kg
Ca	153,767	139,244	127,822	145,550
V	281.99	82.92	84.72	66.86
Cr	51.47	69.48	82.61	68.52
Fe	17,767	30,297	36,355	26,194
Mn	6,952	8,449	6,931	8,556
Co	10.83	8.80	10.83	9.54
Ni	212.26	57.66	57.29	52.42
Cu	203.40	94.40	90.30	83.00
Zn	7,129	342.13	149.03	55.03
Al	12,526	28,130	41,958	103,905
Mg	61,689	42,450	41,408	10,152
Ti	777	2,047	2,685	1,748
As	31.76	4.04	2.18	1.61
Mo	27.45	6.07	4.49	5.21
Se	9.22	<RL	0.45	2.24
Pb	293.08	16.61	5.69	1.60
Hg	<RL	0.06	0.17	<RL
Cd	72.37	2.67	0.78	<RL
Ag	3.50	0.53	0.47	0.47
Si	131,000	47,400	127,000	90,700
P	56,000	12,600	-	19,100
Na	18,000	600	12,500	7,500
K	36,000	6,500	145,000	13,300

Abbreviations;
ICP-MS: Inductively Coupled Plasma-Mass Spectrometry
ICP-OES: Inductively Coupled Plasma-Optical Emission Spectroscopy
EDX: energy dispersive x-ray; MAP: mixed Ash Pond ash samples;
HBP-Hog boiler precipitate ash sample;
MAP-1: particle size range of <75µm to >125µm particle size;
MAP-2: particle size range of >180µm to>300µm particle size;
MAP-3: particle size range of >500µm and above particle size;
<RL: less than reportable limit

4.1.2 Chemical Composition of Fly ash

Table 4.2 summarizes the major chemical components of the two ashes as quantified by the MLA. Both samples contain typical components of fly ash such as lime (CaO), quartz (Si_2O), sodium oxide (Na_2O), potassium oxide (K_2O), magnesium oxide (MgO), alumina (Al_2O_3), iron oxide (Fe_2O_3), manganese oxide (MnO), phosphorus oxide (P_2O_5), and titanium oxide (Ti_2O). Quartz (Si_2O) is the predominant constituent of both samples with over 35% of total chemical composition. CaO and K_2O were also present in a considerable percentage (18-23%) which could account for the samples' strong alkalinity in solution. The Na_2O and MgO would also account for the samples alkalinity but are present in smaller percentage compared to CaO and K_2O. Smaller quantities of P_2O_5, Al_2O_3, and Fe_2O_3 were also detected with traces of Ti_2O and MnO in both samples. Hence, both samples can be classified as class C ash grade in accordance with ASTM C618 as CaO is in the range of (17 – 32wt%) and Si_2O is in the range of (25 – 42wt%). Class C FA is self-cementing and does not require alkaline activator in cement application making it an option for concrete and cement applications. It is also important to note that these samples provide a rich source of SiO_2, CaO, and Al_2O_3 which are important feedstock for zeolite synthesis. The ratio of SiO_2 to Al_2O_3 is higher than 1.5 in both ashes which is ideal for zeolite.

Table 4.2: Major chemical component of the Ash sample

Major component	HBP	MAP-1	MAP-2	MAP-3
Si_2O	37.05	36.36	36.45	36.97
CaO	18.57	20.01	19.19	17.84
K_2O	22.13	22.44	22.87	23.53
Al_2O_3	4.97	4.71	5.82	6.27
MgO	6.22	5.84	6.37	6.62
P_2O_5	8.30	7.71	6.64	6.01
Fe_2O_3	1.54	1.87	1.64	1.76
Na_2O	1.04	0.84	0.92	0.88
MnO	0.01	0.04	0.02	0.02
TiO_2	0.17	0.20	0.09	0.09
LOI*	4.56	12.47	3.32	2.01

LOI*: Loss on ignition

4.1.3 Significance of the Chemical Content of Ash

The adsorption and/or neutralization capability of fly ash is mainly attributed to presence of chemical species such as SiO_2, Al_2O_3, Na_2CO_3, $CaCO_3$ and CaO (Somerset et al., 2004). Neutralization of AMD using FA occurs through dissolution of CaO, Na_2O, K_2O and MgO in the FA to the AMD thereby increasing the pH of the solution. In addition, contaminants such as metals are adsorbed on to the FA. These chemical species (CaO, Na_2O, K_2O, SiO_2, Al_2O_3 and MgO) were equally present in the analyzed FAs in quantities applicable for AMD treatment and PBR application.

SiO_2 and Al_2O_3 are key constituents when forming zeolite via the hydrothermal process. The sodium ions (Keka et al., 2004) form sodium aluminum silicate hydrate ($Na_2Al_2SiO_6.H_2O$) during the hydrothermal process. The ratio SiO_2/Al_2O_3 of the sample

is crucial to zeolite synthesis and its performance as an adsorbent (Rios et al., 2008 and Keka et al., 2004), generally a low SiO_2/Al_2O_3 ratio results in a hydrophilic zeolite, while zeolite with high SiO_2/Al_2O_3 ratio (high silica zeolite; $SiO_2/Al_2O_3 > 2$) will tend to be hydrophobic and organophillic (Rios et al., 2008). The analyzed FA samples contain SiO_2 and Al_2O_3 in a suitable ratio for zeolite synthesis (SiO_2/ Al_2O_3 = 6.0 to 7.7). since the minimum ratio that would favors the formation of faujasite zeolite is SiO_2/Al_2O_3 ratio of 1.5 (Gitari et al., 2005) .

The total concentration of SiO_2, Al_2O_3 and Fe_2O_3 and the alkaline content (Na_2CO_3, $CaCO_3$, CaO, Na_2O, K_2O and MgO) are also important parameters for use as a PRB. Hydrated aluminum-silicate minerals from soluble salts of silicate and aluminates immobilize the contaminants from AMD or contaminated water (Claudia et al, 2009). Heavy metals are retained by oxides and oxy-hydroxides of Al, Fe, Mn, lime, and clay minerals (Antonio and Ayuso, 2008), prior to their subsequent oxidation, neutralization and/or biodegradation. The FA in this study has the total of SiO_2, Al_2O_3 and Fe_2O_3 and the alkaline content (Na_2CO_3, $CaCO_3$, CaO, Na_2O, K_2O and MgO) in the range of 90% and above therefore confirms its suitability for PRB.

4.1.4 Morphology

SEM micrographs examination (fig.4.1a - f) show both samples are similar to published data (Sarkar et al., 2010; Zhou and Haynes, 2010; and Min et al., 2004) The FAs are composed mostly of irregular-shaped amorphous particles with few spherical (micro-

spheres/cenospheres) crystals interspersed between the amorphous phases. There are also amorphous aluminum-silicate glasses with large irregular-shaped and porous carbon particles. Figure 4.1 a, b and c shows that the HBP ash sample contains macro-porous carbon material, amorphous glass, and cenospheres. However, the MAP samples are mostly amorphous phases with elongated or sand-like porous carbon material having dense siliceous particles as shown in figure 4.1(d – f). This type morphology has been reported to impact its leaching behaviour. For instance, for samples with non-porous continuous outer surface and heavy (dense) particle, the leaching of heavy metals may be prevented due to non-permeability particulate nature (Min et al., 2004).

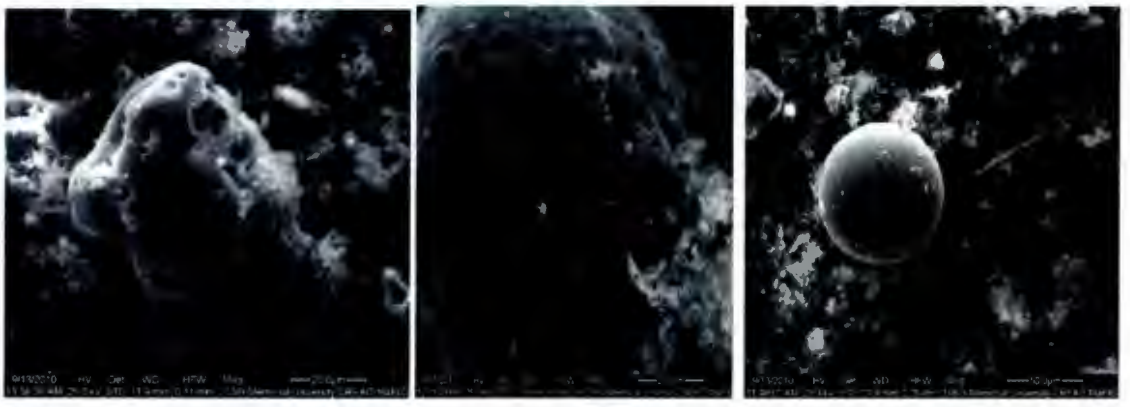

Figure 4.1a **4.1b** **4.1c**

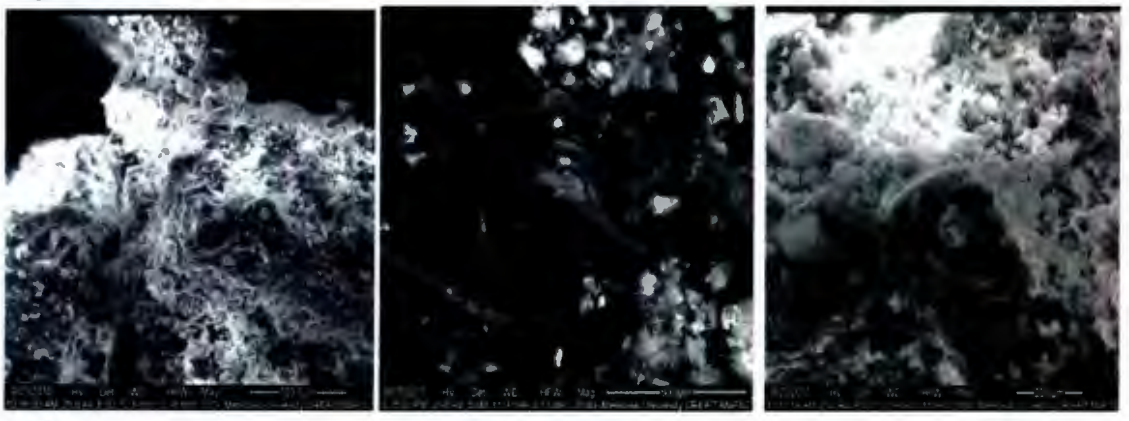

4.1d **4.1e** **4.1f**

Figure 4.1(a-f): Morphological structure of FA particles with SEM.

The presence of porous and carbon materials in the samples indicate that the FAs will be good candidates for adsorption and PRB (with good porosity and permeability).

4.1.5 Amorphous, Crystalline and Mineralogical composition of Fly ash

The X-ray pattern of the ash is shown in figure 4.2. The quantity of different compounds identified by XRD was estimated through the height of the corresponding diffractograms peaks. The peak intensities (count values) suggest the presence of some crystalline mineral phases which are possibly product of combustion. However, the high background intensity in the diffractograms (humps in the region 2θ = 10 – 50°) also indicates a significant fraction of amorphous (glass-like) phases, carbon, and other non glass amorphous minerals. The X-ray diffractograms of the HBP sample shows strong peak intensity for quartz, lime, potassium phosphate, magnesium – copper oxide minerals, and gehlenite while haematite and gypsum are also present in much smaller amounts. In addition to quartz, lime and gypsum the MAP sample also shows strong peaks for calcite but lower peak intensities for haematite, arnorthite, and gehlenite. Traces of other minerals were also recorded with smaller peak intensities as shown in figure 4.2 such as pyrite, rutile, illite, feldspar, ettringite, albite, anhydrite and clay.

The XRD mineral analysis table (table 4.3) corroborates this result showing quartz, lime, calcite and alumino-silicate glass as the major mineral phases. It is important to note that the mineral compounds determined by the XRD analysis are also in good agreement with

MLA analysis as both techniques indicated quartz, lime, and potassium compounds as the major mineral phases of the samples. Furthermore, substantial amounts of glassy materials were recorded for each sample and also each ash contains two or more of the four major crystalline phases.

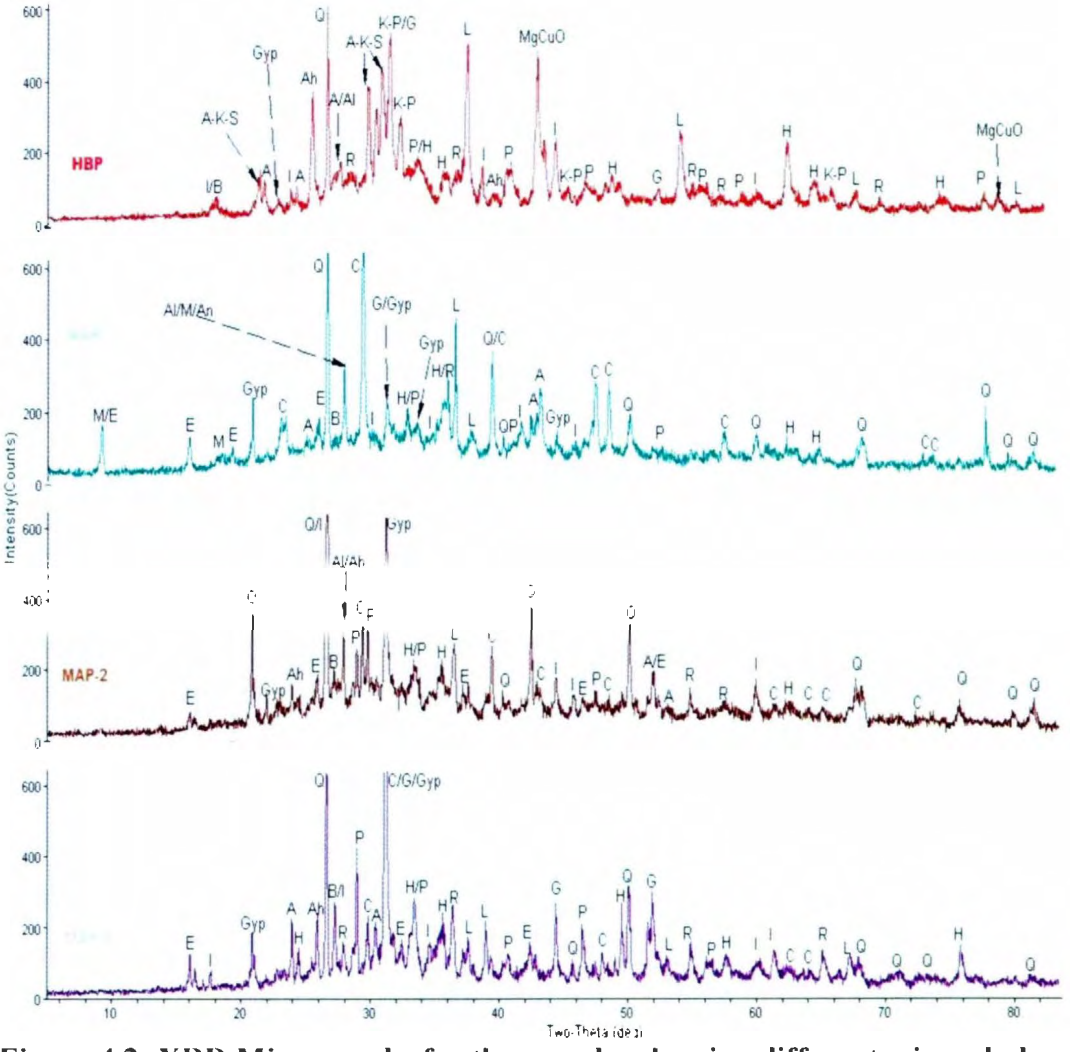

Figure 4.2: XRD Micrographs for the samples showing different mineral phases for all the samples.

Q-Quartz; L-Lime; C-Calcite; P-Pyrite; R-Rutile; I-Illite; H-Haematite; G-Gehlenite; Gyp-Gypsum; Al-Albite; Ah-Anhydrite; E-Ettringite; MgCuO- Magnesium Copper-Oxide; K-P –Potassium phosphate; B-Beidellite; A-Arnorthite; A-K-S – Ammonium-potassium-Sulphate; M-Montmorillonite

Table 4.3: XRD Mineral analysis of ash samples

Mineral	HBP	MAP-1	MAP-2	MAP-3
Alumino-Silicate glass	+	+	+	+
Quartz (SiO_2)	+	+	+	+
Lime (CaO)	+	+	+	+
Calcite ($CaCO_3$)	+	+	+	+
Haematite (FeO_3)	-	-	-	-
Feldspar	-	-	-	-
Rutile (TiO_2)	-	-	-	-
Pyrite (FeS_2)	-	-	-	-
Gypsum (CaSO4.2H2O)	-	-	-	-
Anhydrite($CaO7SrO_3SO_4$)	-	-	-	-
Ettringite ($Ca_6Al_2(SO_4)_3$ -	-	-	-	-
(OH)12.26H2O)	-	-	-	-
Gehlenite ($Ca_2Al_2SiO_7$)	-	-	-	-
Clay	-	-	-	-

+ Major phase, - Minor phase

4.1.6 Important of Minerals in FA

Most of the minerals identified by the XRD are either source materials for zeolite synthesis, adsorption applications, and/or PRB. For instance the amorphous alumina-silicate and ettringite are the complex form of calcium-aluminum-silicate compounds and these compounds are the reactive portion of FA important for zeolite/adsorption applications (Claudia et al., 2009). Calcium-aluminum silicate-hydrate ($Ca_2(Si_9Al_3)O_{24}.8H_2O$) is the major zeolitic material in most adsorption applications especially SO_2 removal from gas streams (Papandedreou et al., 2007 and Moutsatsou et al., 2006). In addition, the presence of transition metals (such as Co, Ni, Cu, Cr, Ag, and V) in conjunction with aluminum, calcium, magnesium, silicon and iron enhance the

adsorptive properties (Papandedreou et al., 2007 and Moutsatsou et al., 2006). In comparison with previous research, the mineral composition present in the samples was in ranges for zeolite, adsorption, and neutralization applications (Papandedreou et al., 2007 and Moutsatsou et al., 2006). Table 4.4 below compares the FA mineral composition with investigated FAs in the literature.

Table 4.4: Mineral composition Comparison between Characterized FA and Literature

Mineral	Zhou and Hynes (2010)	HBP	MAP-1	MAP-2	MAP-3
Alumino-Silicate glass	+		+	+	+
Quartz (SiO_2)	+	+	+	+	+
Lime (CaO)	+	+	+	+	+
Calcite ($CaCO_3$)	+	+	+	+	+
Haematite (FeO_3)	+	-	-	-	-
Feldspar	-	-	-	-	-
Rutile (TiO_2)	N/A	-	-	-	-
Pyrite (FeS_2)	N/A	-	-	-	-
Gypsum (CaSO4.2H2O)	-	-	-	-	-
Anhydrite($CaO7SrO_3SO_4$)	-	-	-	-	-
Ettringite ($Ca_6Al_2(SO_4)_3$ - (OH)12.26H2O)	N/A	-	-	-	-
Gehlenite ($Ca_2Al_2SiO_7$)	-	-	-	-	-
Mullite	-	N/A	N/A	N/A	N/A
Arorthite	-	N/A	N/A	N/A	N/A

+ Major phase, - Minor phase N/A- not applicable

4.1.7 Surface area and pore volume

Nitrogen adsorption-desorption isotherms for the ash samples are shown in figure 4.3(a-d). The HBP ash showed type II isotherm in the Brunauer classification (Pierre et al., 2004) which represents the normal form of nonporous or macro-porous adsorbent

isotherm. It is a form that obtained from unrestricted monolayer-multilayer adsorption and suggests particulate material with its pores and void communicating with its surface (Pierre et al., 2004). However, the MAP samples 1, 2, and 3 do not show the same structure, instead a well defined adsorption-desorption hysteresis (fig.4.3 b, c & d) was present. The hysteresis represents the points where, at a given relative pressure, the volume of gas absorbed is not equal to the volume desorbed during the adsorption-desorption (Pierre et al., 2004) and its implication is accumulation or build up in the pores with time. This behaviour is attributed to capillary condensation taking place in the elongated mesopores (narrow walls) and it occurs when the nitrogen multilayer begins to behave like normal liquid and fill the voids (pores) of the material (Paya et al., 2002). Another characteristic of the samples that may be responsible for the hysteresis is complex pore networks and interconnectivity of tiny and larger pores. The textural properties of the samples were computed (as shown in table 4.4). The calculated area for the samples is between $1.06 \times 10^4 - 4.65 \times 10^5$ cm^2/g which falls within published ranges for fly ash, meanwhile the specific area of the samples can be increased reasonably by steam or hydrothermal treatment.

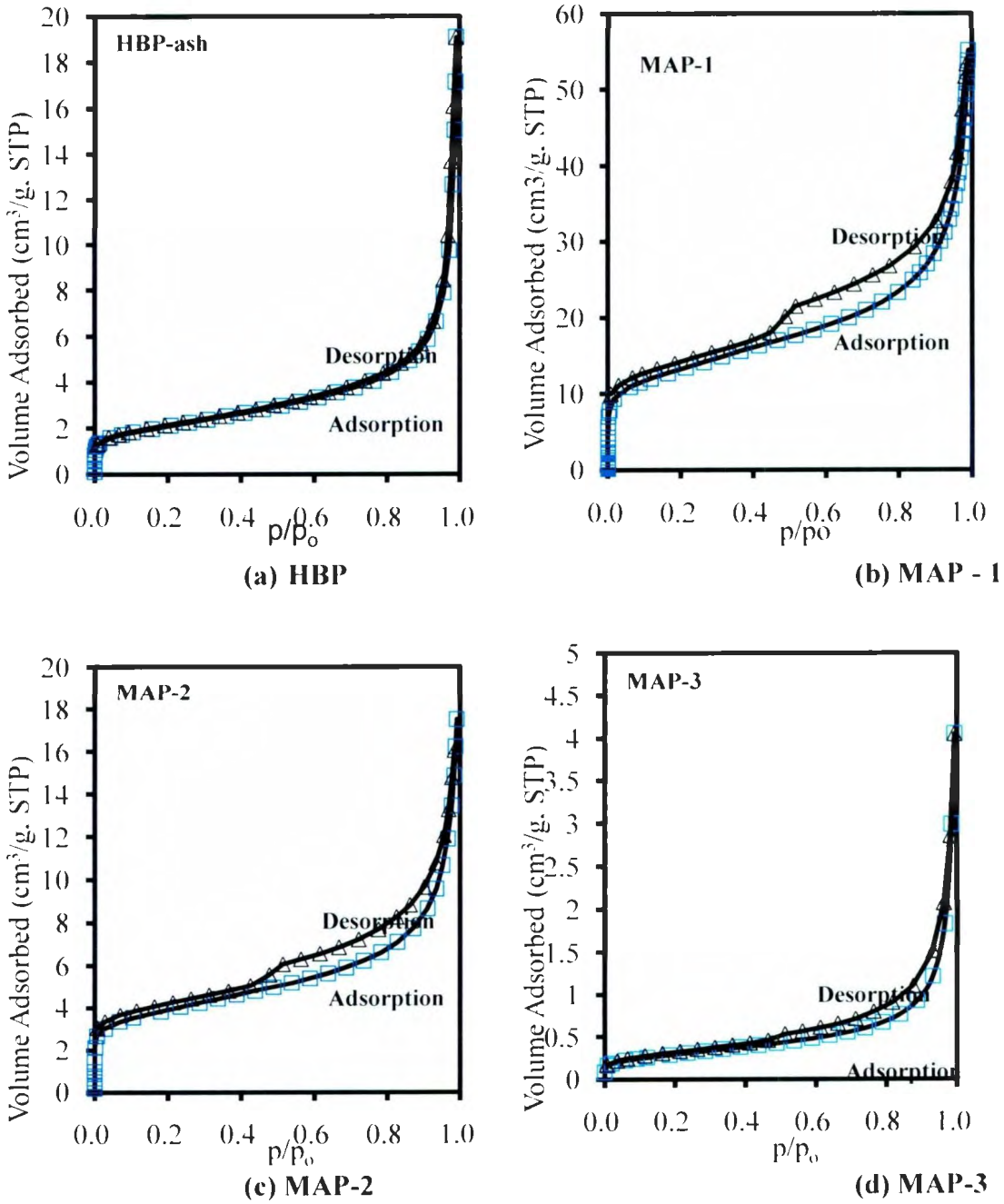

Figure 4.3(a-d): Volume of gas (at STP) sorbed during N_2 adsorption and desorption at 77K vs.

Relative pressure P/P_0 for HBP, MAP-1, MAP-2 and MAP-3 ash samples, with all sample particle size range of 7µm to 125µm

Table 4.5 : Textural properties of ash samples.

Sample	S_{BET} (cm^2/g)	Total pore volume, V_t from P/P_o=0.99 (cm^3/g)
HBP	7.41×10^{-4}	0.029
MAP-1	4.65×10^{-5}	0.085
MAP-2	1.36×10^{-5}	0.027
MAP-3	1.06×10^{-4}	0.005

The MAP-3 sample is predominantly large and dense non porous particle therefore has an overall lower pore volume.

4.1.8 Thermal properties of Fly ash

A series of step-wise thermogravimetric analysis under reactive/inert atmospheres was used to determine the samples' thermal properties as described in section 3.2.6. The total loss on ignition (LOI) observed with HBP sample was approximately 5% and MAP sample with LOI value ranges from 2 – 12% as shown in table 4.5 and its effect on adsorption capacity is explained in section 4.1.9.

Loss of moisture occurred between 35-100°C under an inert atmosphere as shown in figure 4.4a and represented by P1 on the temperature-weight loss profile. Dehydration of hydrated lime started afterwards up to around 400-450°C. The major decomposition of the sample was observed at temperature range of 350 °C to 800 °C. This decomposition represents dehydration, carbonate decomposition and carbon reactivity (carbon oxidation due to reduction of iron under inert condition and carbon oxidation in reactive atmosphere) (Paya et al., 2002 and 1998). Holding the system temperature isothermally at

100 °C for 15 minutes removes all moisture content and reactive oxygen from the samples as described in section 3.2.6. Heating from 100°C to 1000°C in inert atmosphere (N2) at 75mL/min and 20°C/min results in the following proposed reactions (Paya et al., 1998):

$$XCa(OH)_2 \rightarrow (heat) \rightarrow CaO + XH_2O \ (400\text{-}450^oC) \quad (4.1)$$

$$XMg(OH)_2 \rightarrow (heat) \rightarrow MgO + XH_2O \ (400\text{-}450^oC) \quad (4.2)$$

$$XCa(Si_9Al_3)O_{24}.8H_2O_7 \rightarrow (heat) \rightarrow XCa(Si_9Al_3)O_{24} + 8XH_2O_7 \ (400\text{-}500^oC), \quad (4.3)$$

Equations 4.1 to 4.3 above represent dehydration of hydrated lime.

$$CaCO_3 \rightarrow (heat) \rightarrow CaO + CO_2 \ (700\text{-}800^oC) \quad (4.4)$$

$$MgCO_3 \rightarrow (heat) \rightarrow MgO + CO_2 \ (700\text{-}800^oC) \quad (4.5)$$

Equations 4.4 and 4.5 represents Carbonate decomposition

$$Fe_xO_y + C \rightarrow (heat) \rightarrow Fe_xO_{y-1} + CO \ (700\text{-}1000^oC) \quad (4.6)$$

$$Al_xO_y + C \rightarrow (heat) \rightarrow Al_xO_{y-1} + CO \ (700\text{-}1000^oC). \quad (4.7)$$

$$Fe_2O_3 + C \rightarrow (heat) \rightarrow Fe_2O_2 + CO \quad (4.8)$$

Equation 4.8 represents typical carbon oxidation due to reduction of iron under inert condition

To determine the remaining organic carbon, samples were cooled from 1000°C to 100°C with 20°C /min cooling rate under N_2 at 75mL/min flow rate. The samples were then heated from 100-1000°C at a heating rate of 20°C /min in air at 75mL/min flow rate. The remaining inorganic carbon is oxidized (a reaction which is exothermic) in the ash with general chemical reaction shown below:

It is important to note that dehydration and decomposition of other complex hydrated minerals and some other slag formed during fuel combustion also accompanied the process but are insignificant and occurs simultaneously with other major decomposition in the temperature range of 380-850°C.

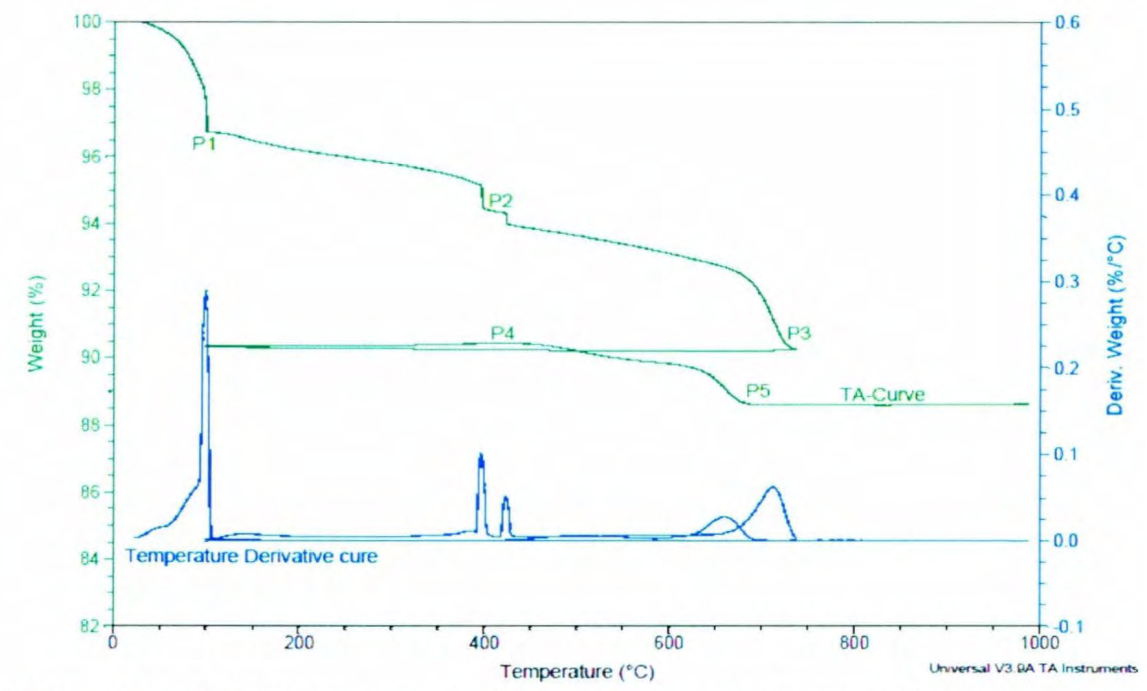

Figure 4.4a: TGA Thermogravimetric curve showing decomposition (%wt. change) of the ash sample with temperature and temperature derivative curve.

Abbreviations: P1: Loss of Moisture content at 30-100°C (under N_2 atmosphere)

P2: Dehydration of hydrated lime at 400°C (under N_2 atmosphere)

P3: Carbonate decomposition and reduction of iron by carbon oxidation at 700-800°C (under N_2 atmosphere)

P4: Oxidation of metals (insignificant amount) into metallic oxides at 350-450 (under pure O_2 atmosphere)

P5: Oxidation of organic carbon into CO_2 at 450-700 (under pure O_2 atmosphere)

To verify the inorganic carbon an alternative process was used by acid treatment (as described in section 3.2.6) prior to TGA analysis. In this procedure decomposition approximates loss of moisture content, dehydration of hydrated limes under inert (N_2) atmosphere and organic carbon oxidation under reactive (O_2) atmosphere. The estimated TOC values with this technique were in good agreement with the EDT technique (table 4.5). Figure 4.4c shows the temperature-weight loss profile for the analysis and table 4.5 compared values of TOC for both TGA and EDT technique.

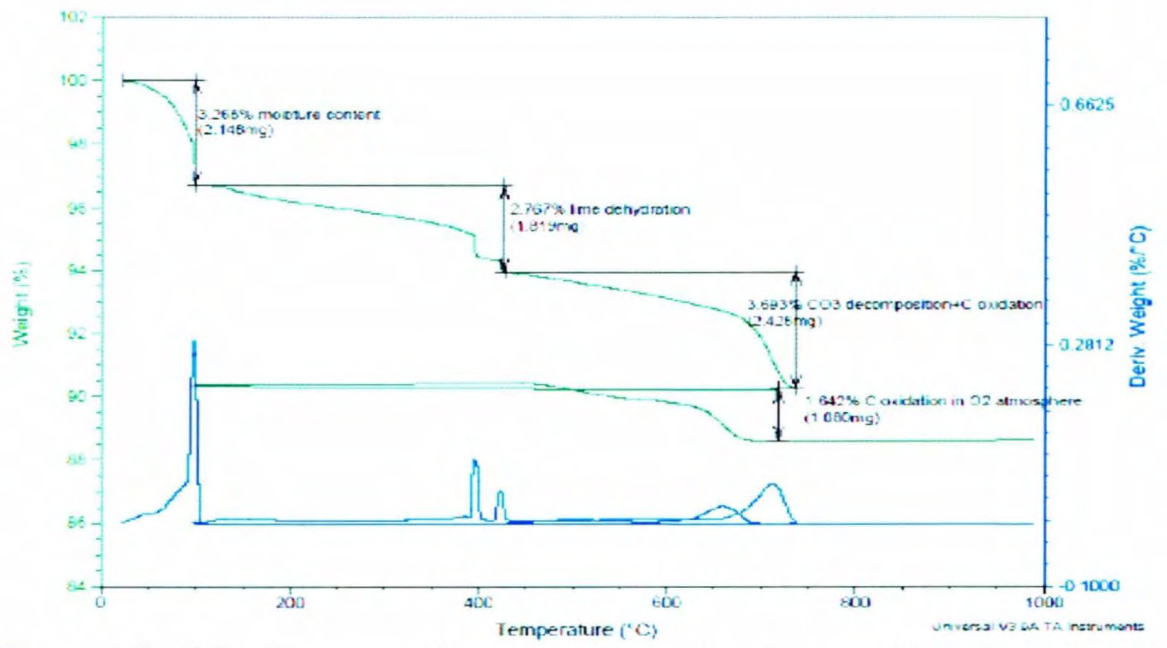

Figure 4.4b: TGA Thermogravimetric curve showing decomposition (%wt.change) of the ash sample with temperature and temperature derivative curve.

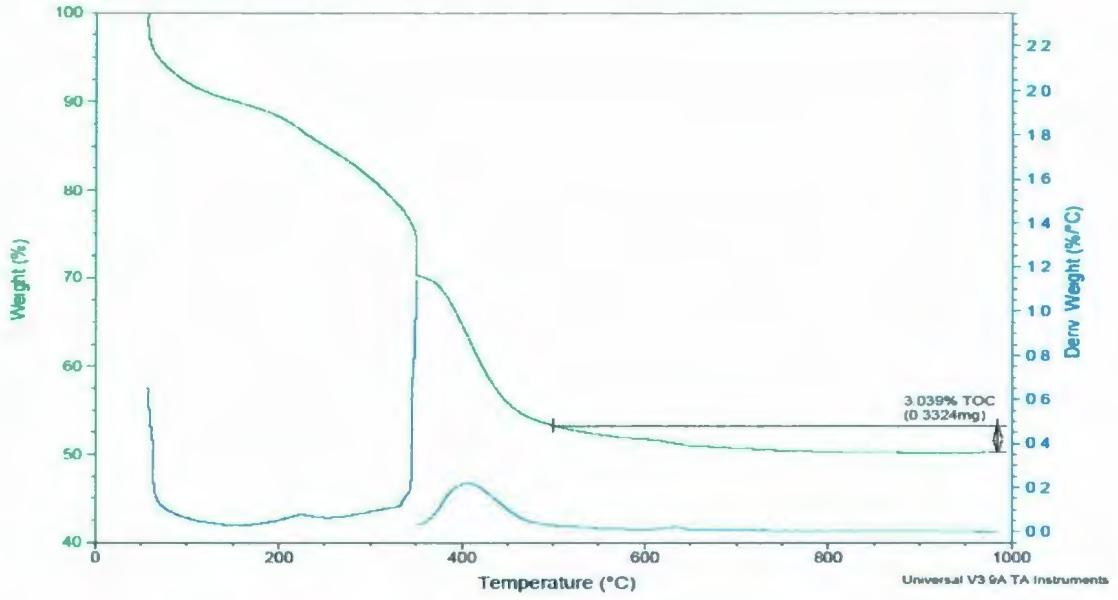

Figure 4.4c: TGA Thermogravimetric curve showing decomposition (%wt change) of the acidified sample with temperature and temperature derivative curve.

Table 4.6: Total Carbon and Total Organic Carbon (TOC) Determination using EDT and TGA

Total Carbon and Total Organic Carbon Determination				
Sample ID	Mean % Total Carbon by EDT	% inorganic carbon by EDT	% Free organic carbon by EDT	% Free organic carbon by TGA
HBP	3.08	1.43	1.65	1.86
MAP-1	9.54	5.71	3.83	3.04
MAP-2	2.56	1.46	1.19	1.28
MAP-3	0.11	0.05	0.06	0.11

4.1.9 Surface Area, Free Carbon Content and Adsorptive Property of the Samples

Generally, the larger the surface area of an adsorbent material, the larger the adsorption capacity of the material. The surface area of an adsorbent depends on the textural properties and surface area to volume ratio of a material. Therefore the TOC content

determines in part the adsorptive capacity of a material. The free organic carbon materials of the FAs are the porous fraction. The total organic carbon content (TOC) in the MAP-1 FA is approximately 3.83%. MAP-1 FA has the highest percentage of free organic carbon among all the analyzed FAs and therefore has the largest pore volume ($0.085cm^3/g$) and largest surface area (4.65×10^5 cm^2/g) as shown in table 4.4. The percent free organic carbon contents recorded by HPB and MAP-2 FAs are almost equal (table 4.4) therefore the values of surface area and pore volume recorded by both FAs are also very close (table 4.5). MAP-3 has the lowest percent of free organic carbon and the lowest pore volumes and surface area. The difference between the EDT estimated MAP-3 free organic carbon and the TGA estimated value could be that the EDT technique is less accurate for smaller value of free organic carbon. The surface area of the analyzed FAs are within the published values in a study by Davini (1996). In Davini's study for SO_2 adsorption surface areas showing good absorption were in the range of $1 \times 10^4 - 3 \times 10^5$ cm^2/g while similar work by Teong et al., (2003) varied from $1.89 \times 10^5 - 8.64 \times 10^5$ cm^2/g.

4.1.10 Other physcio-chemical characteristics

Table 4.6 outlines the pH and buffering capacity of the FAs. The pH values range from 10.54 to 13.08 or strongly basic. The total lime (CaO) and potassium oxide (K_2O) content is approximately 45wt% as shown in the table 4.2 and contributes to the FAs high pH. Small percentage of MgO and Na_2O might also contribute to the samples alkalinity making an approximate 50wt% total (CaO, K_2O, MgO and Na_2O) content.

The HBP sample has a higher buffering capacity at 4.9 mmol/unit-pH than the MAP sample at 0.5-0.6 mmol/unit-pH. The buffering capacity is defined as the amount of acid or base required to change the pH of one molar solution by one unit, the higher the buffering capacity, the better the material is able to absorb very low or very high pH solutions without an appreciable change in the pH of the material. Hence, HBP FA has a better neutralization capacity than the MAP FA. The differences in how the HBP and MAP are handled at the pulp and paper plant may explain the large difference in buffering capacity. The HBP is precipitated from the effluent gas stream while the MAP ash sample is flushed with high pressure water stream through the sluiceway; therefore some of the soluble alkaline content of MAP FA may have been lost into the water stream prior to its collection. This could also explain the small gap between the pH values between the two types. Nevertheless, the pH values of both samples makes them good alkaline materials for neutralization of an acid, and for pH control of contaminants in solution.

Table 4.7: pH and Buffering power of ash samples

Sample	pH	Buffering Power (mmol/pH units)
HBP	13.08	4.90
MAP-1	10.54	0.50
MAP-2	11.38	0.60
MAP-3	11.51	0.50

Table 4.8 below outlines the density and porosity of the samples. The HPB densities are low on both a dry and wet basis which portrays its true nature (light weight ash/fly ash). Hollow particles such as cenospheres or plerospheres including carbon particulate matters

might be present in HBP resulting in the low density. The MAP-1 sample was slightly higher in density. Again, this could be a result of the high carbon as both samples (HBP and MAP-1) had higher carbon percentage (table 4.5). MAP-2 and MAP-3 samples are denser than the former two samples. There is less porous and carbonaceous matter (table 4.5) in these two samples.

Table 4.8: physical properties of the Ash samples

		Density (g/Cm^3)		
Sample	porosity %	Density Dry basis (g/cm^3)	Density Wet basis (g/cm^3)	True Density (g/cm^3)
HBP	75	1.13	0.27	1.41
MAP-1	67	1.28	0.97	2.00
MAP-2	67	1.76	1.59	2.04
MAP-3	30	2.33	2.10	2.43

4.2 Mine tailings Characterization Results

4.2.1 Chemistry and elemental composition

Table 4.9 summarizes the analysis of the mine tailings collected from a VALE mine site. Major, trace, and minor metals are present. Iron (Fe) and sulphate (SO_4) are the dominant species which is not unexpected as the mines process iron sulphide ores.

Table 4.9: Mine Tailing Elemental Composition

Element	Mine Tailing (mg/kg)
Fe	514,156
SO_4	273,160
Ca	8,584
Ni	3,211
Al	2,311
Ti	1,834
Mn	711
Cu	682.20
Br	202.80
Zn	167.92
Co	92.06
Se	82.29
V	69.30
Cr	69.19
Pb	12.71
Mo	3.48
As	2.12
Ag	1.56
Cd	0.86
Hg	Below detection limits

4.2.2 Crystalline, amorphous and Mineralogical properties

The mine tailing is characterized by strong crystalline mineral peaks and very weak amorphous background peaks. Minerals detected at high levels included (Appendix A) pyrrhotite ($Fe_{1-x}S$), pyrite (FeS_2), magnetite (Fe_3O_4), chromium manganese sulphide ($(Cr_{0.77}Mn_{0.99})S$), titanium sodium hydrogen phosphate hydrate ($TiHNa(PO_4)_2.2H_2O$), tetrascandium hexachloride nitride (Sc_4Cl_6N) and boron iron terbium silicon ($(B_5Fe_{70}Si_2Tb_8)_{0.024}$ with small quantity of silicon aluminum compound ($Sr_4Cs_{1.1}(Al_{12}Si_{36}O_{96})$). The high levels of metals and sulphur result in a tailings effluent with a low pH (AMD) which in turn will result in precipitation of metals.

4.3 AMD Generation and Treatment with FA

4.3.1 Chemistry of Generated AMD Water

As outlined in chapter 3, the tailings were placed in humidity cells and the leachate (AMD) collected for analysis and treatment. Table 4.9 outlines the chemistry of the AMD. Figure 4.6 outlines the pH of the AMD collected over eight weeks which varied from 1.8 to 3.5. The pH trend showed in the figure 4.6 below indicates that the AMD increases in acidity in the first three weeks and strongly acidic AMD solution was generated in the fourth week. There was increase in the pH in the fifth week and stables at pH of approximately 2.5 afterwards. The metal ions and acidic nature of AMD represent important environmental hazards to freshwater resources and aquatic ecosystem. Sulphate ions is the major anion in the analyzed AMD ranged from 8,729 mg L to 38,202 mg L while Fe^{2+} is the dominant cation with concentrations ranging from 3,300 mg L to 181,00 mg L.

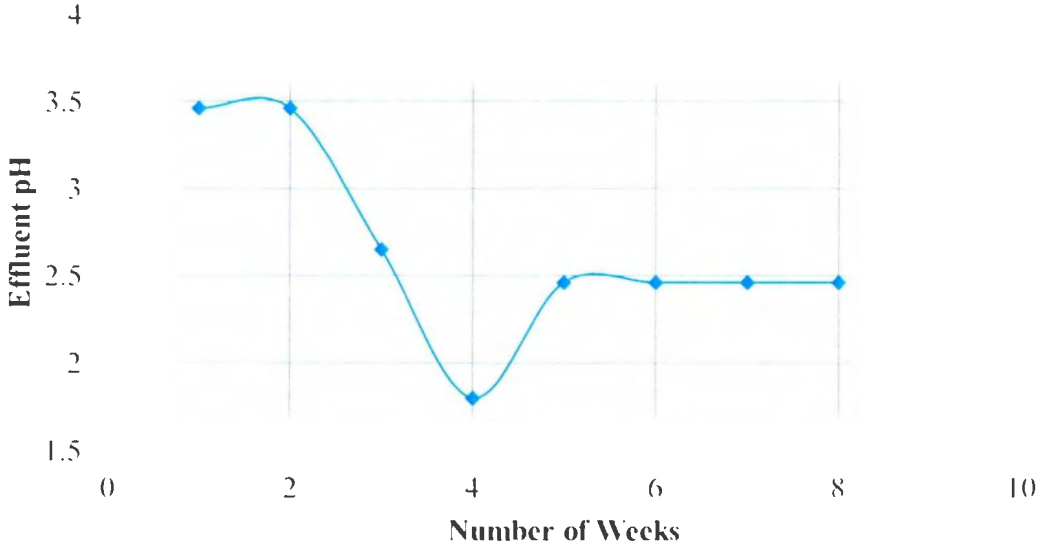

Figure 4.6: Effluent (AMD) pH profiles

Table 4.10: Chemistry and pH of AMD generated for the first 4 weeks

Metals (mg/L)	AMD 1st week	AMD 2nd week	AMD 3rd week	AMD 4th week
SO_4^{2}(mg/L)	8,729	10,922	31,771	38,202
Fe(mg/L)	3,683	4,853	3,294	18,058
Ca (mg/L)	995	951	798	761
Ni(mg/L)	513.66	492	465	1,618
Mg (mg/L)	277	199	697	544
Mn(mg/L)	41.12	40.98	36.86	104.50
Co(mg/L)	8.53	8.36	7.62	350
Cu(mg/L)	0.40	0.92	0.93	0.09
Cd(mg/L)	0.24	0.15	0.07	<RL
As(mg/L)	0.03	<RL	0.08	<RL
Zn(mg/L)	<RL	1.46	0.11	2.80
Mo(mg/L)	<R L	0.09	<RL	0.11
Hg(mg/L)	<RL	0.15	0.04	0.22
Pb(mg/L)	<RL	0.05	0.01	0.10
Final pH	3.46	3.46	2.65	1.80

NB: This research is limited to characterizing and using of the generated AMD to simulate the adsorption properties/profiles of specific materials (FA) and **not for long period kinetic/static test for weathering simulation** on mine tailing which usually takes minimum period of 25-40 weeks.

4.3.2 AMD: FA Neutralization Result

The elemental analysis of neutralized (treated) and raw (untreated) AMD is presented in table 4.11. The amount of major contaminants removed increases with increasing FA concentration. The final change in pH as a function of time of the mixtures is outlined in figure 4.7. The immobilization of contaminants from the AMD is a complex process which could comprises of adsorption, ion exchange, precipitation and co-precipitation of metal hydroxide complexes on active sites of the sorbent (FA/Zeolite).

Table 4.11: Chemistry of FA: AMD Neutralization outlet process Water

MAP ASH	AMD B4	M N10	M N30	M N 50	M N100	M N250	M N500
Ash doses(g\l)	0	10	30	50	100	250	500
Mg	199	516	710.	924	1,154	870	675
SO_4	10,922	7,128	5,277	6,426	12,192	7,736	5843
Ca 43	951	1,081	1,587	1,391	1,365	1,262	1,073
Fe 54	4,853	1,487	1.59	0.20	23.94	1.78	8.90
Mn	40.98	110.80	126.60	71.20	18.99	4.49	6.62
Co	8.36	7.63	1.40	0.01	0.11	0.05	0.09
Ni	492	377	126	11.82	1.77	0.77	3.78
Cu	0.92	0.45	0.024	0.12	1.10	1.18	1.07
Zn	1.46	17.09	0.30	0.28	1.75	0.45	0.28
Mo	0.09	0.09	0.09	0.09	0.10	0.18	0.19
Hg	0.15	0.09	0.08	0.08	0.12	0.08	0.08
Pb	0.05	0.05	0.04	0.04	0.05	0.05	0.05
HBP ASH	AMD B4	H N10	H N30	H N50	H N100	H N250	H N500
Ash doses(g\l)	0	10	30	50	100	250	500
Mg	199	523	610	195	2.00	1.00	30.00
SO_4	10,922	9,463	6,584	6,428	8,820	8,854	10,536
Ca 43	951	737	638	667	692	678	780
Fe 54	4853	1,244	3.12	4.36	1.25	0.40	3.42
Mn	40.98	66.84	0.38	0.08	0.08	0.15	2.30
Co	8.36	10.14	0.06	0.04	0.02	0.03	0.00
Ni	492	293	0.15	0.13	0.02	0.47	0.33
Cu	0.92	1.23	1.15	1.18	1.01	0.94	0.99
Zn	1.46	32.85	0.20	0.56	1.21	4.87	3.45
Mo	0.09	0.08	0.47	0.66	1.18	2.21	1.91
Hg	0.15	0.08	0.08	0.08	0.08	0.08	0.13
Pb	0.05	0.12	0.05	0.04	0.04	0.14	0.06

NB: AMD B4 represents Raw Acid Mine Drainage before treatment with FA
M represents MAP FA sample; H represents HBP FA samples while N(x) stands for sample dosage in g/L e.g. HN20 stands for 20g of HBP FA/Liter of AMD

pH Profiles

The pH trends observed with both FAs during neutralization are similar to those observed and reported by Gitari et al. (2010), and Kumar et al., (2008) from similar experiments (fig.4.7c). The types and volumes of ash were different but trends were the same as outlined in figure 4.7 a and b.

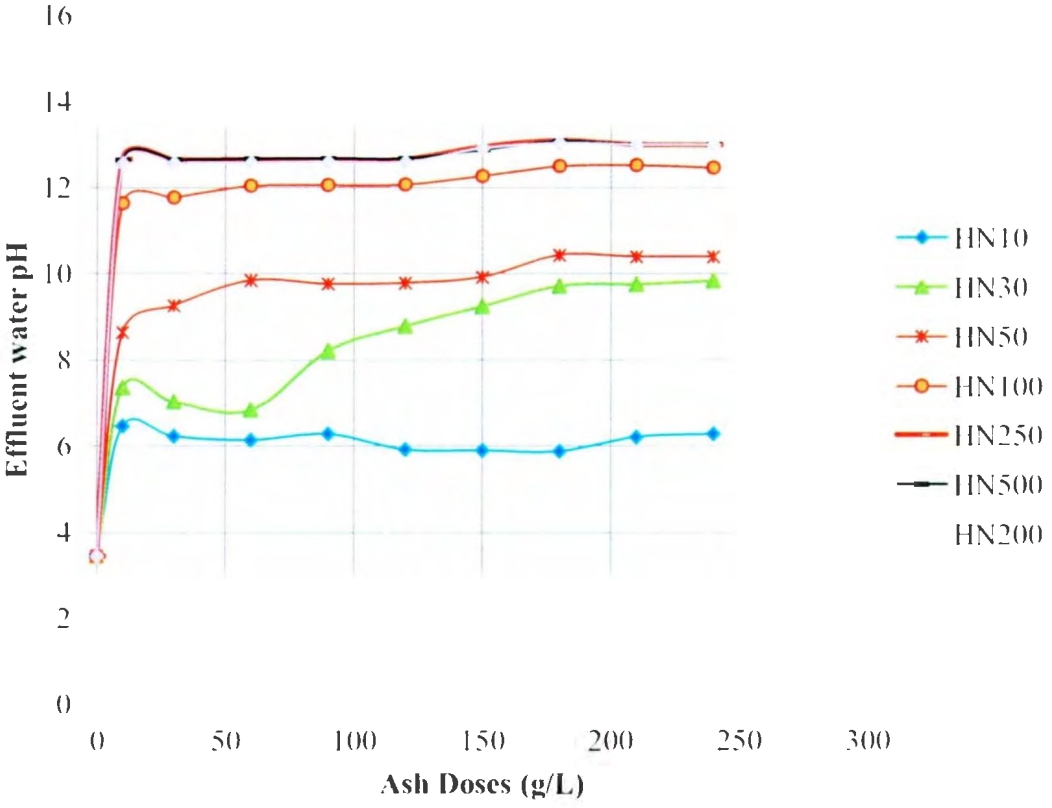

Figure 4.7a: Change in pH of AMD solution with time for doses of (HBP) Sample

NB: H represents HBP FA samples while N(x) stands for sample dosage in g L e.g. HN20 stands for 20g of HBP FA Liter of AMD

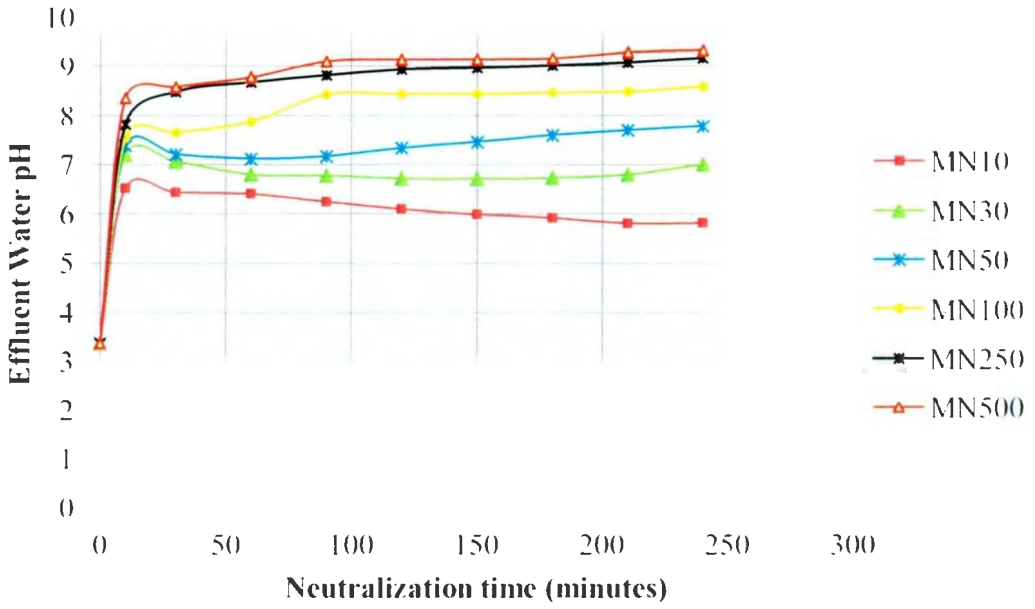

Figure 4.7b: Change in pH of AMD solution with time for doses of (MAP) Sample
NB: M represents MAP FA sample; while N(x) stands for sample dosage in g L e.g. MN20 stands for 20g of MBP FA Liter of AMD

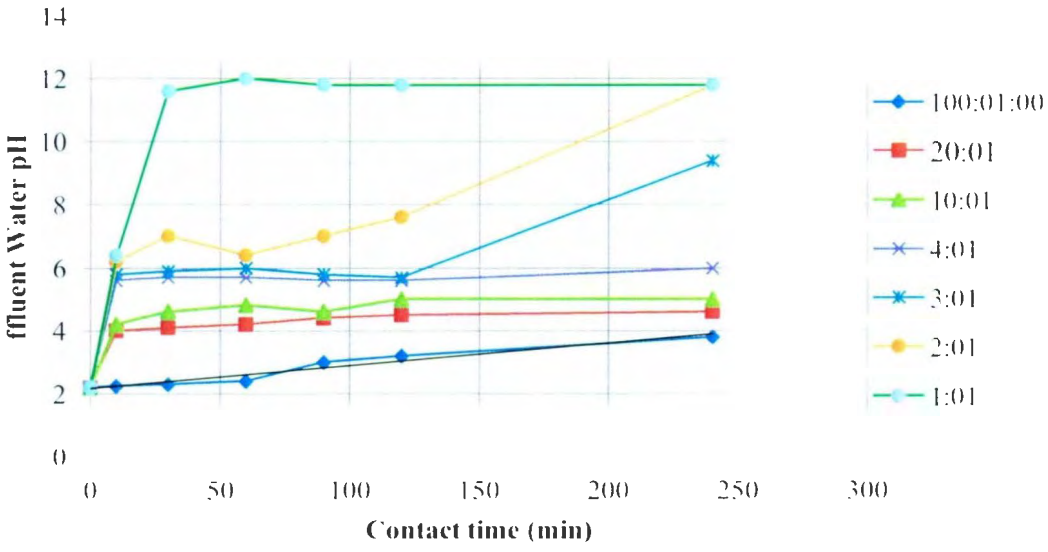

Figure 4.7c: pH as a function of time for various AMD: FA neutralization ratios (modifed from Kumar et al., 2008)
NB: 100:01; 20:01; 10:01 etc… represents various AMD: FA ratios during neutralization.

4.3.4 Basics of AMD treatment with Fly Ash (FA)

The neutralization of AMD is a function of the insolubility of contaminants under basic conditions. Soluble lime (CaO) and other soluble metal oxide such as MgO, Na_2O and K_2O are present in considerable amounts in the FA (Gitari et al, 2010, Muluken et al., 2010, Kumar et al., 2008, Gitari et al., 2005 and Komnitsas et al, 2004). The dissolution of these compounds is the first step in the neutralization process when FA comes in contact with AMD (aqueous solution) to form hydrated lime in solution. Dissociation of alkaline compound in solution yields more hydroxide $(OH)^-$ groups that triggers the solution pH (Aube, 2004), according to the reactions below:

$$CaO + H_2O \rightarrow Ca(OH)_2 \quad (4.10)$$

$$Ca(OH)_2 \rightarrow Ca^{2+} + 2(OH)^- \quad (4.11)$$

$$MgO + H_2O \rightarrow Mg(OH)_2 \quad (4.12)$$

$$Mg(OH)_2 \rightarrow Mg^{2+} + 2(OH)^- \quad (4.13)$$

Dissociation of more $(OH)^-$ groups into the solution leads to the hydroxide ions interacting and combining with dissolved cations in solution to produce precipitates (Aube, 2004), according to equations below:

$$Fe^{2+} + 2(OH)^- \rightarrow Fe(OH)_2 \quad (4.14)$$

$$Co^{2+} + 2(OH)^- \rightarrow Co(OH)_2 \quad (4.15)$$

$$Al^{3+} + 3(OH)^- \rightarrow Al(OH)_3 \quad (4.16)$$

By increasing the AMD solution pH to certain set-point, precipitation of some metals (in form of metal hydroxides) occurs, Fe, Zn, and Cu precipitated at typical pH of 9.5 while other metals such as Ni, Pb, Mn and Cd requires higher pH value (10.5 - 11) precipitate and settle out (Aube, 2004 and Younger et al., 2002).

The acidity of AMD solution is a result of mineral acidity such as metal sulphide and hydrogen ions depending on geological formation of the mine site, (Skousen, 1997). At lower solution pH, the more soluble ions of Fe^{2+} and Mn^{2+} are oxidized to their less soluble form Fe^{3+} and Mn^{3+}. Fe^{3+} and Mn^{3+} then combine with hydroxyl groups to form insoluble precipitates (Younger et al., 2002). As more sulphate ions and hydrogen ions are removed from the solution, the solution pH increases. Other dissolved metals also precipitate out of solution by forming insoluble metal hydroxide with the OH groups while sulphate ions combine with cations such as Ca^{2+}, Fe^{2+}, Mg^{2+}, to form insoluble metal sulphate and/or with Na^{+} to form soluble Na_2SO_4 as illustrated below:

$$2H_2O + M(SO_4) + Ca(OH)_2 \rightarrow M(OH)_2 + CaSO_4.2H_2O\ ; \qquad (4.17)$$

where M represents metals e.g. (Cu, Zn, Fe) (Chalkley et al., 1989).

NaOH is often used preferably over $Ca(OH)_2$ in AMD treatment due to the lower volume of sludge (less precipitation) generated. Hydrated sodium sulphate ($Na_2SO_4.10XH_2O$) formed from NaOH is highly soluble therefore sulphate precipitates are not generally formed (Chalkley et al., 1989). In general, suphate ions might still be present in NaOH treated AMD due to soluble $Na_2SO_4.10XH_2O$ and Na_2SO_4. The Na_2O in the FA could produce NaOH in the AMD and subsequently form $Na_2SO_4.10XH_2O$ and Na_2SO_4. This would explain part of anomalous behaviour of suphate ion adsorption as discussed in the section 4.3.5.

4.3.5 Adsorption and Leaching Characteristics of AMD: FA Neutralization

Fe Removal

More than 70% of Fe was removed with a concentration 10g L of both FAs and all detectable amounts were removed with 30, 50, 100, 250 and 500g L of HBP. At 30g L MAP FA all detectable Fe was removed. HBP FA concentrations except 10g L, all Fe^{2+} and Fe^{3+} were completely removed from the solution (final pH of 7.0 – 12.5). This is attributed to a rapid oxidation of Fe^{2+} to Fe^{3+} and subsequent hydrolysis of Fe^{3+} to insoluble hydroxides (Kumar et al., 2008). The insoluble amorphous hydroxides and or oxy-hydroxides are retained on the solid FA residue.

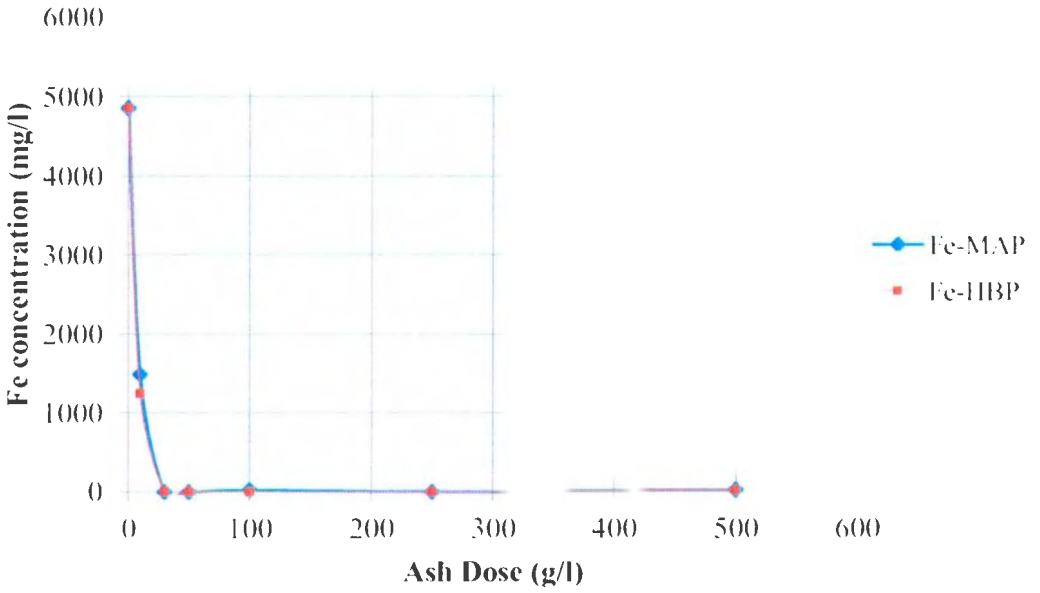

Figure 4.8: Iron removal profile from AMD solution

The sharp decrease in total iron in the AMD is likely due to oxidation of Fe^{2+} to Fe^{3+} at lower pH of 4 - 4.5 and subsequent precipitation of insoluble oxyhydroxide of iron out of

the AMD. Studies by Gitari et al. (2010), Kumar et al. (2008), Gitari et al.(2005) and Komnitsas et al. (2004), showed similar behaviour. (figure 4.9 below compares data from Kumar et al., 2008)

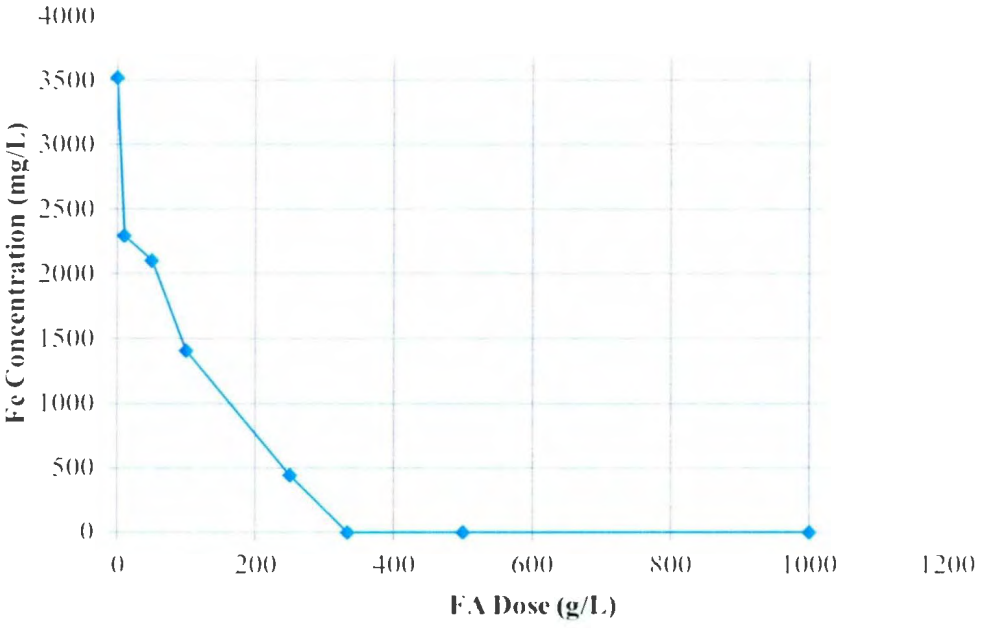

Figure 4.9: Fe removal profile from AMD using FA (modified from Kumar et al., 2008)

Ca, Zn, and Mn Removal

The treated AMD with the MAP showed increases in the Ca concentration indicating that Ca was leached from the MAP FA. This result followed the trend observed by Kumar et al., (2008). In Kumar investigation, alkaline reagents leach such elements like Ca, Na, and K into solution. In contrast, Ca does not leach into the process water as HBP FA dosage increases for AMD treatment. This behaviour could be as a result of interaction of calcium and sulphate ions in solution to precipitate gypsum ($CaSO_4.2H_2O$) (Kumar et al., 2008).

Zn and Mn also leached into solution from both FAs at the lowest concentration of FA (10g L) but reverse this trend at higher concentrations (fig.4.10a and 4.10b). The neutralization pH profiles (fig.4.7a and b) show that the solution pH for both sample with 10g L was below 7.0 well below the pH region where Zn and Mn precipitates, but as the FA doses increases the solution pH also increases to above 7.0 resulting in precipitation of these metals (Zn and Mn) onto the solid residue hence, their concentration in solution decreases.

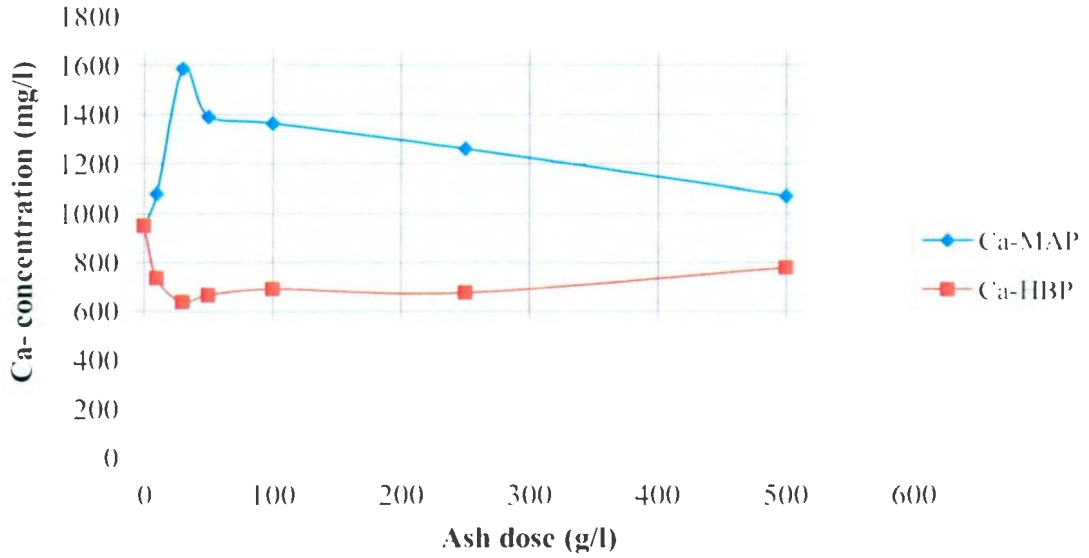

Figure 4.10a: Calcium profile from treated AMD solution

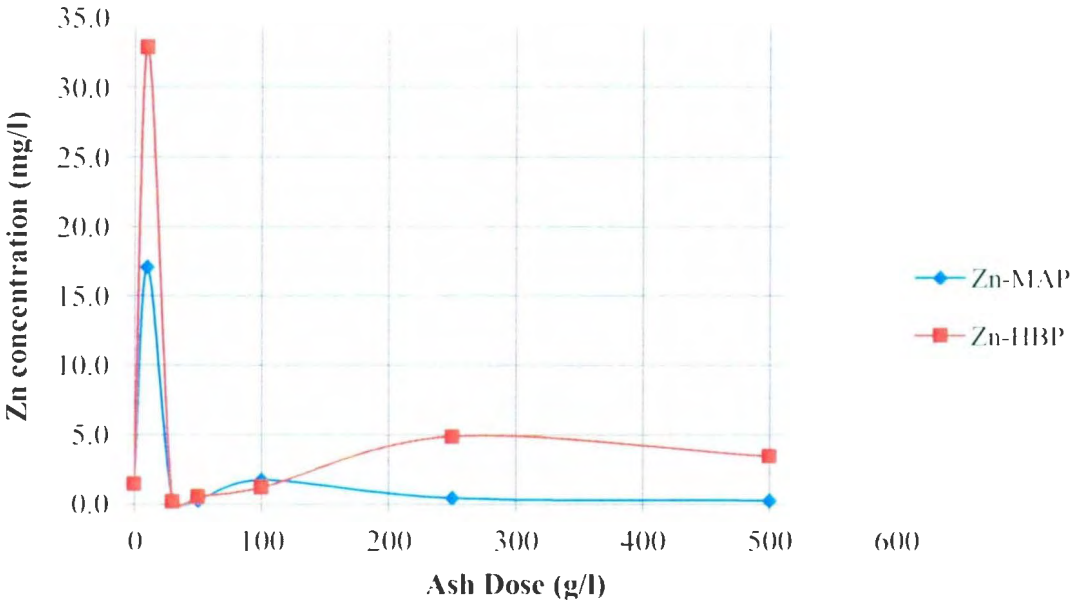

Figure 4.10b: Zinc removal profile from AMD solution

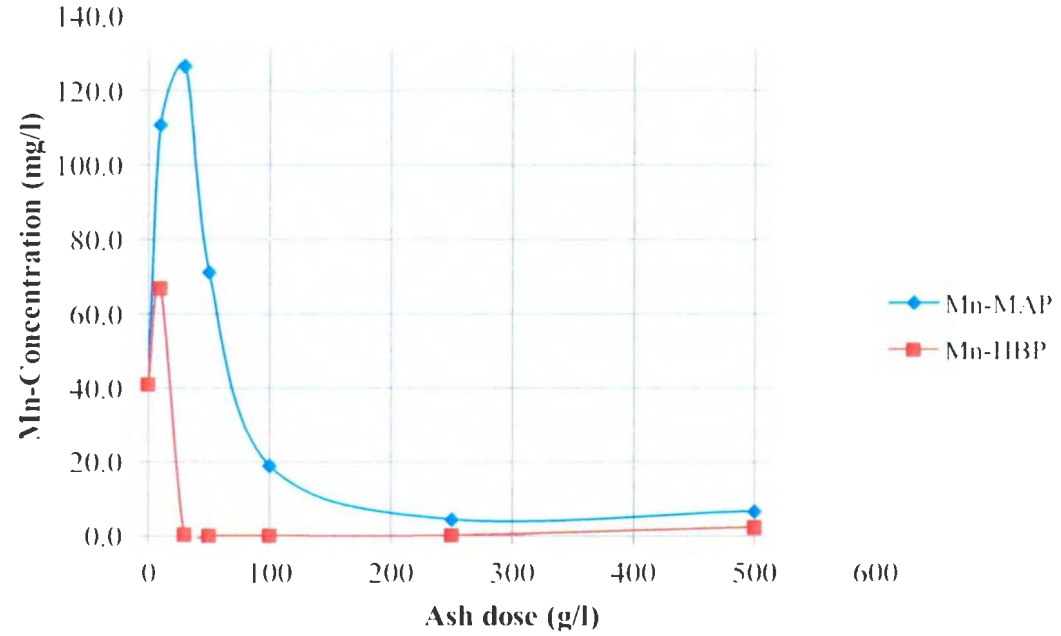

Figure 4.10c: Manganese removal profile from AMD solution

Leaching of Ca and Mg into the solution was also reported by Kumar et al., (2008) from FA – AMD neutralization. According to Kumar et al., (2008), the treatment of AMD with alkaline reagents leaves Ca and Mg in the final effluent water due to formation of soluble salts of these metals.

Sulphur Removal

The sulphur removed from the AMD is shown in figure 4.11. As the concentration of FA creased from 10 to 50 g/L there was approximately 50% drop in sulphate in solution. Various mechanisms could have responsible for SO_4^{2-} removal such as dissolution of CaO from FA and in the presence of acidic AMD Ca^{2+} ions released into the solution precipitated gypsum ($CaSO_4.2H_2O$) on interaction with SO_4^{2-} causing the initial sharp decrease (as shown in figure 11 below). Barium (Ba) and Strontium (Sr) salts present in the FA could also dissolve interacting with SO_4^{2-} resulting also in subsequent precipitation of barite ($BaSO_4$) and celestite ($SrSO_4$) or both (Kumar et al, 2008). At pH <- 7, oxy-hydroxides of Al such as alunite, basaluminite and jurbanite could have interacted with SO_4^{2-} forming Al-oxy-hydroxysulphates of these compounds resulting also in sharp decrease of SO_4^{2-}. Furthermore, at pH > 7 iron-oxy-hydroxides precipitates remove SO_4^{2-} in large quantities (Gitari et al, 2010), therefore could have also contributed to SO_4^{2-} removal.

Further increase in FA dosage from 100 – 200g/L shows an increase in SO_4^{2-} concentration in the effluent water. Formation of soluble $Na_2SO_4.10XH_2O$ and Na_2SO_4 in solution could be responsible for the increase in solution as discussed earlier in section

4.2.4. Furthermore, since the volume of AMD is constant for all the ash doses, it may be that cations released into the solution (e.g Ca^{2+}, Ba^{2+}, and Sr^{2+}) with 30 – 50g L FA doses. Therefore the increase in the SO_4^{2-} ion concentration in solution while using the HBP FA may indicate it contains more soluble sulphate salt than MAP FA.

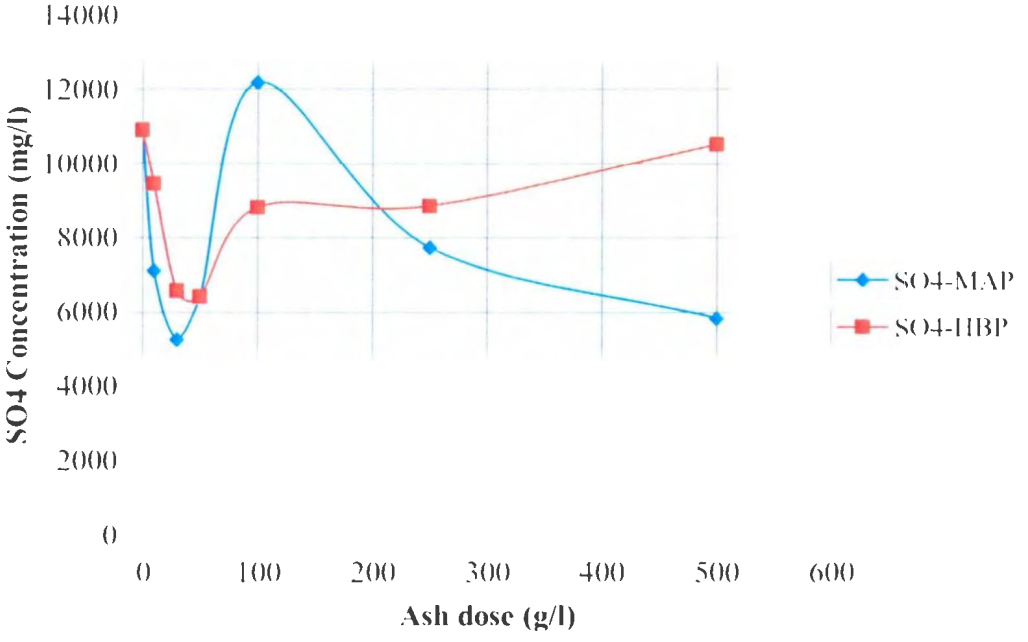

Figure 4.11: Sulphur removal profile from AMD solution

According to Kumar et al., (2008) several mechanisms could be responsible for sulphate removal including gypsum ($CaSO4.2H_2O$) , barite ($BaSO_4$), and or celestite ($SrSO_4$) formation. As the solution pH increases to 3, oxidation of Fe^{2+} to Fe^{3+} with subsequent precipitation of amorphous ferric hydroxide may also absorb SO_4. At a pH of 5-7 this absorption reaches a maximum (Kumar et al., 2008 and Gitari et al., 2005). Gitari et al (2010) found that when the FA doses were doubled, the SO_4 concentration was not doubled in treated solution therefore suggesting that solubility control for SO_4 does

exists. Removal profiles oberved for the suphate ions during neutralization is similar and took the same trend as that reported by Gitari et al., (2005).

Co and Ni Removal

A sharp decrease in concentration was observed with cobalt and nickel as shown in figure 4.12a and 4.12b below. The concentration of Co was high in solution initially at lower pH (pH < 7) in the 10g/L of HBA FA and was later on removed accordingly as the FA dose increases. MAP FA does not recorded any leaching of Co into the solution as there was no any initial increment in Co concentration with all dose of MAP FA .This removal could be attributed to precipitation of both metals at pH greater than 9.0. At pH of 9.5 or greater, Ni^{+1} precipitated as $Ni(OH)_2$ and adsorbed onto precipitated amorphous Al or Fe oxy-hydroxides while Co precipitate as $Co(OH)_2$ and adsorbed onto the FA surface (Kumar et al., 2008).

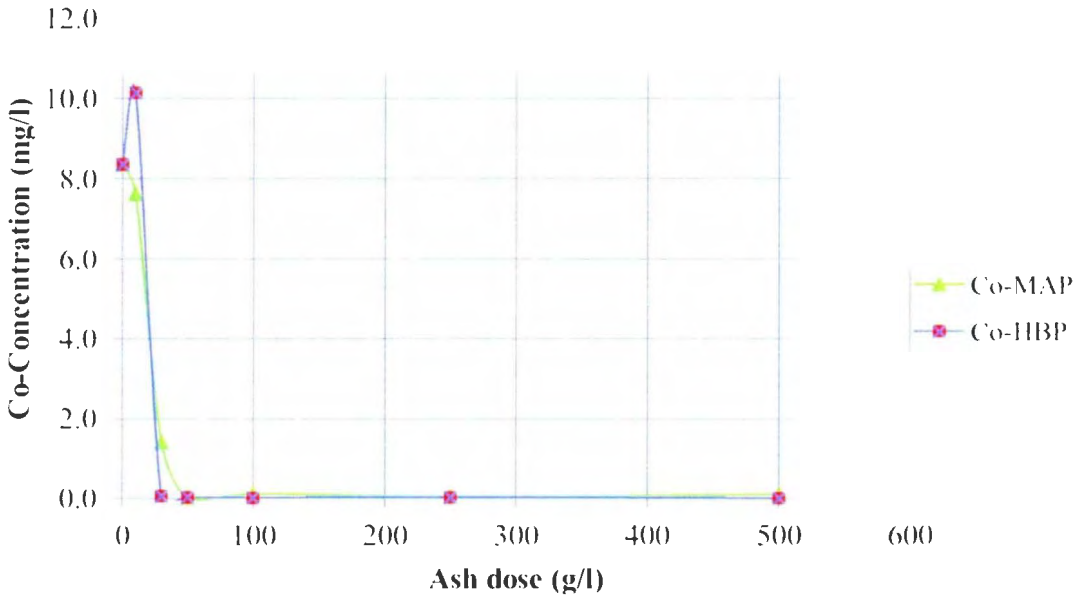

Figure 4.12a: Cobalt removal profile from AMD solution

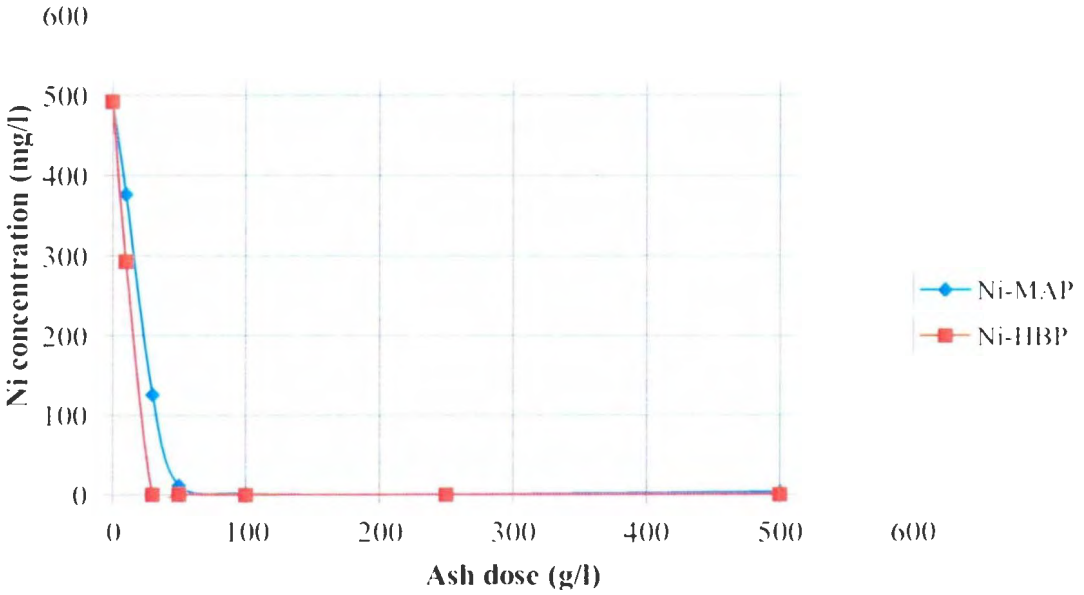

Fig.4.12b: Ni removal from Ash: AMD neutralization

Almost complete removal of Ni, Co and Mn occured as reported in investigations by Gitari et al. (2010 and 2005) and Muluken et al. (2010). Near complete removal of these metals was observed at pH of 7 – 9. The metals are removed through precipiation as insoluble metal hydroxyde at certain pH ranges (4.5 to 9.5 and above) (Aube, 2004; Younger et al., 2002; and Chalkley, 1989).

Neutralization of AMD with raw fly ash on a larger scale should be investigated as efficiencies achieved in the lab may not fully translate to larger scale. However, the lab scale results indicate the FA is an effective treatment system for AMD with removal of metals such as Fe, Ni, Co, Mg and Zn at 70%+. The concentration of SO_4^{-2} in the AMD is relatively unchanged at high FA concentrations for the HBP FA, due to the reasons outlined above. As long as the pH stays above ~6 (Skousen et al., 1997) the salts will not disassociate, however below this pH the sulphate could be released into solution resulting in a drop in pH. This needs to be further investigated to ensure this reaction does not reverse thereby releasing sulphate into the environment.

4.3.6 FA- Neutralization Efficiency

Neutralization efficiency estimates the relative effectiveness of the FA in neutralizing AMD acidity and subsequent contaminant removal from the effluent water stream. The contaminant removal efficiency by the FA is thus evaluated as;

$$\int = \{(C_1-C_2)/C_1\} * 100 \qquad (4.18)$$

where ∫ represents removal efficiency, C_1 represents the initial contaminant concentration before neutralization and C_2 represents final contaminant concentration after neutralization. Hence, the overall treatment efficiency using raw FA: AMD neutralization was estimated to be 85%.

4.3.7 Process Water Final pH

The final process water pH for all analyzed FA-AMD neutralization was greater than 6.0 except 10g/L MAP FA which is 5.8 (fig.4.7 a-b). The observed pH fluctuations in the first 90 minutes of contact time could be attributed to chemical interactions but become stable after 150 minutes. Process water of all FA doses hit the maximum pH in 240 minutes and these values remained stable for several weeks. The FA: AMD ratio considered as the optimum dosage for this research was 100g/L HBP FA and 250g/L MAP FA. The difference in the optimum FA doses between the two samples was attributed to higher buffering power and pH of HBP FA.

4.3.8 Adsorption Mechanism

The pH is a very important parameter for this process due to the solubility and mobility of metals such as Fe, Zn, Co, Pb, Al, and Mn. At high pH levels these metals form complex amorphous solids (Kuyucak, 2006) that retained on the surface of adsorbents.

As the solution pH increases, an increase in the metal ions in solution occurs resulting in the precipitation and/or co-precipitation metal hydroxides, oxides, carbonates, sulphides, sulphates and phosphates (Zhou and Haynes, 2010). Specific adsorption includes metals

ions and/or anions exchange on various charged surfaces. The amorphous and crystalline Fe, Al, Mn oxides and the aluminosilicates carries varying charged surfaces on which adsorptions occurs (Zhou and Haynes, 2010). The mineralogical and chemical analysis has shown that the FA particles are composed primarily of amorphous ferro-aluminosilicate, calcium-aluminosilicates, iron oxides, and aluminum oxides. Also, the high pH of FA favours specific adsorption and/or surface precipitation of metal cations and anions to its surface (Zhou and Haynes, 2010).

4.3.9 Optimization and Scale up design

The optimum contaminant removal was achieved with 100g/L HBP FA and 250g/L MAP FA during the laboratory scaled experiment. After 4 hours 100g/L HBP FA recorded final pH of 12.2 while 250g/L MAP FA showed final pH of 9.2 and at these pH (pH~9.0 to 12.0) the solubility limit of common metals such as Cu, Zn, Cd, Mn, Pb and $Fe^{2,3}$ is exceeded therefore are less soluble and hence precipitated. This experiment was carried out at ambient condition of temperature and pressure. Most AMD treatment plant requires final effluent pH of circum-neutral (6.8) to 9.0 therefore recycling of lime in the final process water may be required. Since a stable effluent pH was achieved at 150 minutes of stirring, the reaction/residence time could also be reduced to less than 3 hours (2hours 30minutes). Mixing/stirring speed has no effect on the final effluent pH and removal efficiency therefore a minimum speed of 40rpm is reasonable for this process.

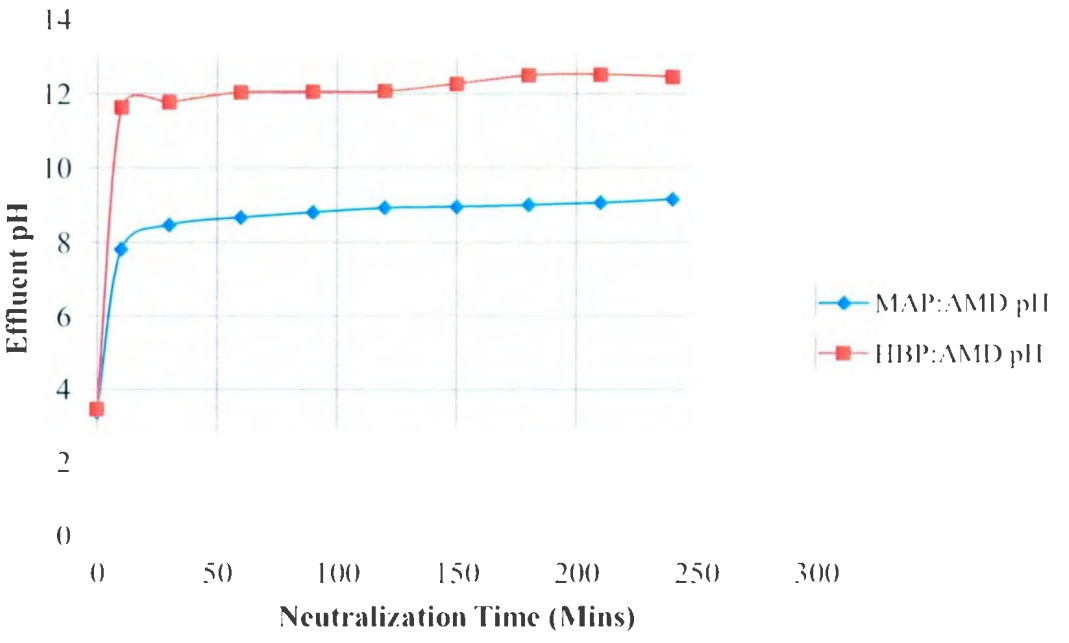

Figure 4.13: Optimum FA treated effluent water pH profile

4.3.10 Scale Up

The scale-up of this process requires additional research, however calculations to reflect feasibility are shown below;

Assuming a mining effluent (AMD) pond 3.816 x 10^6L day (1.008 x 10^9GPD) effluent discharge. An equivalent amount of FA that would be required for the FA AMD neutralization process is 381.6 tonnes day of HBP FA and 954 tonnes day of MAP FA. This is strictly based on the AMD that has the same level of contamination as those analyzed. On average these values represent approximately 0.05% of FA that is generated annually in Canada. Furthermore, if the effluent pH is more than 9.5, excess lime can be recycled back to the FA mixing tank therefore the amount of feed FA can be reduced

accordingly by balancing the final effluent pH and quantity of FA introduced from the feed. Hence, the solid residue generate from FA: AMD neutralization would be recycled for zeolite application as described in section 3.4.

4.3.11 Tailing weathering and natural degradation

Mineral weathering is usually associated with some naturally occurring degradation (Younger et al., 2002). Many carbonate and silicate minerals are weathered by AMD and in the process the AMD pH is reduce pH and it acts as a buffer. This is a process that occurs naturally with subsequent precipitation of amorphous and insoluble minerals prior to or during any treatment. Dissolution of minerals such as calcite, anorthite, albite, aluminosilicate and felsdspar are classic examples of weathering that neutralizes or reduces acidity (Younger et al., 2002). Calcite and feldspar dissociate rapidly and sufficiently control the pH of process water (Younger et al., 2002). This phenomenon was observed in our experiments in untreated AMD although it is very slow process. Greyish precipitates formed at the base of AMD containers and were analyzed using XRD techniques. The XRD analysis identified the precipitate as predominantly gypsum ($CaSO_4.2H_2O$). Example of such dissociation that occurs during mineral weathering is outlined below:

$$CaCO_3(s) + H^+ \quad \leftrightarrow \quad Ca^{2+} + HCO^{3-} \qquad (4.19)$$

$$KAlSi_3O_{8(s)} + H^+ + 9/2H_2O \quad \rightarrow \quad 2H_4SiO_{4(aq)} + 1/2Al_2Si_2O_5(OH)_{4(s)} \qquad (4.20)$$

4.4 Permeable Reactive Barrier

4.4.1 AMD pH profile

The change in pH with AMD pore volumes flowing through the reactive columns for both FA samples are represented in the figure 4.14. The pH of the AMD was below 2.0 at the start of experiment. The effleunt pH gradually increased from 1.8 to 12.5 just after the first pore volume (approximately 400cm^3 AMD) passed through the HBP reactive barrier column. The process water had a pH of 12.4-12.6 and became constant. Dissolution of some metal oxides such as MgO, CaO, Na_2O and K_2O likely contributed to this rapid pH increase. The increase in the pH may also be due to the oxidation of Fe^{2+} to Fe^{3+}, hydrolysis of AMD-FA constituents such as Fe^{3+}, Al^{3+}, and subsequent hydrolysis to iron and/or aluminum hydroxides as described by Kumar et al., (2008). The HBP FA had a higher buffering capacity than MAP FA. The process water pH of the MAP reactive column showed similar profile as that of HBP reactive column, however the overall pH and buffering capacity was lower. Buffering plateaus occurred at pH of 6.0 to 8.4 as shown in the figure 4.8 and became stable after the sixth pore volumes of AMD. This indicated that HBP sample has higher neutralization capacity (as discussed in section 4.1.10) than the MAP FA which is in agreement with the characteristics of the FA with respect to pH and buffering power of the FAs.

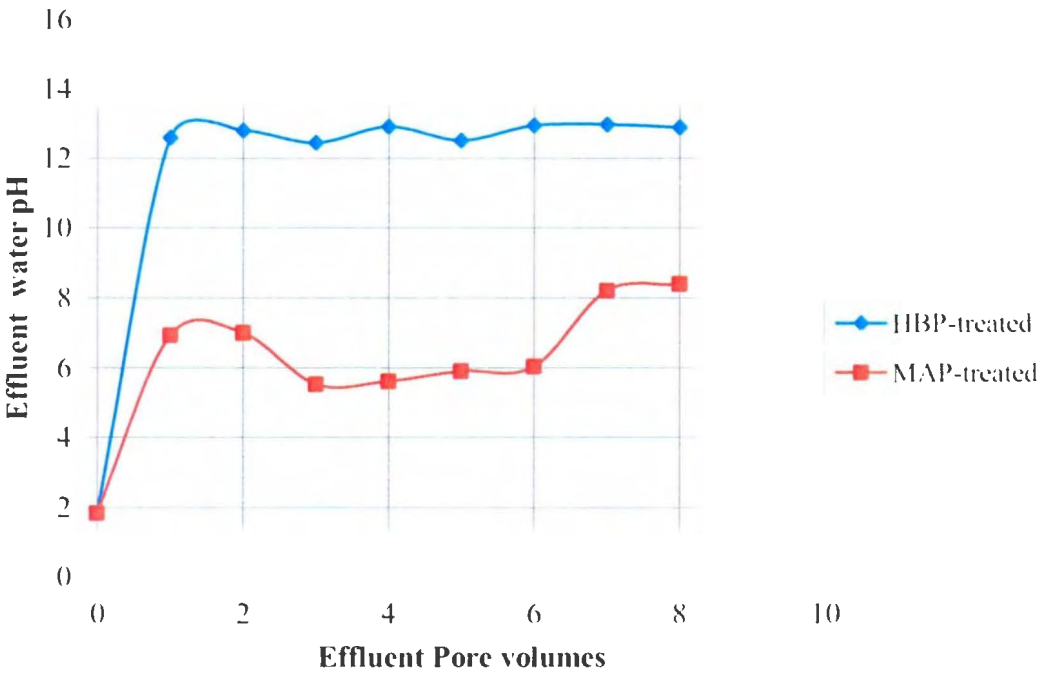

Fig.4.14 : pH profile for both ash samples (PRB Column)

4.4.2 Effect of Chemical Interactions on Flow rate and residence time

The permeable reactive column function is to immobilize metals and increase the pH promoting sulphate reduction and metal sulphate precipitation. As the AMD passes through the reactive barrier, several physical and chemical interactions occur such as dissolution of soluble salts, hydrolysis, oxidation, precipitation and co-precipitation that may alter the flow through the column. This is likely the cause of the unstable region between the 2nd and 7th pore volumes in the pH profile of the effluent.

The volumetric flow rate of the column system was initially 1.860cm^3 day for MAP FA column and 1.440cm^3 day for HBP FA column with average residence time of 7.1 hours

and 7.5 hours respectively. After some time during the process, the flow rate and residence time decreased significantly due to precipitation visualized through the column wall in the first 0 – 8cm mark of the column. This precipitation occoured in both FA, MLA analysis of the precipitate FA mixture indicated an increase in Fe and Ca of the FAs. The XRD analysis confirmed large amounts of gypsum ($CaSO_4.2H_2O$), Fe_2O_3 and $FeSO_4$. After four pore volumes, the flow rate was reduced from 1,860cm^3 to 1200cm^3/day for the MAP FA column and from 1,440cm^3 to 960cm^3/day for HBP FA column. This is because the pore spaces of the reactive barrier were partially blocked by ($CaSO_4.2H_2O$), Fe_2O_3 and $FeSO_4$ in both cases thereby reducing the volumetric flow rates. The chemical reactions desribed below are likely examples of such possible reactions which are:

Calcite dissolution has little or no overall effects on barrier but results in the removal of lime and calcite from the barrier matrix (Chalkley et al., 1989) :

$$CaCO_3 + H^+ \rightarrow Ca^{2+} + HCO_3^- \qquad (4.21)$$

Siderite ($FeCO_3$) formation results in replacement of chemical species in barrier material;

$$CaCO_3 + Fe^{2+} \rightarrow FeCO_3 + Ca^{2+} \qquad (4.22)$$

$$FeCO_3 + H^+ \rightarrow Fe^{2+} + HCO_3^- \qquad (4.23)$$

Gypsum precipitation has the potential for precipitation and blockage of pore spaces in barrier;

$$Ca^{2+} + SO4^{2-} \rightarrow CaSO4.2H_2O \qquad (4.24)$$

Finally iron precipitation drops the pH of the solution due to production of more protons into the solution by hydrolysis;

$$4Fe^{2+} + O_2 + 10H_2O \rightarrow 4Fe(OH)_3 + 8H^+ \quad (4.25)$$

(Chalkley et al., 1989)

The total iron removal from solution results in iron precipitation that causing pore space blockage in the barrier which was largely responsible for the change in the flow rates and residence times.

A major pH increase was observed between 1th and 2nd pore volumes in both cases and chemical interaction might be responsible for the pH fluctuation between the 2nd and 6th pore volumes (fig.4.14).

4..4.3 Chemistry of PRB Process Water Before and After Treatment

Table 4.12 summarizes effluent contaminant removal through the permeable reactive barrier application using the two FA samples. An appreciable amount of contaminats were removed as more AMD pore volumes passed through the reactive barrier. The pH trend of the final effluent water is similar to those investigated by and Muluken et al., (2010) and Komnitsas et al, (2004).

Table 4.12 Percentage of effluent contaminant removal.

		Percentage contaminant Removal (%) from each Pore volumes							
Element	Raw AMD (mg/kg)	MAP FA-Treated							
		1	2	3	4	5	6	7	8
Mg	544	L	L	L	L	L	L	L	L
Al	2.06	63.11	L	69.90	69.42	58.25	0	14.56	L
SO4	31776	63.17	61.24	87.56	80.63	73.20	74.55	85.38	77.19
Ca 43	761	L	L	L	L	L	L	L	L
Fe 54	18058	100	100	100	100	100	100	100	100
Mn	104.5	99.14	98.91	99.81	99.92	99.90	99.92	99.88	99.60
Co	35	100	98.66	99.80	99.97	99.94	99.91	100	99.46
Ni	1618	99.59	99.40	99.98	100	99.98	100	99.98	99.99
Cu	0.09	L	L	L	L	L	L	L	L
Zn	2.8	46.79	L	53.93	59.64	49.64	71.43	40.36	L
Mo	0.11	L	L	L	L	0	L	18.18	L
Hg	0.22	27.27	54.55	31.82	63.64	9.09	L	63.64	L
Pb	0.1	L	L	30	L	L	L	L	L
Element	HBP FA-Treated								
Mg	544	99.97	99.82	99.79	99.88	99.87	99.86	99.76	99.92
Al	2.06	92.23	61.65	58.25	25.73	L	37.86	60.68	98.06
SO4	31776	63.31	53.46	92.20	77.32	98.46	89.89	69.34	98.75
Ca 43	761	L	L	L	L	L	L	22.47	L
Fe 54	18058	99.81	99.81	99.80	99.80	99.79	99.81	99.82	99.81
Mn	104.5	99.21	99.93	99.89	99.78	99.89	99.66	99.83	99.81
Co	35	100	99.94	99.23	99.97	99.94	99.94	99.97	99.94
Ni	1618	99.99	99.96	99.98	100	100	99.93	99.99	99.99
Cu	0.09	L	L	L	L	L	L	L	L
Zn	2.80	L	L	L	L	15.00	L	L	0.36
Mo	0.11	L	L	L	L	L	L	L	L
Hg	0.22	68.18	68.18	63.64	68.18	63.6364	68.18	68.18	54.55
Pb	0.1	L	L	L	L	L	L	L	L

L*: Represents leaching of metals from FA into AMD solution (its % cannot be estimated)

Efficiency was evaluated using the correlation $\int = \{(C_1-C_2)/C_1\} * 100$ as described in section 4.3.6.

Fe, Ni, Co, and Mn Removal

The raw AMD sample was characterized by high Fe^{2+} Fe^{3+} levels (18,058mg L) as shown in table 4.12. Iron was removed almost completely from the effluent stream after the first pore volume. The behaviour is very similar in both ash samples as it can be seen from adsorption profile (fig. 4.15a). The MAP ash sample removed the iron completely after first pore volume while HBP ash sample removed iron to value less than 35mg L. This happened at circum-neutral pH (pH almost 7.0) for the MAP but at pH of around 12.8 for the HBP sample. As previously mentioned a dark-grey precipitate was noticed in the first column in the first 0 – 8cm of the reactive column.

Mn, Ni and Co showed similar trends as Fe for both ash sample. The effluent Mn concentration after first pore volume decreased significantly to below 1.0 mg L for both FA samples. This was the same for Ni, and Co for both FAs as shown in figure 4.15(b – d) except that Ni in the MAP sample was completely removed after the 3rd pore volume. Komnitsas et al. (2004), reported similar removal profile for Fe, Co, Ni, and Mn with PRB application.

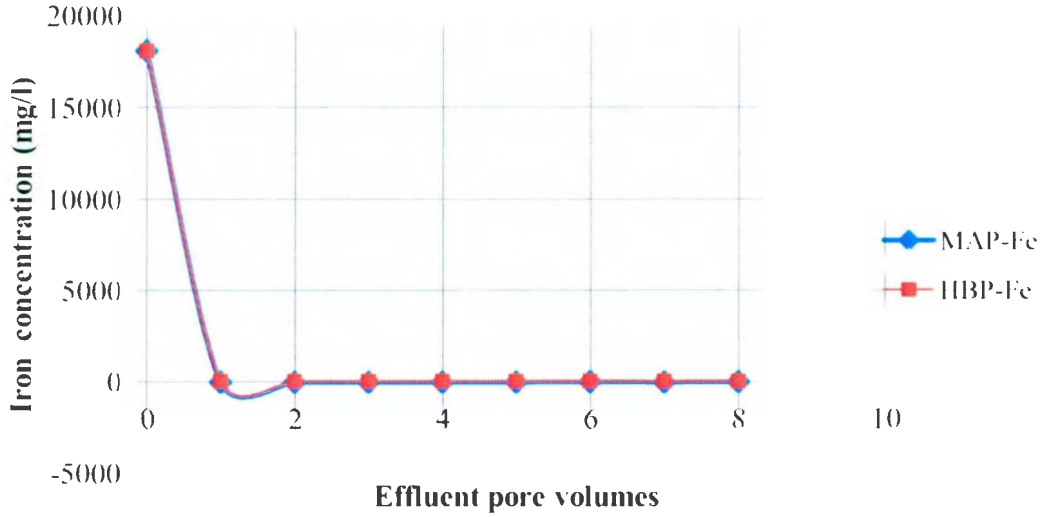

Figure 4.15a : Iron removal from effluent water stream by PRB

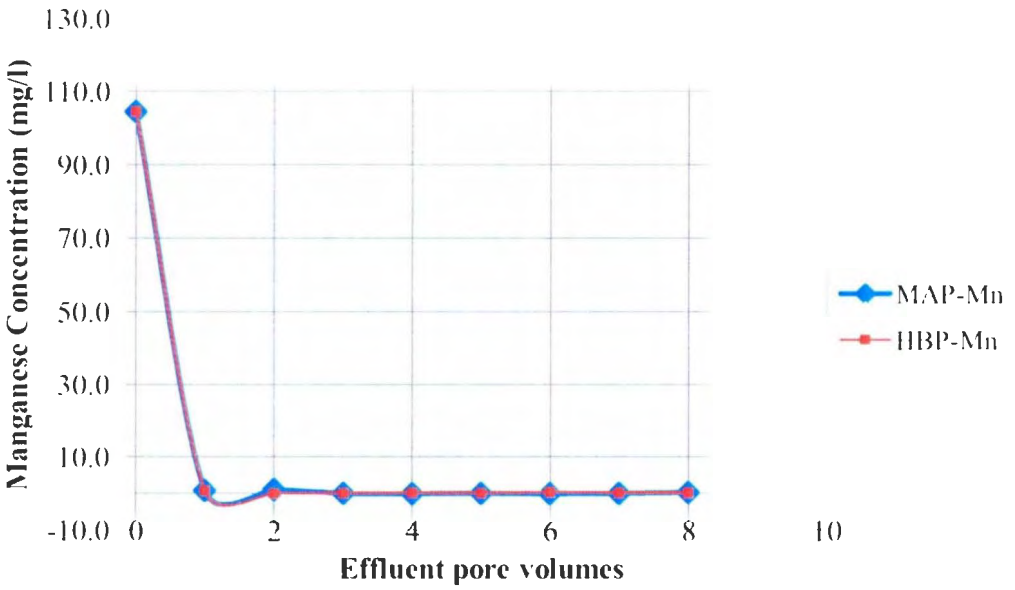

Figure 4.15b : Manganese removal from effluent water stream by PRB

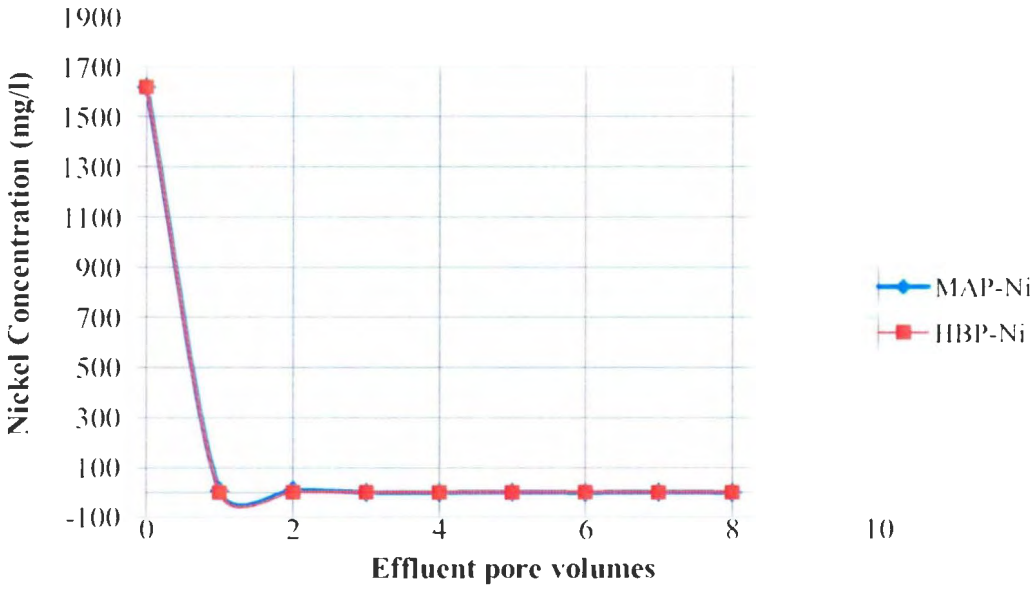

Figure 4.15c: Nickel removal from effluent water stream by PRB

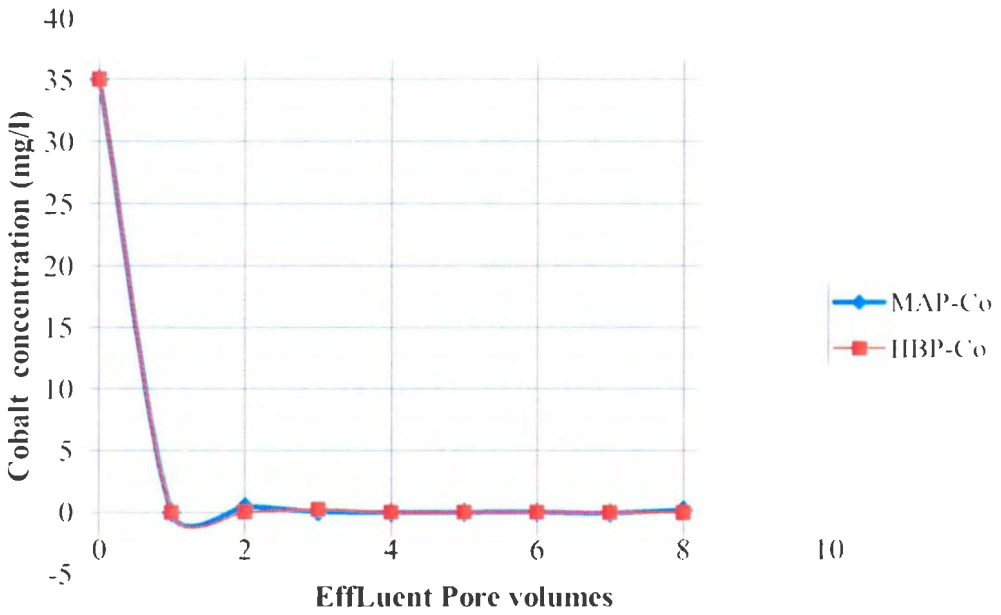

Figure 4.15d : Cobalt removal from effluent water stream by PRB

SO_4 Removal:

The sulphate ion represents the dominant anion of the AMD and the inlet concentration was approximately 31,776 mg L as shown in table 4.12. After the passage of the 1st pore volume, the sulphate concentration for both FA column dropped signifficantly to approximately 11,000 mg L. The next noticeable reduction in SO_4^{2-} concentration was after the 3rd pore volumes when the concentration dropped to less than 3,000mg L and 4,000mg L for HBP and MAP FA respectively. This occured at the high pH region (6.0 and above) for both ash as shown in figure 4.16. After the 3rd pore volume the SO_4 begins to increase. The final effluent still had SO_4 of less than 500mg L for HBP while for MAP sample, it showed a value slightly above 7,000mg L. This indicated that HBP sample is

more effective in sulphate removal than the MAP sample. The increase in sulphate concentration suggested that there are soluble salts of sulphate in the fly ashes which dissolved leached into the effluent stream. Formation of gypsum ($CaSO_4.2H_2O$) is most likely major precipitate of this interraction as suggested by Muluken et al (2010). As discussed in section 4.2.2 the anomalous behaviour of sulphate ions in solution could also responsible for the unstable nature of SO_4 adsorption profile as shown. Similar removal profile were also reported by Muluken et al., (2010), but explanations reasons as to increasing behaviour of SO_4 ions in solution was not provided.

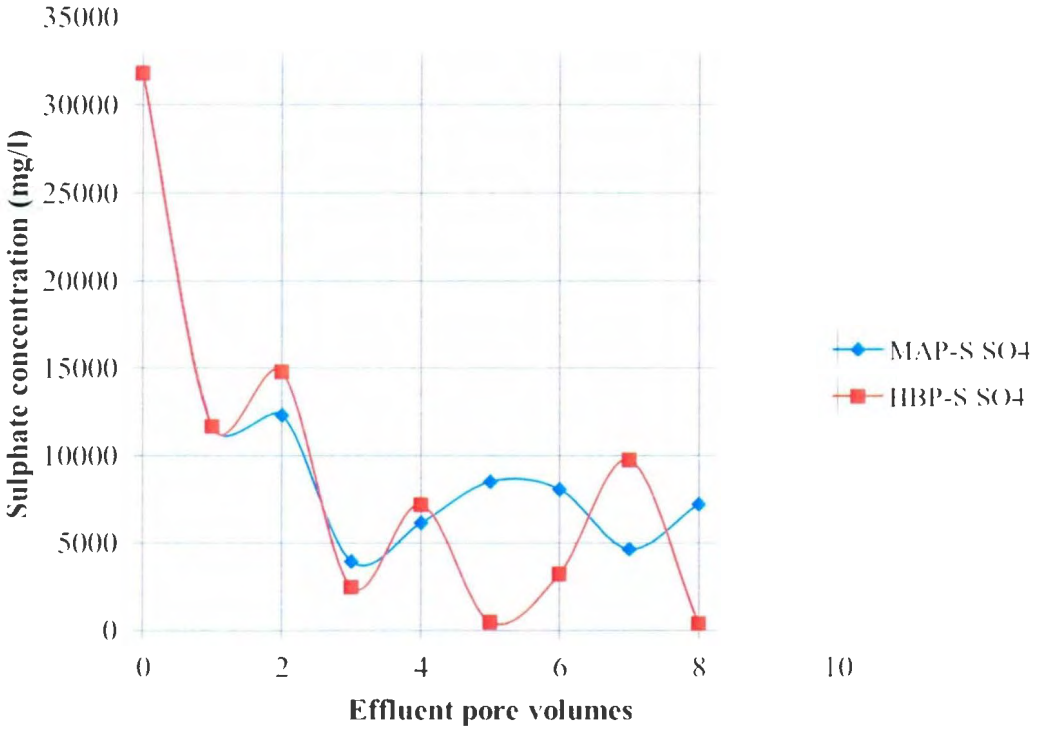

Figure 4.16: Sulphur removal from effluent water stream by PRB

Ca, Mg, Cu, Mo and Zn Removal:

A Large amount of Ca was released from both FAs into the AMD solution as shown by the trend in the figure 4.17a. The leaching characteristics follows the trend described by Kumar et al. (2008). as discussed earlier (section 4.2.5.2). Mg also showed similar leaching trend with MAP FA but no leaching of Mg was detected with HBP FA, this could be that there are no soluble salts of Mg in the HBP FA. Mo initially leached into the AMD solution over the first three pore volumes and was adsorbed afterwards when the solution pH increased to the solubility limit (6.0 and above). Leaching of Zn was also observed in both FAs as shown in figure 4.17d. Cu also leached into the effluent with MAP FA but very little from the HBP FA.

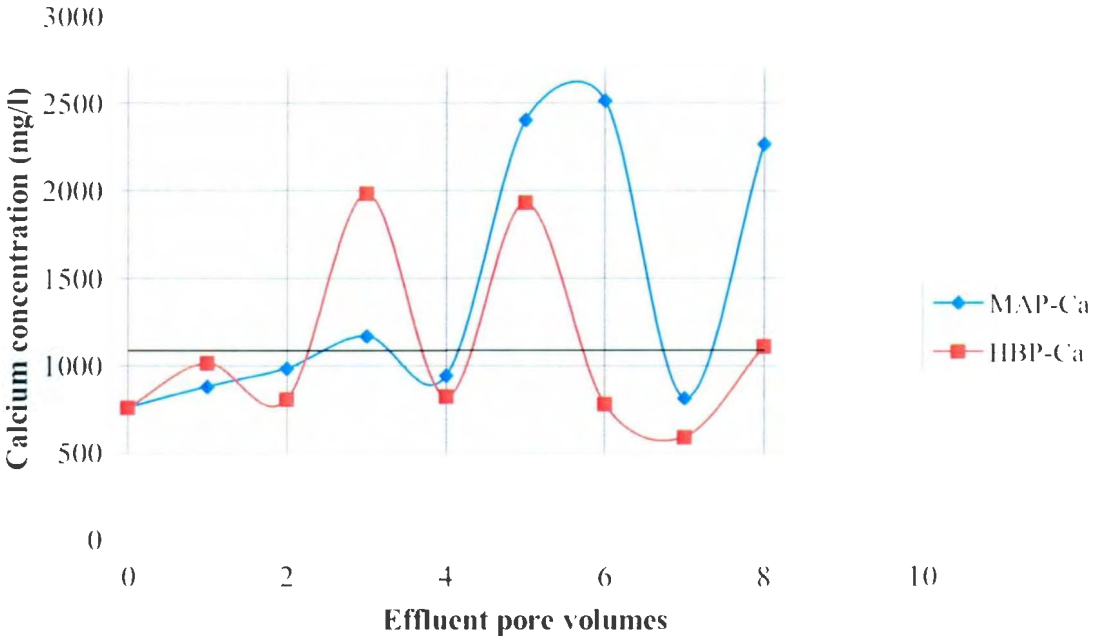

Figure 4.17a : Calcium profile in the effluent water stream through PRB column

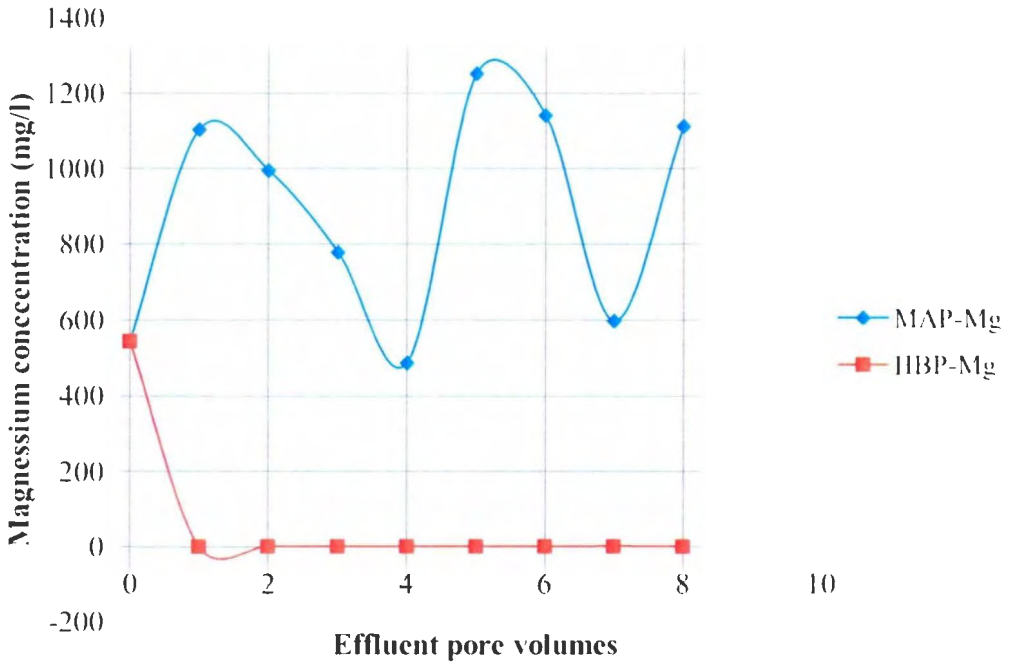

Figure 4.17b : Magnesium removal/profile in effluent water stream by PRB

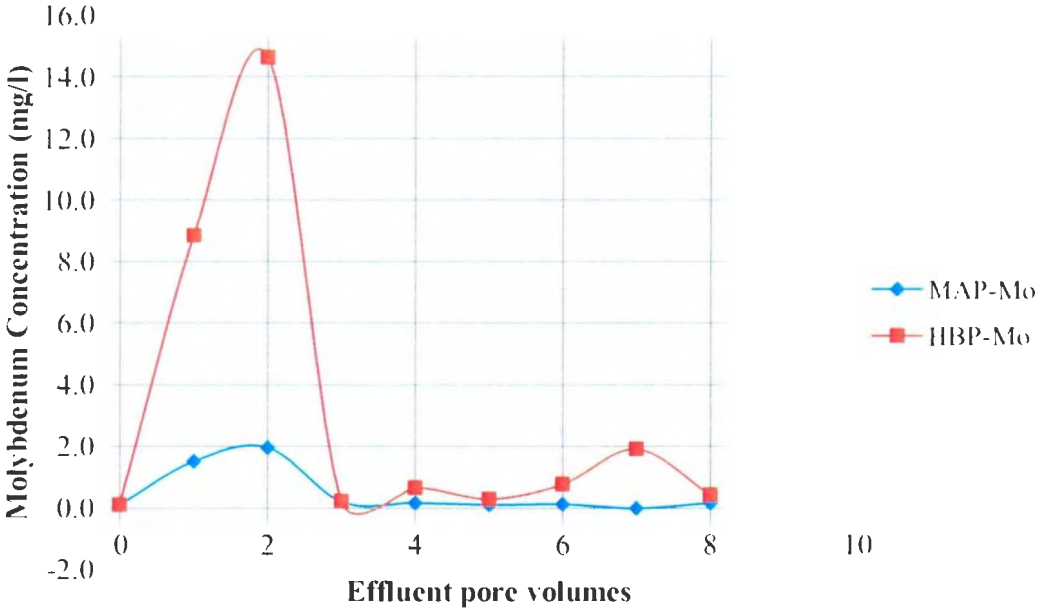

Figure 4.17c : Molybdenum removal/profile in effluent water stream by PRB

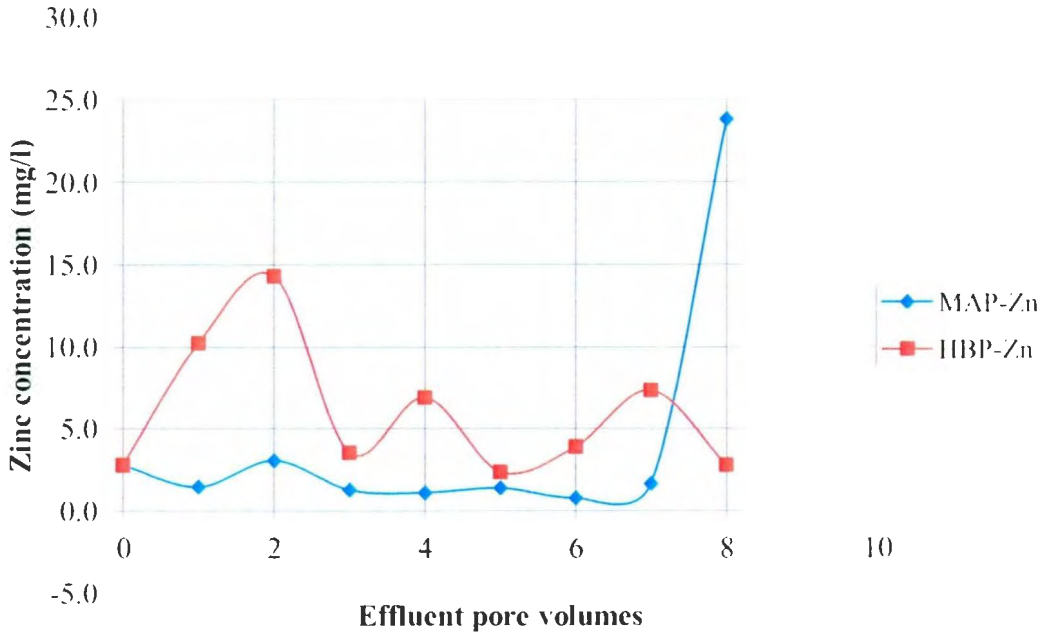

Figure 4.17d : Zinc profile in effluent water stream by PRB

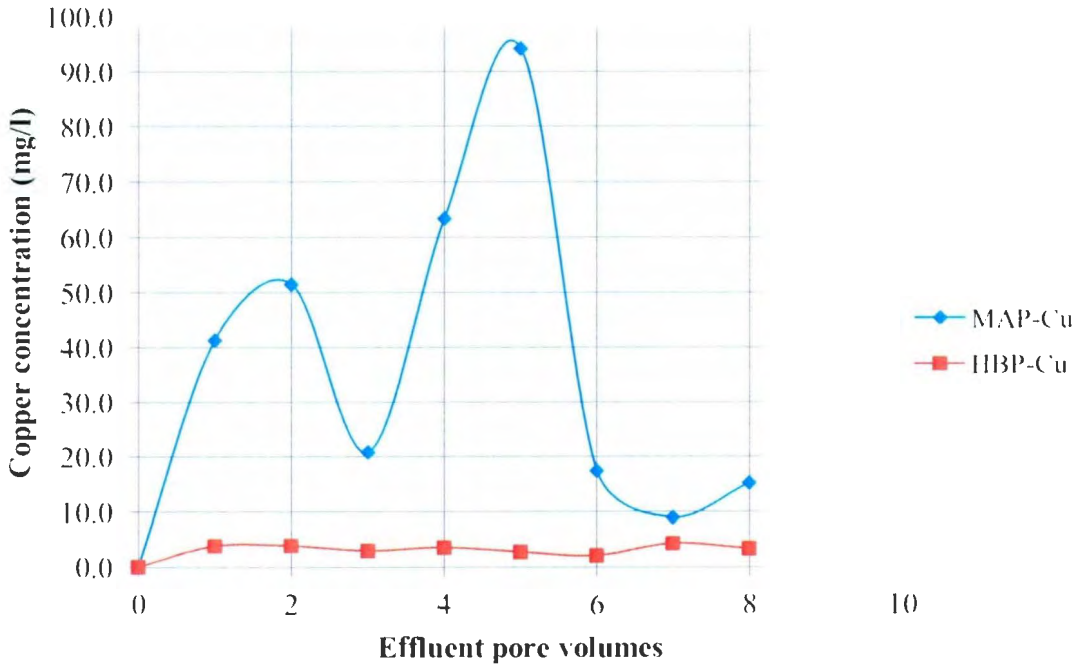

Figure 4.17e : Copper profile in effluent water stream by PRB

4.4.4 PRB Treatment Efficiency

The removal mechanism of PRB techniques is similar to that of neutralization and approximately 97% efficiency was recorded. Similar expression was also used to evaluate the PRB efficiency (i.e. $\int = \{(C_1-C_2)/C_1\} * 100$). Almost complete removal of Fe^{2+}/Fe^{3+}, Ni, Co, and Mn was achieved and metals that leached into the solution include Ca, Mg, Mo and Cu. Therefore going by the evaluated efficiencies, PRB is more efficient than the neutralization method in terms of contaminant removal. In terms of pH increase and stability, the FA: AMD neutralization shows better pH control than the PRB. This could be attributed to constant mixing during neutralization, nevertheless, PRB also achieve final process water pH of above 8.0 (by MAP FA) and above 12.0 (by HBP FA) which is reasonable.

4.4.5 PRB Optimization

PRB optimization can be defined in terms of finding the balance between contaminant capture/removal, residence time and the stability of PRB that produces a minimum cost. In this investigation the amount of FA used for the PRB column was fixed unlike the neutralization study and the volumetric flow rate was kept constant under gravitational free flow. There was a significant reduction in the volumetric flow rate over time due to blocking of pore spaces in the first 30% of the first column with amorphous precipitates. As more contaminant was removed from the AMD, more reactive barrier spaces were blocked and less volume of AMD flow through the barrier and therefore more residence time were required for the process. Hence at the end of the 8^{th} pore volumes, the

unblocked part of FA (85%) of total volume still has the quality almost equal to that of fresh FA. Optimum design requires a mechanism that would maintain constant flow rate throughout the life cycle of the FA and hydraulic perforation or subsequent removal of the spent FA at the upper section of the column.

4.5 Zeolite Characterization Result

4.5.1 Mineral Content, Amorphous and Crystallinity

The XRD analysis of the FA produced zeolites showed a sharp peak of sodium aluminum silicate hydrates (zeolite) and potassium aluminum silicate hydrate (Appendix A). The main zeolites formed are the sodium aluminum silicate hydrate ($Na_6Al_6Si_{10}O_{32}.12H2O$), potassium aluminum silicate hydrate ($K_{2.52}Al_{10.68}Si_{27.36}O_{72}$).$(H_2O)_{25.5}$) and the lawsonite-zeolite that is calcium aluminum silicate zeolite ($CaAl_2(Si_2O_7)(OH)_2(H_2O)$. Gypsum, aluminum silicate, quartz and muscovite are also present in significant amounts. There is an indication that the aluminum silicate salts crystallize to various zeolitic materials during hydrothermal process (Keka et al, 2004).

The conventional hydrothermal treatment with alkali (NaOH) uses the NaOH as an activator during fusion process at high temperature (500 – 650 °C) combining with aluminum silicate sub-building units to form soluble groups (Keka et al, 2004).

4.5.2 Surface area and textural properties

Table 4.13 shows the surface area and pore volumes of modified FAs after hydrothermal treatment. The pore volume of the modified fly ash increased 2.5 times for the MAP FA

and 15 times for HBP FA. The specific surface area increased approximately twice and six times for MAP and HBA FA respectively

Table 4.13 Textural properties of ash samples.

Sample	S_{BET} (cm^2/g)	Total pore volume, V_t from P/P_o–0.99 (cm^3/g)
MAP	3.93×10^5	0.20
MAP-zeolite	7.94×10^5	0.50
HBP	1.01×10^5	0.02
HBP-zeolite	5.85×10^5	0.30

4.5.3 Zeolite-AMD Neutralization and Adsorption of Contaminants

The adsorption capacity of the zeolite synthesized from FA was compared with that of commercial activated carbon. The pH profile of the process water after treatment with FA-zeolite in figure 4.19 showed similar characteristics as those for FA: AMD neutralization and PRB. The solution pH is stable on the same time scale as the PRB without fluctuations as observed with PRB. The maximum pH achieved using synthesized zeolite was 8.8 by HBP-Zeolite and 8.4 by MAP-zeolite at the end of 240 minutes of reaction. It is important to note that process water pH remained stable after treatment for a number of weeks. During the hydrothermal treatment of FA with NaOH, most of the leachable metals have been dissolved into solution during the process and as such, there is no significant amount of metal leached into the process water treated by the synthesized zeolites.

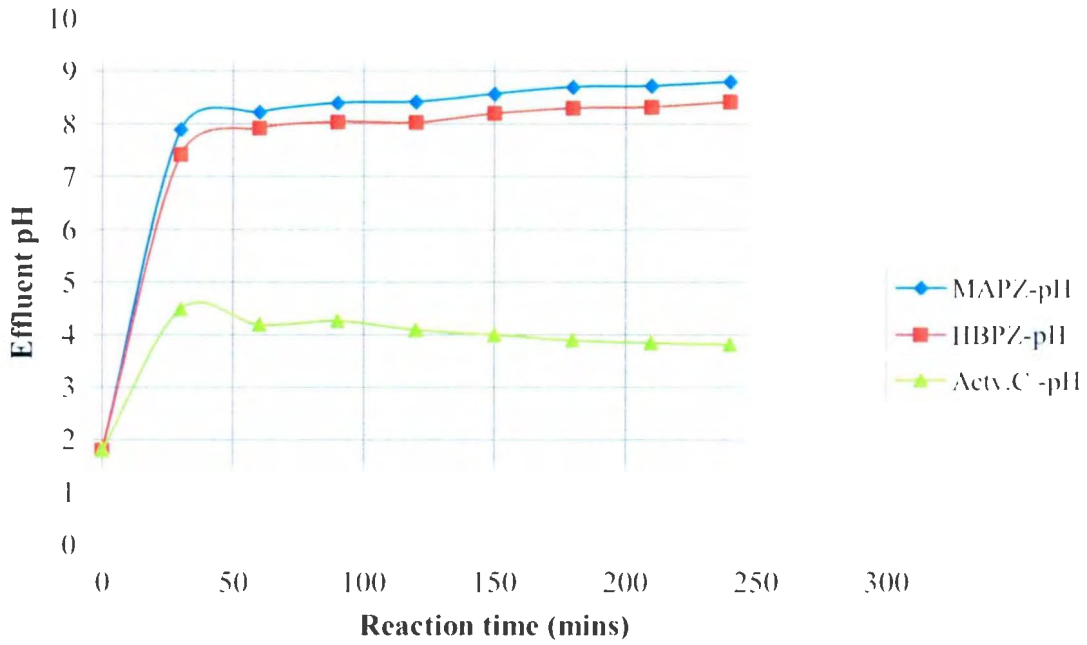

Figure 4.19: Effluent pH trend with time on neutralization with synthesized zeolites
NB: MAPZ represents MAP FA Zeolite treated AMD; Actv.C represents commercial activated carbon treated AMD and HBPZ represents HBP FA treated AMD

Table 4.14 and 4.15 respectively shows the effluent contaminant concentration and efficiency before and after treatment. A 200g L MAP–zeolite dose and 100g L of each of HBP – zeolite and commercial activated carbon were used for AMD treatment under the same condition of mixing. In comparison with equivalent doses of raw FA treated AMD, the modified ash samples (Zeolites) showed higher efficiency for contaminant removal (adsorption) than raw fly ash. Contaminant concentration in the raw AMD treated by raw and modified samples is quite different, therefore it is better to compare their removal efficiency rather than concentration of contaminants removed. The major contaminants, Fe and SO_4, are almost four times more concentrated in the raw AMD treated by the

zeolite compared to those treated by raw FA. MAP and HBP zeolite show a 99.79% Fe removal and more than 85% for SO_4 removal. Overall, the modified samples shows almost 80% efficiency with only copper leached into the solution while the raw FA sample shows average performance of 58-60% efficiency with leaching in such metals as Ca, Mg, Mo and Cu.

Table 4:14 Concentration of Contaminant in FA-Zeolite Treated Effluent Water

		Modified FA (Zeolite) Treatment			Raw FA Treatment		
	Raw AMD	HBPZ(100g/L)	MAPZ(200g/L)	AC Treated	Raw AMD	M N250	H N100
Mg	544	492.47	85.32	177.15	199	870	2.00
SO_4	38,202	5,047	3,179	<RL	10,922	7,736	8,820
Ca	761	728	320	238	951	1,262	692
Fe	18,058	37.80	37.54	869.74	4,853	<RL	<RL
Mn	104.50	0.86	0.25	13.63	40.98	4.49	0.08
Co	35.00	0.01	0.03	2.24	8.36	0.05	0.02
Ni	1,618	0.47	0.65	103.74	492	0.77	0.02
Mo	0.11	0.03	0.03	0.04	0.09	0.18	1.18
Zn	2.796	0.70	1.90	3.64	1.46	0.45	1.21
Cu	0.09	0.26	0.46	0.25	0.92	1.18	1.01
Hg	0.22	0.37	0.08	0.08	0.15	0.08	0.08
Pb	0.10	0.03	0.05	0.15	0.05	0.05	0.04

NB: HBPZ represents HBP FA Zeolite treated AMD; MAPZ represents MAP FA Zeolite treated AMD; AC represents commercial activated carbon treated AMD; M represents MAP FA sample; H represents HBP FA samples while N(x) stands for sample dosage in g/L e.g. HN20 stands for 20g of HBP FA/Liter of AMD.

Table 4.15 Percentage removal of contaminant with synthesized FA-Zeolite

	Synthesized Zeolite Treated AMD			Raw Ash Treated AMD	
	% contaminant removal			% contaminant removal	
	MAPZ(200g/L)	HBPZ(100g/L)	Actv.C(100g/L)	MAP(250g/L)	HBP(100g/L)
Fe	99.79	99.79	95.18	100	100
Mn	99.76	99.18	86.96	89.00	99.80
Co	99.91	99.97	93.59	99.00	99.81
Ni	99.96	99.97	93.59	100	100
Mg	84.31	9.47	67.43	L	99.03
SO_4	91.68	86.79	100.19	29.00	19.25
Ca	57.89	4.32	68.67	L	27.17
Mo	72.74	72.74	68.40	L	L
Hg	63.88	66.42	63.88	45.00	45.22
Pb	52.55	64.79	58.40	0.00	20.00
Zn	31.96	74.96	30.07	70.00	17.22
Cu	L	L	L	L	L

NB: L signifies metal leaching into the process water; HBPZ represents HBP FA Zeolite treated AMD; MAPZ represents MAP FA Zeolite treated AMD; AC represents commercial activated carbon treated AMD; M represents MAP FA sample; H represents HBP FA samples while N(x) stands for sample dosage in g/L e.g. HN20 stands for 20g of HBP FA/Liter of AMD.

The 100g/L dose of commercial activated carbon was used for AMD treatment. A result similar to the modified FAs was recorded but 100% SO_4 removal and its final effluent pH was low (below 4.0). This is an indication that commercial activated carbons are for SO_4 adsorption but unsuitable for AMD pH control (neutralization). In comparison with modified FA, it shows an overall removal efficiency of 75% which is below 80% recorded by modified FA (zeolite). Its efficiency in all contaminants other than SO_4 is less than modified FA efficiency.

4.5.4 Zeolite Efficiency

The overall efficiency of both modified FA in contaminant removal (using $\int - \{(C_1-C_2)/C_1\}^* 100$ as described in section 4.3.6.) was approximately 97% with almost complete removal of Fe, Ni, Co, Mn and SO_4 and leaching recorded only with Cu.

The final process water pH was 8.4 and 8.8 respectively for modified HBP and MAP FAs. The major difference between using the modified FAs and the raw FAs for AMD treatment was that there is no significant amount of metal leaching with modified FA treatment. The modified FAs removed a lager percent of SO_4. Furthermore the final process water pH of raw FA treated is higher than those treated by the modified FAs. These differences could be attributed to dissolution of the soluble alkaline compound from the modified FAs during hydrothermal process.

4.5.5 Optimization

This investigation was not extended to the effects of the hydrothermal reaction parameters such as hydrothermal process temperature, FA/NaOH ratio, caustic reagent molarity, fussion temperature, nucleation time and temperature, reaction time e.t.c... The dose of modified FAs used for AMD treatment was 100 g/L and 200 g/L of HBP and MAP respectively.

CHAPTER FIVE: CONCLUSSION AND RECOMMENDATION

5.1 Characterization

The physical, mineralogical, chemical and physicochemical characteristics of AV Cell fly and boiler ash was characterized for suitability in applications to adsorption, PRB, and neutralization. Potential applications in the areas of AMD treatment (neutralization and permeable reactive barrier) and zeolite application of neutralization residue were explored experimentally.

The FAs are of ASTM C618 class C with good pozzolanic properties and MLA analysis shows that these samples provide a rich source of SiO_2, CaO, and Al_2O_3 which are feedstock for zeolite synthesis. The analyzed FAs have high ratios of SiO_2/Al_2O_3 (ranges from 6.0 to 7.7) which are conducive to high performance zeolite.

The mineralogical and chemical analysis indicate FA particles are composed primarily of amorphous ferro-aluminosilicate, calcium-aluminosilicates, iron oxides, silicon oxides and aluminum oxides. These compounds are key species for adsorption applications.

The high pH of FA enhances adsorption and/or surface precipitation of metal cations and anions to its surface. The FA pH were in the ranges of 10.54 - 13.08 with buffering capacity of 0.5 - 4.9mmol/pH hence, suitable for AMD mitigation through neutralization and/or permeable reactive membrane (PRB).

The mitigation of CO_2 emissions through adsorption onto FA or fly ash modified material is a low cost and sustainable approach to CO_2 capture and control. The chemical make-up

and resulting adsorptive capacity of the fly ash studied make it a possible treatment option. The presence of cementing agent such as hydrated lime, quicklime, gypsum and clay indicated the ash could also be used in cement and concrete application.

In conclusion, there are a number of areas of alternative use for the fly-ash. The most promising and perhaps the most applicable in the natural resource context is use in mining effluent treatment/mitigation, cement/concrete application and carbon capture.

5.1.2 Treatment Application

In the second phase of this research we conducted laboratory scale experiments in the use of the FAs to mitigate acid mine drainage (AMD) from mine waste. The optimum FA dose for neutralization of AMD is 100g/L HBP FA and 250g/L MAP FA and the final pH of the treated AMD rose from approximately 2.0 to 12.4 and 9.2 respectively. Both samples showed high contaminant removal efficiency (> 90%) for Fe, Co, Mn and Ni. The impact on sulphate concentration in the AMD was difficult to evaluate due to the reactivity and solubility of the sulphate and formed soluble sulphate salts. However, the variation in sulphate concentration did not impact the final process water acidity. The synthesized zeolite effectively decontaminated AMD water with high overall contaminant removal efficiency (approximately 97%) and final pH of above 8.0 that remained stable over 11 weeks

The AMD was effectively treated when the FA was used as a PRB. A laboratory scaled reactive barrier column was constructed and AMD introduced at the top. Flow rates and residence times of the AMD in the column were 1860 cm^3/day and 7.5 hrs for MAP FA and 1440cm^3/day and 7.5 hour for HBP FA. Under these conditions, all contaminants of concern were completely removed from the AMD, and the final process water pH varied between 8.2 – 12.2 with leaching from Ca, Mg, Mo and Cu.

The mechanism of contaminate removal is proposed as; (i) solution pH increase due to alkaline species dissolving from FA to AMD, (ii) oxidation of Fe^{2+} and Al^{2+} to Fe^{3+} and Al^{3+} at low pH to circum-neutral pH and subsequent hydrolysis and precipitation as a separate phase (iii) adsorption of hydroxide of Ni, Cu Mn and Co onto the surface of FA at high pH (iv) co-precipitation of Cu, Zn and Co. Hence the major inorganic species Fe, SO_4, Mn, Ni, Co and Zn were removed probably through precipitation of amorphous oxides, oxy-hydroxides and hydroxyl-sulphates.

There are still challenges with respect to larger scale application of FA as a PRB and/or AMD neutralization agent. Saturation of pore spaces of the reactive barrier material with amorphous precipitates at high pH occurs and therefore the PRB design will need to be optimized to either eliminate or mitigate this issue. In terms of contaminant removal, the PRB and zeolite production are more efficient the use of the FA as a neutralization agent. Reuse of neutralization residue has proved successful in zeolite application therefore suggesting total continuous recycling of FA with neutralization process.

AMD treatment with FA provides a low cost, environmentally safe and beneficial use of what would be considered a waste.

5.1.3 Research Contribution

1. Mineralogically and chemically, most researchers have characterized and quantified various samples of FA using common techniques such as XRF, SEM,XRD, AND ICP-MS and/or ICP-OES. Using Mineral Liberation Analysis (MLA) technique has not been found from literature for FA characterization. MLA is a robust technique with inbuilt automated features for high degree of precision in studying physical, chemical and mineralogical characteristics of mineral grains exploration, processing and refining. The accurate and full characterization of FA is a critical step in development of alternative uses.

2. In addition, most FA neutralization application studies have not addressed the issue of the neutralization residue generated. Kumar et al., (2008) investigated using the solid residue generated from neutralization for backfill and construction materials. In this investigation new uses of solid residue generated from FA was been investigated for recycling in zeolite synthesis and proved successful as the modified FAs showed an improved adsorption properties.

3. Most published work on laboratory scaled PRB employed the use of synthetic (simulated) AMD for PRB purposes. For instance Komnitsas et al., (2004) investigated

the acidic leachate clean up with FA barriers by using simulated AMD. Another instance was using FA-bentonite mixtures as a reactive barrier (Muluken et al., 2010). This investigation considered the real site situations by using raw AMD for the study and possibility of less energy input to the PRB system. The vertical flow of AMD (under gravity) through barrier column could be cost effective due to less energy input (does not requires the service of pumps and vacuum). Operating parameters on larger scale must be investigated to address feasibility of the process.

4. A 50-50% by volume of FA: silica sand was studied in this research and time taken for partial and total blockage of the barrier pore spaces was reduced.

5.2 Recommendation for Future Studies

1. Future research could explore other suitable areas of FA applications such as binding, agglomeration and paste technology, CO_2 sequestration and capture, SO_2 and other toxic gas adsorption from effluent gases, cement and concrete applications. The analyzed FAs are of ASTM C618 class C with good pozzolanic properties therefore taking advantage of its cementitous characteristics to control the formation of acid mine drainage (AMD) from mine waste through binding and/or co-placement would be worthy of investigation and its final strength and compaction should be tested for backfill applications. Also cement and concrete application would require large volume of FA hence should also be investigated.

2. Long-term evaluation of PRB should also be studied with proper and adequate design to study the reactive barrier materials longevity to volumetric flow rate, residence time on contaminant removal, and final effluent pH. This research investigated a vertical flow gravity PRB design and therefore a horizontal system should also be studied which would require pumps, gates and other flow devices.

3. Scale-up for all proposed systems (PRB and neutralization) needs to be further explored as key issues may not present themselves on a small scale.

4. In the hydrothermal process for zeolite synthesis, the effect of ratios of caustic reagent, caustic molarity, fusion temperature, nucleation time, fusion temperature, reaction time etc... were not investigated and should be included for investigation in the future research. In addition the modified FA (zeolite) and the raw FA show high efficiency in heavy metals removal but less so for SO_4 ions while commercial activated carbon shows 100% efficiency in SO_4 removal but low efficiency in heavy metals removal. Possibly a small portion of activated carbon could be combined with the modified FA or raw FA to achieve better contaminant removal.

References

Amaratunga, L. M. and Yaschyshyn D.N (1997). Development of a high Modulus paste fill using fine gold mill tailings. *Geotechnical and Geological Engineering 1997. 15. School of Engineering, Agglomeration Research Group, Laurentian University, Sudbury, Ontario, P3E 2C6, Canada* , 206 - 211.

American Coal Association 'Coal Bottom Ash/Boiler Slag''2760 Eisenhower Avenue, Suite 304 Alexandria, Virginia 22314. Available at: http:/ www.tfhrc.gov hnr20/recycle waste cbabs1.htm.

Antonio G. S and Ayuso E.A. (2008). Soil remediation in mining polluted areas. *Conference of Soil remediation in mining polluted areas*, (pp. 76 - 82). Salamanca Spain.

Arenillas, A. et al., (2005). CO2 capture using some fly- ash derived carbon materials. *Fuel, Nottingham Fuel and Energy Center, School of Chemical , Environmental and Mining Engineering, University of Nottingham, University Park, Nottingham NG7 2RD, UK* , 2205-2207.

Association of Canadian Industries Recycling Coal Ash CIRCA. (2010). Origins and Applications Of Bottom Ash. *Origins and Applications Of Bottom Ash Technical Fact sheet # 9* , pp. 1-3.

Aube, B., P. Eng., M.A.Sc., (2004). The Science of Treating Acid Mine Drainage and Smelter Effluents. *361 Aumais, Ste-Anne-De-Bellevue, Quebec, H9X 4A9, Canada.*

Bably Prasad, and Robert J.G.M (2010). Treatment of Acid Mine Drainage Using Fly Ash Zeolite. *Journal of Water Air Soil Pollution. Central Institute of Mining and Fuel Research, Dhanbad 826015 Jharkhand, India. Email: drbablyprasad@yahoo.com* .

Behera, R. K. (2010). *Characterization of Fly Ash for their Effective Management and Utilization, Bachelor Thesis, National Institute of Technology.* Rourkela, Orissa.

Benner, S. G. et al., (1999). Geochemistry of a permeable Reactive Barrier for Metals and Acid Mine Drainage. *Journal of Environmental Science and Technology 33, 2793-2799, Department of Earth Sciences, University of Waterloo, Waterloo, Ontario, N2L 3G1 Canada.* , 2795 - 2798.

Bologo V. Maree J.P. and Zvinowanda (2009). Treatment of Acid Mine Drainage Using Magnesium Hydroxide. *International Mine Water Conference, Pretoria, South Africa.*

Carette, G.G. and Malhotra V.M. (1986). *Characterization of Canadian Fly ashes and their performance in Concrete.* Ottawa, Canada: Canadian Center for Mineral and energy Technology (CANMET). ISBN 0-660-12208-1.

Canadian Center for Occupational Health and safety (CCOHS), (1998). *Coal-Fired fly Ash Chemical Hazard Summary.* Hamilton: CCOHS. ISBN 0-660-12772-5.

Canadian Council of Ministers of the Environment (CCME), (2010). *A Review of the Current Canadian Legislative Framework for Wastewater Biosolids.* ISBN 978-1-896997-95-7 PDF

Chalkley, M. E. et al. (1989). Tailing and Effluent Management . *28th Annual Conference of Metallurgists Of CIM, Proceedings of the International Symposium, Volume 14* (pp. 11 - 19). Halifax: Pergamon Press. ISBN 0-08-037289-9.

Ciccu, R. et al., (2001). Heavy metal Immobilization Using Ash in Soils Contaminated by Mine Acitvities. *International Ash Utilization Symposium, Center for Applied Energy Research, University of Kentucky, USA.*

Claudia, B. et al., (2009). Zeolite Synthesized from fused Coal Fly Ash at Low Temperature Using Seawater for Crystallization. *Journal of Coal Combustion and Gasifification Products (CCGP)* , 7 - 12.

Coal-Bottom-Ash/Boiler-Slag. (May; 2010). Coal Bottom Ash/Boiler Slag; ''Material Description'' ' *available at: http:www.tfhrc.gov/hnr20/recycle/waste/cbabs1.htm downloaded on 17th of May; 2010.*

Davini, P. (1996). Investigation of the SO2 adsorption properties of Ca(OH)2 fly ash systems. *Fuel Vol. 75 No. 6, Chemical Engineering Department, Pisa University, 2 Via Diotisalvi, 56126 Pisa, Italy* , 714 - 716.

Diehl .S.F. et al (2003) Trace metals sources and their release from mine wastes: Examples from Humidity cell tests of hard rock mine waste and from warrior basin coal. *Presented at 2003 National Meeting of the American Society of Mining and Reclamation and 9th Billings Land Reclamation Symposium, Billing MT, June 3-6, Lexington, Kentucky, KY 40502.*

Elliott, A. and Mahmood T. (2005). A review of secondary sludge reduction technologies for the pulp and paper industry. *Paprican, 570 St. John's Boulevard, Pointe-Claire, Que., Canada H9R 3J9, Pulp Paper,. 79 (12): p. 49.*

Envis-Newsletter. (January 2006). *State of the Environment, Orissa: Fly Ash Management, Center for Environmental Studies N-3/56, IRC Village, Bhubaneswar-751015, Fores and Environment Department, Gorvernment of Orissa.* Orissa: Environmental Information System India.

EPA (2008), QAPP for the Characterization of Coal Combustion Residues; Appendix A, Quality Assurance Project Plan Category III/ Technology Development Final. *Contract No.EP-C-04-023, Work Assignment No.4-26.*

Feuerborn Hans-Joachim (2005) ''Coal Utilization over the world and in Europe'' *Workshop on Environmental and Health Aspects of Coal Ash Utilization*, International workshop, Tel-Aviv, Isreal.

Gitari, W.M. et al., (2010). Partitioning of major and traced inorganic contaminants in fly ash acid mine drainage derived solid residues. *International Journal of Environmental Science Technology 7 (3), 519 - 534* , 520-527.

Gitari, W.M. et al., (2005). Treatment of AMD with Fly Ash: Removal of Major, Minor Elements, SO4 and Utilization of the solid residues for Wastewater Treatment. *2005 World of Coal Ash (WOCA)*, (pp. 4-8). Lexington, Kentucky, USA.

Gonzalez A., Navia R. and Monero A. (2009). Fly Ashes from Coal and Petroleum Coke Combustion: Current and Innovative Potential Applications. *Waste Management and Research* , p. 977.

Headwater Resources Bulletin (Bulletin Number -16), Rev. 3/05. Fly Ash for Block Manufacturing, available at: *http://www.flyash.com data upimages press TB.16*.

Hellier William, W. (1998). Abatement of Acid Mine Drainage Pollution to Upper Three runs by Capping an Acid Producing Reclaimed Surface Mine With Fluidized Bed Combustion Fly Ash. *Department of Environmental Protection, Pennsylvania.*

Hewitt M. (2006) '' Jeddo Abandoned Mine Drainage Passive vs. Active Treatment Cost Estimates'' *Eastern Pennsylvania Coalition for Abandoned Mine Reclamation (EPCAMR),* Watershed Outreach Coordinator, available at : http://www.orangewaternetwork.org/storage/watersheds/Nescopeck_Watershed_Treatment_Appendix_B.pdf

Hohne, A. W. (2009). A Novel Approach To The Handling and Disposal of Caol Combustion Products. *2009 World of Coal Ash (WOCA)*, (pp. 1 - 7). Lexington, KY, USA.

James C. Hower et al., (2004) Major and Minor Element Distribution in Fly Ash from Coal-Fired Utility Boiler in Kentucky. *Energy Sources, Part A, 28: 79-95, University Of Kentucky, Center for Applied Energy Research, Lexington, Kentucky, USA.*

James, J. G. and Figueroa L.A. (2009). *Mitigation of Metal Mining Influenced Water Volume 2.* Littleton, Colorado: Society for Mining , Metallurgy, and Exploration, Inc. ISBN 13: 978-0-87335-270-3.

Jang, A. and Kim IN S. (2000). Technical Note on Solidification and Stabilization of Pb, Zn, Cd, and Cu In Tailing Wastes Using Cement and Fly Ash. *Journal of Minerals Engineering Vol. 13, Department of Environmental Science & Engineering, Kwangju Institute of Science and Technology, 1 Oryong-dong, Puk-gu, Kwangju 500-712, Korea* , 1660-1661.

Karthik, Obla. Ph.D., P.E (2009). *Fly Ash Concrete with Acceptable performance , Managing Director, Research and Materials Engineering, NRMCA, funded by The Department of Energy's Combustion Bye-products Research Consortium (West Virginia University).* (West Virginia University) USA.

Keka O., Pradhan N.C. and Samanta N.A. (2004) Zeolite from Fly Ash: Synthesis and Characterization. *Department of Chemical Engineering, Indian Institute of Technology, Kharagpur 721 302, India. Bulletin of Material Science, Volume 27, No.6, P 555-564.*

Kelley A. Reynolds and Leslie Petrik; ''The use of Fly Ash for the Control and Treatment of Acid Mine Drainage'' *Eskom Holdings, R&S Division, CR &D Department, Private Bag 40175, Cleveland, 2022, Johannesburg, SA. Email: Kelley.reynolds@eskom.co.za.*

Komnitsas K. Bartzas G. and Paspaliaris (2004). Clean up of Acidic Lachates Using fly Ash Barriers: Laboratory Column Studies. *The International Journal Vol.6 No. 1, Technical University of Crete, Department of Mineral Resources Engineering , 73 100 Chania, Greece* , 82 - 87.

Kumar, V. R. et al., (2008). Neutralization of acid Mine Drainange using fly ash, and strenght devlopment of the resulting solid residues. *South African Journal of Science 104*, 317-319.

Kuyucak N. (2006). Selecting Suitable Methods For Treating Minning Effluents. Prepared for the *''PerCan Mine Closure'', pp. 1-30., Golder Associate Limited, Kanata, Ontario K2K 2A9, Canada*

Matsi, T. and Keramidas V.Z. (1999). Fly ash application on two soils and its effect on soil salinity, pH, B, P and on ryegrass growth and composition. *Journal of Environmental pollution 104 , Soil Science Laboratory, Aristotle University, Thessaloniki, 54006, Greece* , 108-111.

McCubbin Neil (1983). *The Basic Technology of The Pulp and Paper IndustrY and Its Environmental Protection Practices.* Ottawa, Ontario Canada: Environmental Protection Services, Environment Canada.ISBN 0-662-12850-8.

Min, L. et al., (2004). Characterization of Solid Residues from Municipal Solid Waste Incinirator. *State Key Laboratory of Coal Combustion, Huazhong University of Science and Technology, Power Engineering, 430074 Wuhan, Hubei, China.*

Misra, M., Yang K. And Mehta R.K. (1996). Application of fly ash in the agglomeration of Reactive Mine Tailings. *Journal of Hazardous Materials 51 (1996), Department of Chemical and Metallurgical Engineering/MS 170 Mackay School of Mines, University of Nevada, Reno, NV 89557, USA* , 182- 191.

Moutsatsou A. et al., (2006), ''The Utilization of Ca-rich and Ca-Si- rich fly ashes in Zeolite production.'' *Laboratory of Inorganic and Analytical chemistry, Deparment of Chemical Engineering , National Technical University of Athens, 9Iroom polytechnoustr. 15780, Athens Greece.*

Muduli, S.D., Nayak B.D and Dhal N.k. (2009), CO2 Sequestration Through Mineral Carbonation of Fly Ash and its Use in Agriculture, *Institute of Minerals and Materials Technology, Bhubaneswar. Email: surabhidipali@gmail.com.* Institute of Minerals and Materials Technology, Bhubaneswar.

Muluken, B.Y., Shang J. Q. And Ernest K.Y. (2010). Feasibility of using Coal Fly Ash for Mine Waste Containment. *Journal of Environmental Engineering, Department of Civil and Environmental Engineering Universty of West Ontario London, Ontario Canada N6A 5B9* , 683 - 686.

Muluken, B.Y., Shang J. Q. And Ernest K.Y. (2009). Chemical and Mineralogical Transformations of Coal Fly Ash after Landfilling. *2009 World of Coal Ash (WOCA) Conference*, (pp. 4-6). Lexington, KY, USA.

Muluken, B.Y., Shang J. Q. And Ernest K.Y. (2009). 'Long-term evaluation of Coal fly ash with mine tailings co-placement: A site-specific study'. *Journal of Environmental Engineering, Department of Civil and Environmental Engineering Universty of West Ontario London, Ontario Canada N6A 5B9* , 683 - 686.

Nature'swayResources. *Nature's way Resources ''Boiler Ash'' Available at: http://www.natureswayresource.com.* Texas : 101 Sherbrook Circle, Conroe, Texas 77385-7750, (9360)321-6990 Metro, (936)273-1200 Conroe. Fax (936) 273-1655.

Paine, P. (1987). Historic and Geographic Overview of AMD. *Proceedings Acid Mine Drainage Seminar/Workshop* (pp. 22, 40 - 41). Citadel Inn, Halifax Nova Scotia: Minister of Supply and Services Canada. ISBN 0-662-55005-6.

Papandedreou A., Strournaras C. J., and Panias D. (2007),''Copper and Cadmium adsorption on Pellets made from fired coal fly ash.''*CERECO S.A. Journal of Harzadous Materials, 148(2007) 538-547, Ceramics and Refractories Technological Development company, 72nd km. Of Athens-Lamia National Rd, P.O.Box 18946, 34100 Chalkida, Greece.*

Paya J. et al., (2002) Loss on Ignition and Carbon Content in Pulverized Fuel Ashes (PFA): two crucial parameters for quality control. *Journal of Chemical Technology and Biotechnology, Vol. 77: 251-255.*

Paya J. et al., (1998) Thermogravimetric Methods for Determining Carbon Content in Fly Ashes. *Journal of Cement and Concrete Research, Vol.28, No. 5, pp. 675-686.*

Reynolds K.A and Petrik, L. The use of Fly Ash for the Control and Treatment of Acid Mine Drainage. *Eskom Holdings, R&S Division, CR &D Department, Private Bag 40175, Cleveland, 2022, Johannesburg, SA. Email: Kelley.reynolds@eskom.co.za.*

Phelps J.T., Roh Y. and Roberts J.L (2204). Biogeochemical Processes Utilizing Fly Ash for Carbon Sequestration. *Environmental Science Division, Oak Ridge National Laboratory, Oak Ridge TN 37831-6036. Email: phelpstj@ornl.gov; 865-574-7290.*

Pierre D., Frederic V., and Manuel P, (2004), ''Surface area, Porosity and Water adsorption properties of fine Volcanic Ash Particles''*Bulletin Volcanol Vol. 67: pp. 160-169. Department of Earth & Environmental Sciences, Universite Libre de Bruxelles, Ave. F. Roosevelt 50, B-1050 Brussels, Belgium.*

Piyush K.P. and Raj K.A. (2002). Utilization of mixed pond ash in integrated steel plant for manufacturing superior quality bricks. *Building and Material Science, Vol 25 No 5, Bhilai Institute of Technology, Bhilai House, Durg 491 002, India* , 444 - 446.

Pond P.A. et al., (2005) Accelerated Weathering of Biosolid-Amended Copper Mine Tailings. *Department of Soil, Water, and Environmental Science, University of Arizona, 429 Shantz Building #38, Tuscon AZ 85721.*

Querol, X. et al. (2002). Application of Zeolitic Material Synthesized from fly Ash to the decontamination of waste Water and flue Gas. *Journal of Chemical Technology and Biotechnology* , 292-298.

Querol, X. et al. (1999) Synthesis of Zeolites from Fy Ash in a Pilot Plant Scale. Examples of Potential Environmental Applications. *International Ash Utilzation Symposium, Centre for Applied Energy Research, University of Kentucky, USA.*

Ram L. C. and Masto R.E. (2010). An Appraisal of the potential use of fly ash for reclaiming coal mine spoil. *Journal of Environmental Management. Environmental Management Division, Central Institute of Mining and Fuel Research (Digwadih Campus), PO: FRI, Dhanbad, Jharkand 828108, India.*

Rao, M., Parwate A.V. and Bhole A.G. (2002). Removal of Cr6+ and Ni2+ from aqueous solution Using Bagasse and fly ash. Journal of Waste Management Vol. 22, pp. 821-830. *Civil Engineering Department, College of Engineering, Badnera 444 701, Maharashtra, India.*

Reid, I. (1998.). *Pulp Paper Canada, 99(4).*

Rios C.A, Williams C.D, and Roberts C.L (2007). Removal of heavy metals from acid mine drainage (AMD) using coal fly ash, natural clinker and synthesis zeolites. *Journal of Hazardous Material, Escuela de Geologia, Universidad Industrial de Santander, A.A 678, Bucaramanga, Colombia.*

RENEL (Romanian Energy and Electricity Authority). (1994). *Ash Handling, Disposal, and Ash Pile Remediation at Romanian Coal fired power Plants., US Agency for International Development.* San Francisco, California: Bechtel Corporation.

Rio Algom (1997), MEND PROJECT. *Characterization and stability of acid mine drainage treatment sludges. Kidd Creek division of Falconbridge Ltd,* Energy Mines and Resources Canada.

Roberts M.B. et al., (2010). Removal of Lead from Contaminated Water. *International Journal of Soil, Sediment and water: Vol.3: Iss. 2, Aticle 14.* , 4-5.

Saponaro A., Cumbo D. and Gazzino M. (2007). Mild Coal - Combustion Technology for Future Zero Emission Power Plant. *Italian Section of the Combustion Institute*, (pp. 1 - 4).

Sarkar, A. Rano R. and Kumar A. (2010,). Characterization of High Carbon Ash From Thermal Power Station Using Pulverized Fuel Combustor. *Energy Sources Part A: Recovery, Utilization and Environmental Effects"* , pp. 607 - 619.

Scott .J. et al., (2005). Landfill Management, Leachate generation, and Leach Testing of Solid Wastes in Australia and Overseas. *Critical Reviews In Environmental Science and Technology* , pp. 239, 241 - 246.

Skousen, J., Hilton T. and Faulkner B. (1997). Overview of Acid Mine Drainage Treatment with Chemicals. *Downloaded from Agricultural & Natural Resources Development Home Page, West Virginia University Extension Service* .

Sinclair, R. (2006). An Analysis of Resource Recovery Opportunities in Canada and the Projection of Greenhouse Gas Emission Implications. *Minerals and Metals Sector, NRCan* , pp. 227 - 258.

Solanki, P., Gupta V. and Ruchi K. (2010). Synthesis of Zeolite from Fly Ash and Removal of Heavy Metal Ions from Newly Synthesized Zeolite. *E-Journal Of Chemistry*, 1201-1205.

Somerset V. *et al* (2005), ''Acid Mine Drainage Transformation of Fly Ash into Zeolitic Crystalline phases'' *Department of Chemistry, University of Western Cape, Private Bag x17, Bellville 7535, South Africa*

Somerset V.S. et al (2004), ''Alkaline Hydrothermal Zeolites Synthesized from Fly Ash SiO_2 And Al_2O_3'' *Department of Chemistry, University of the Western Cape, Private Bag X 17, Bellville.vsomerset@uwc.ac.za.*

Sturn, J. W. (1987). Materials handling for Mine Spoils and Coal Refuse. *Proceedings Acid Mine Drainage Seminal/Workshop*, (pp. 321 - 355). Citadel Inn, Halifax, Nova Scotia.

Storm-and-Wastewater,. (2003). *Biosolids Management Programs.* Federation of Canadian Municipalities.

Tarun R. Naik, Ph.D., P.E. and Singh S.S. (1993). Fly Ash Generation and Utilization - An Overview. *Department of Civil Engineering and Mechanics, College of Engineering and Applied Science, The University of Wisconsin-Milwaukee, P.O.Box 784, Milwaukee, WI 53201.*

Teong, L.K, Bhatia S. and Mohamed A.R (2003). Preparation and Characterization of adsorbent prepared from coal fly ash for Sulphur dioxide (SO2) Removal. *School of Chemical Engineering, Engineering Campus, University Sains Malaysia, Seri Ampangan, 14300, Nibong Tebal, Seberang Perai, Penang, Malaysia.*

Usmen, M. (1988). ''Disposal and Utilization of Electric Utility Wastes''. *American Society of Civil Engineers, in conjunction with the ASCE National Convention, Nashville, Tennessee. 345 East 47th Street, New York 10017-2398.* , pp. Pg.36-37. ISBN 0-87262-642-3.

Wang, H. et al., (2006). Utilization of Antikokan Coal Fly Ash in acid rock drainage control from Musselwhite Mine Tailings. ' *Department of Civil and Environmental Engineering, the University of Western Ontario, London, ON N6A 5b9, Canada.*

Wang, S. and Wu h. (2006). Environmental-benign Utilization of fly ash as low cost adsorbents. *Journal of Hazardous Materials, 2006. 136(3), Department of Chemical Engineering, Curtin University of Technology, GPO Box U1987, Perth, WA 6845, Australia* .

Wang H.J. et al (2009). Application of Coal Fly Ash to replace Lime in the management of Reactive mine tailings. *Department of Civil and Environmental Engineering, the University of Western Ontario, London, ON N6A 5b9, Canada.'' Appropriate Technology for Environ mental Protection in the Developing World.*

Webber, M.D. and Sidhwa P, (2010). *Land application of sewage biosolids: Are Canadian trace metal guidelines/regulations over-protective for crop production?* Burlington,: Webber Environmental, 590 Barons Court, Burlington, ON L7R 4E4, Canada.

Wigley F. and WilliamsonWilliamson, J. (2005). *Coal Mineral Transformations - Effects on Boiler Ash Behaviour.* Imperial College of Science, Technology and Medicine, Department of materials , London.

Younger P.L., Banwart S.A. and Hedin R.S. (2002). *Mine Water hydrology, Pollution, Remediation* . Pittsburgh, USA: Kluwer Academic Publishers. ISBN 1-4020-0137-1

Zhou Y.F and Haynes J.R. (2010) 'Sorption of Heavy Metals by Inorganic and Organic Components of Solid Wastes: Significance to Use of Low-Cost Adsorbents and Immobilizing Agents'*Critical Reviews In Evironmental Science and Technology, 40: 11, 909-977.*

Zouboulis A.I. and Mavros. Z. (1992). 'Use of Fly Ash for the Removal of Nickel Ions from Wastewaters. *Fresenius Environmental Bulletin 1: 382-387., Department of Chemistry, Aristotle University, GR-540 06 Thessaloniki, Greece.*

APPENDIX

APPENDIX A : X-ray Diffraction of FAs, FA-Zeolites and the Permeable Reactive Barrier Residues

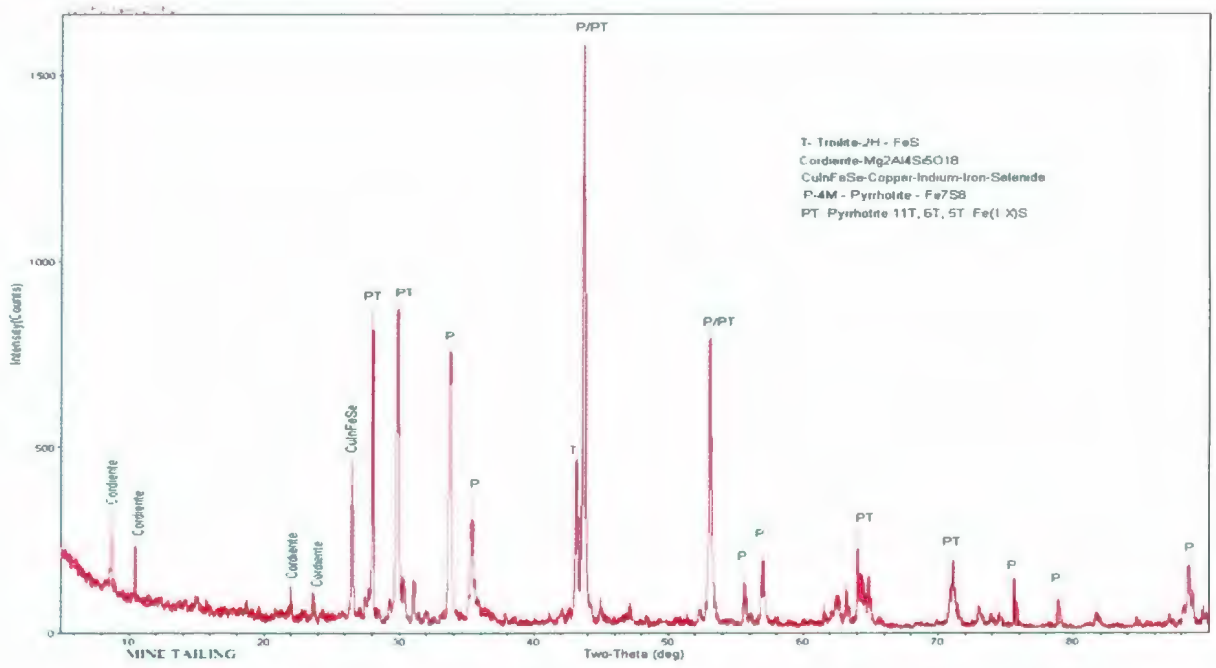

Figure A-1: XRD Micrographs showing different mineral phases for the Mine Tailing

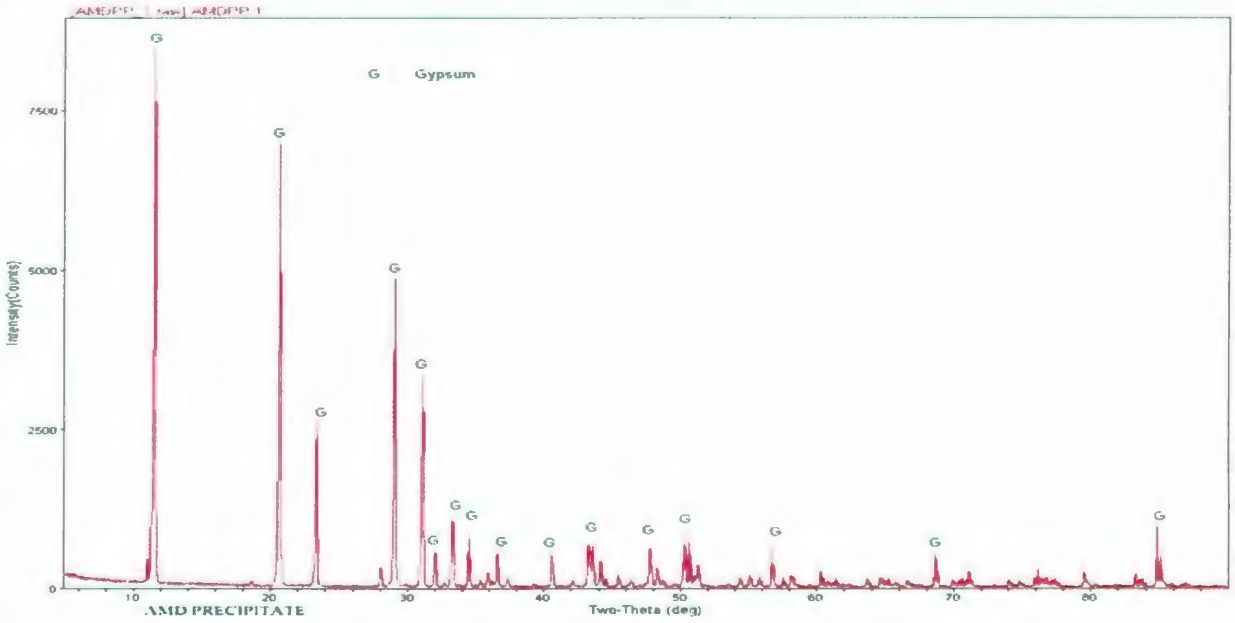

Figure A-2: XRD Micrographs showing different mineral phases for the AMD Precipitate

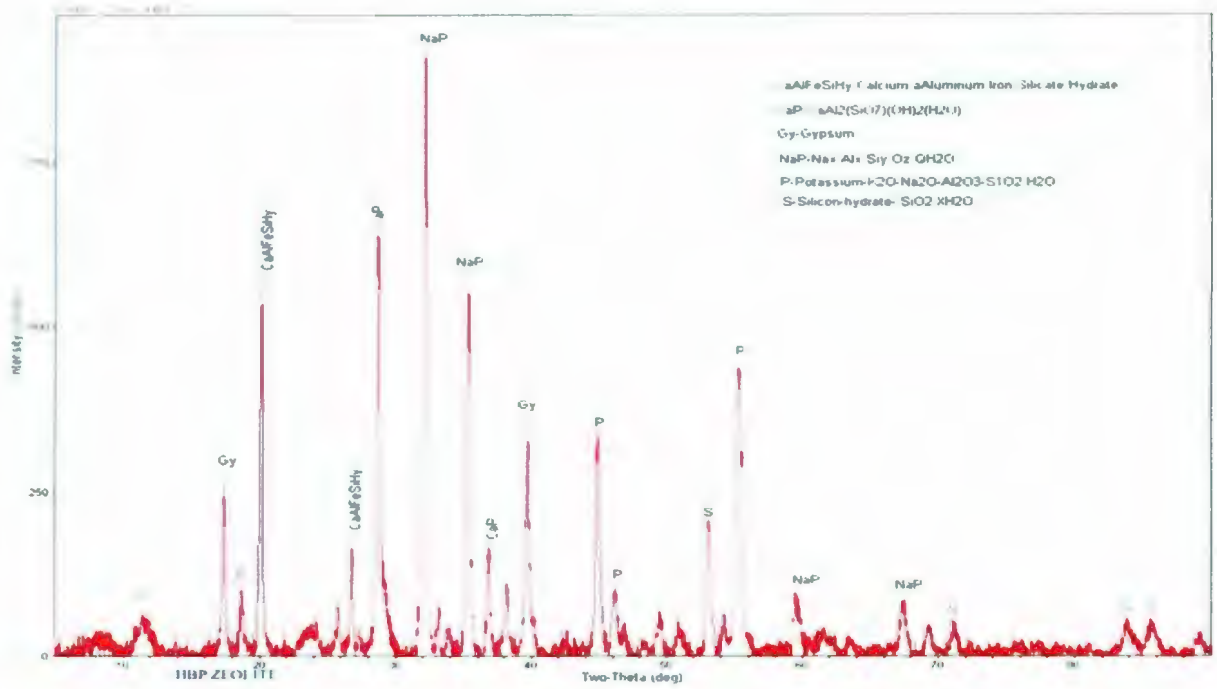

Figure A-3: XRD Micrographs showing different mineral phases for the HBP-Zeolite

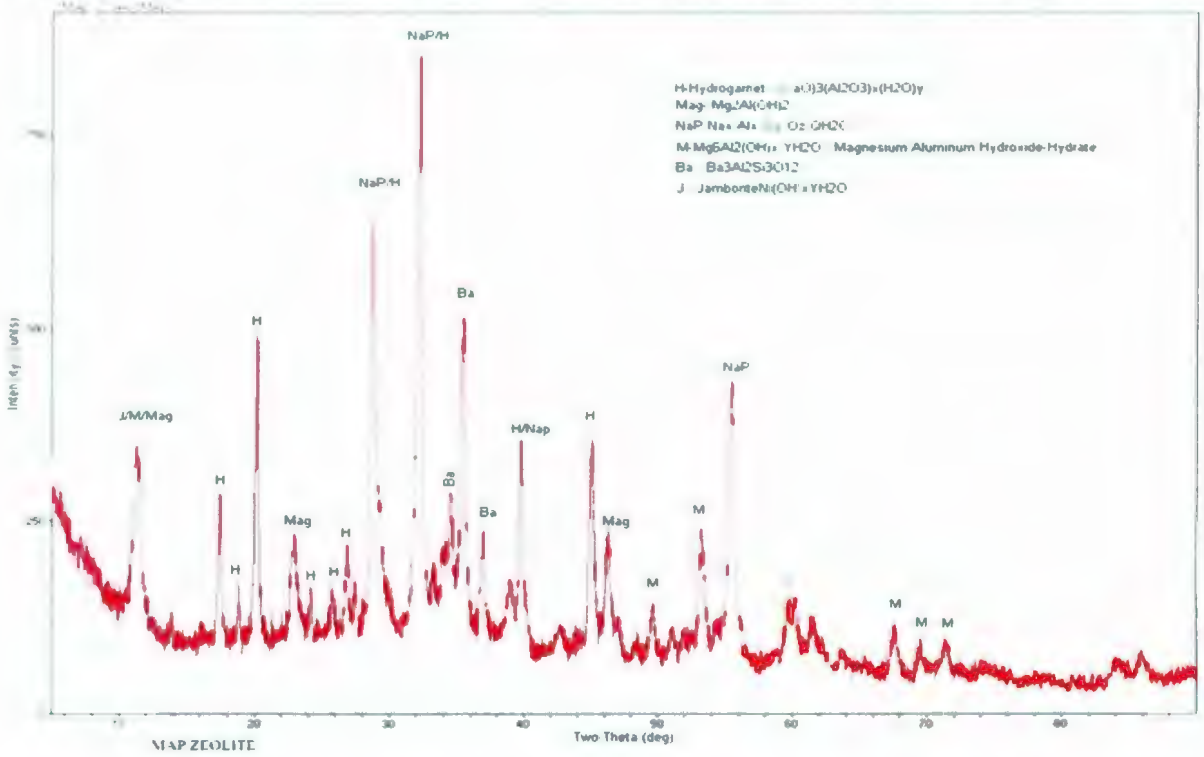

Figure A-4: XRD Micrographs showing different mineral phases for the MAP - Zeolite

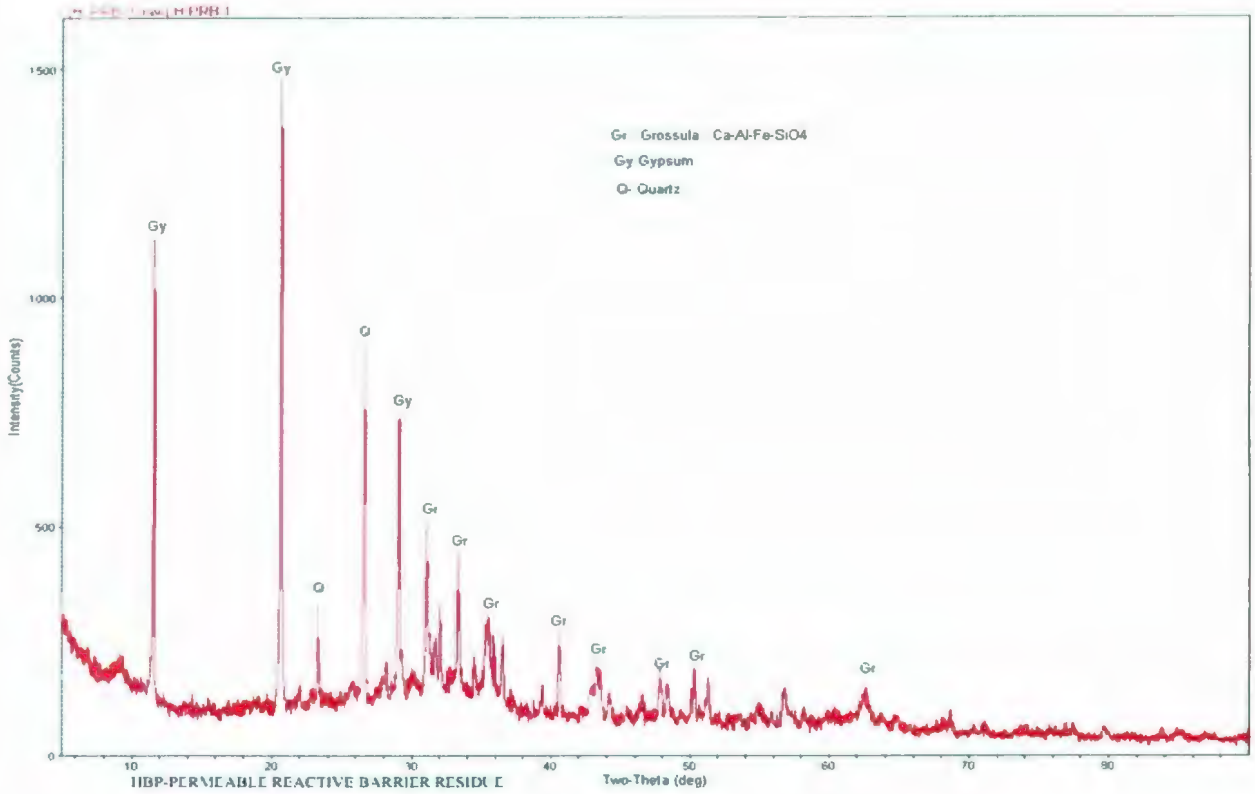

Figure A-5: XRD Micrographs showing different mineral phases for the HBP- PRB-Resisdues

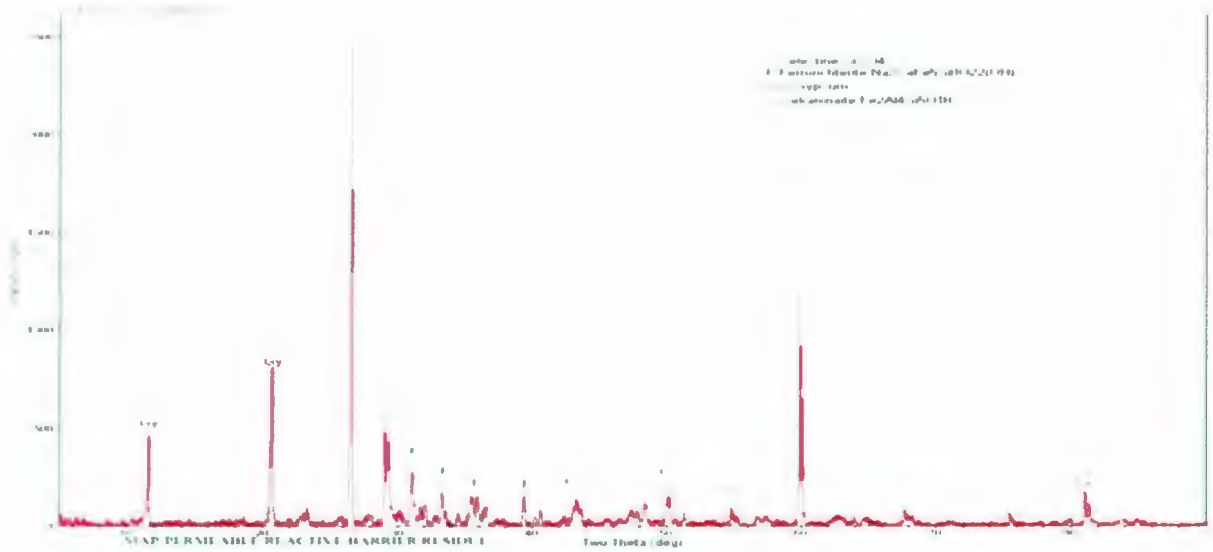

Figure A-6: XRD Micrographs showing different mineral phases for the MAP- PRB-Resisdues

APPENDIX B: Volume of gas (at STP) sorbed during N adsorption and desorption at 77K vs. Relative pressure *P/Po* for HBP FA, HBP-Zeolite, MAP FAand MAP-Zeolite

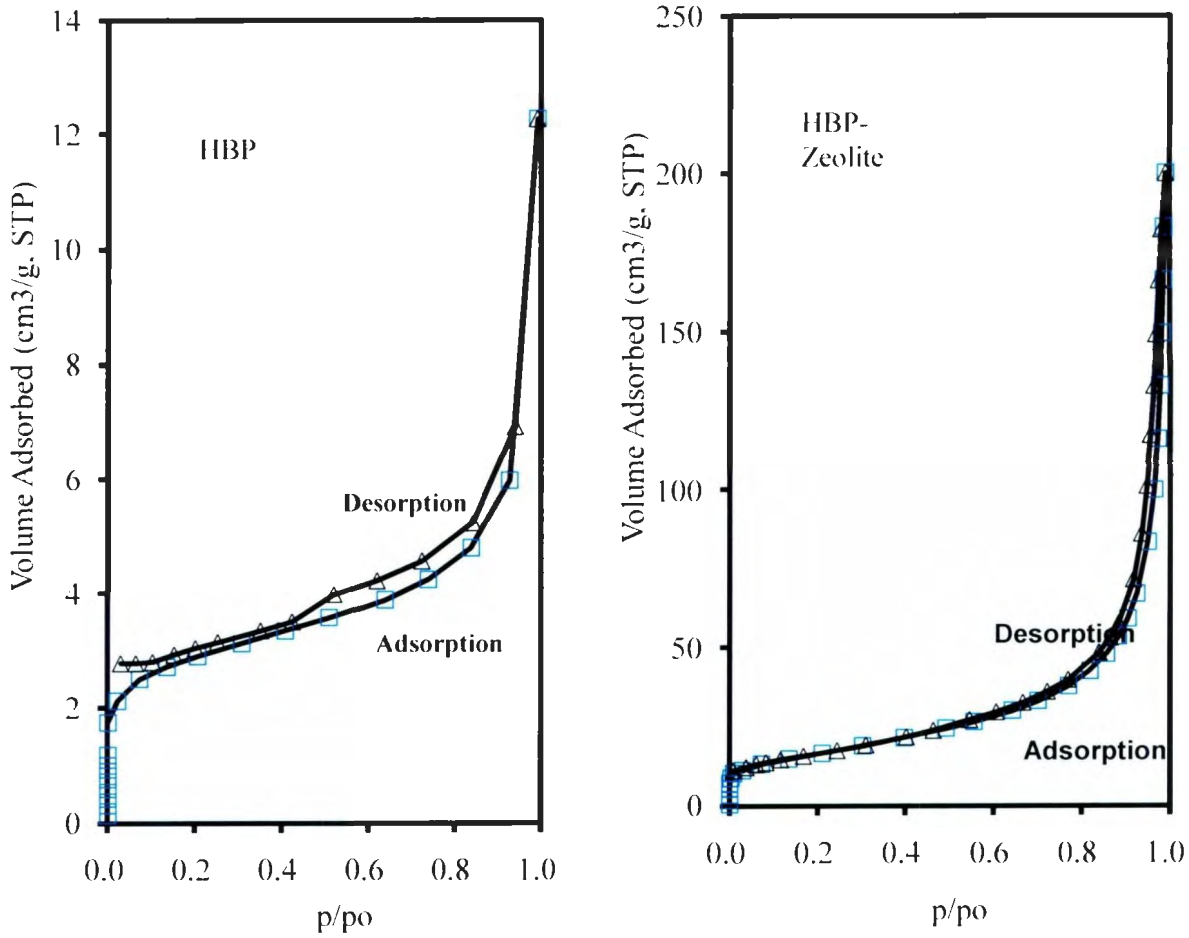

Figure B - 1: Volume of gas (at STP) sorbed during N adsorption and desorption at 77K vs. Relative pressure *P/Po* for HBP FA and HBP-Zeolite.

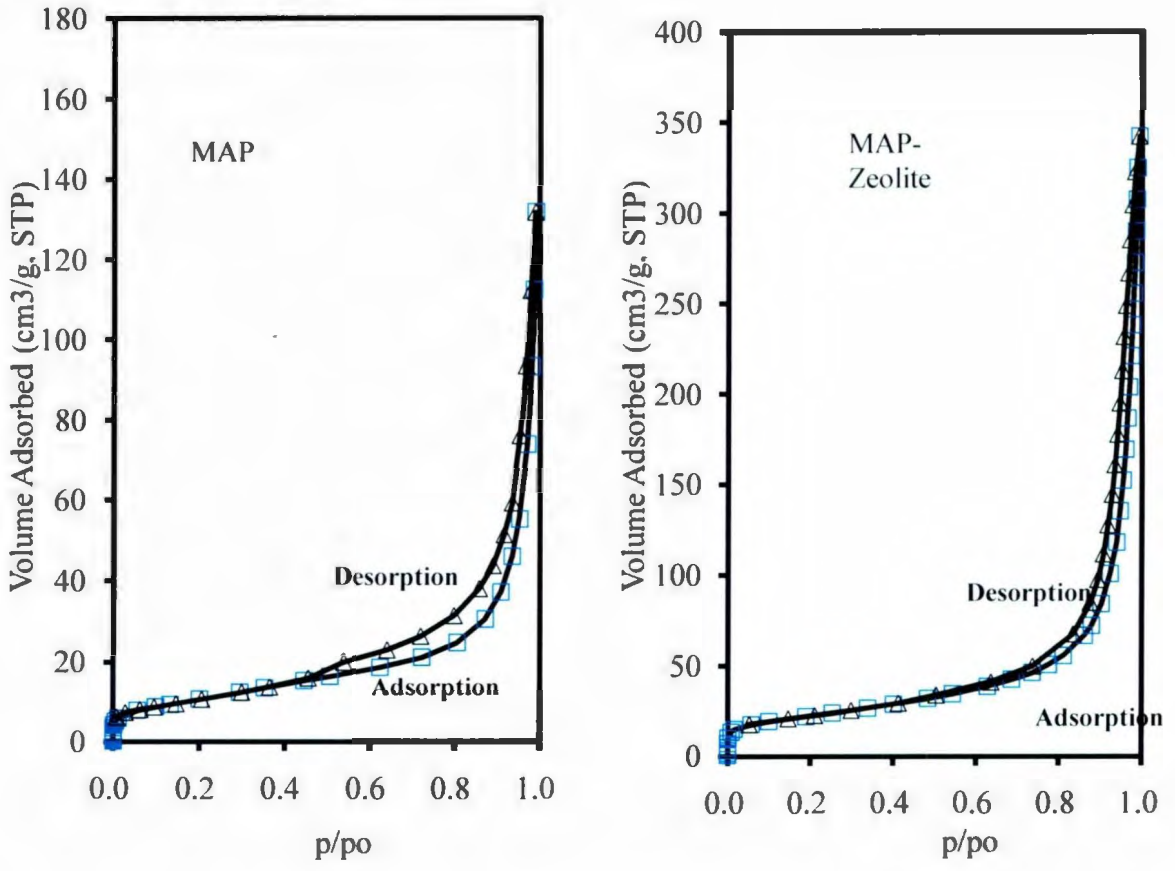

Figure B - 1: Volume of gas (at STP) sorbed during N adsorption and desorption at 77K vs. Relative pressure *P/Po* for MAP FA and MAP-Zeolite.

Table B-1. Textural properties showing improved surface area and pore volumes.

Sample	S_{BET} (cm^2/g)	Total pore volume, V_t from P/P_o=0.99 (cm^3/g)
Map	3.934×10^4	0.199
Map-zeolite	7.938×10^5	0.503
HBP	1.01×10^4	0.019
HBP-zeolite	5.853×10^5	0.295

APPENDIX C: Morphological structure of FA and Zeolite particles with SEM

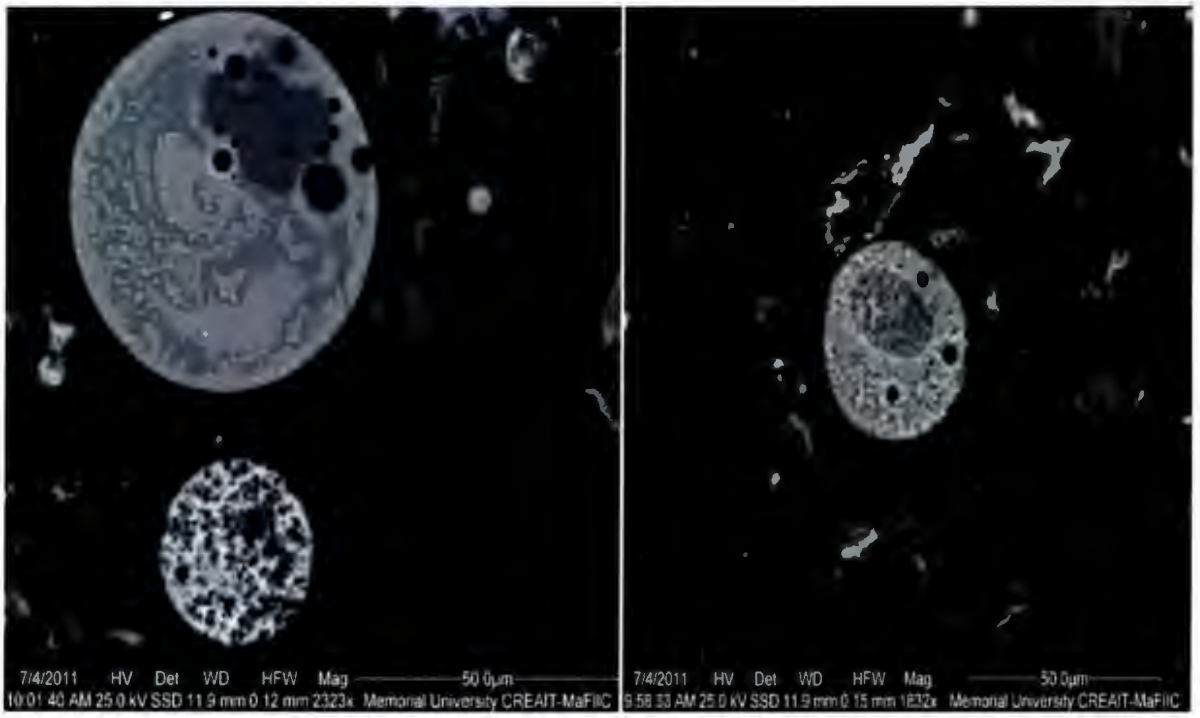

Figure C-1: HBP FA Morphology (50µm)

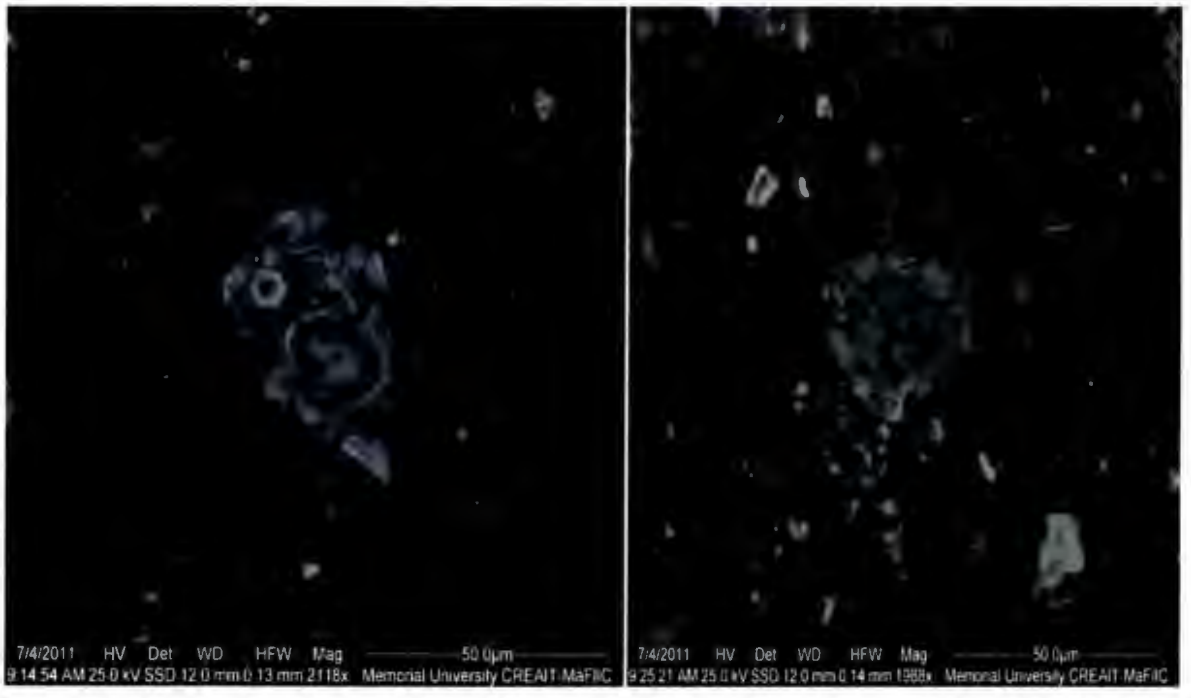

Figure C-2: HBP -Zeolite Morphology (50µm)

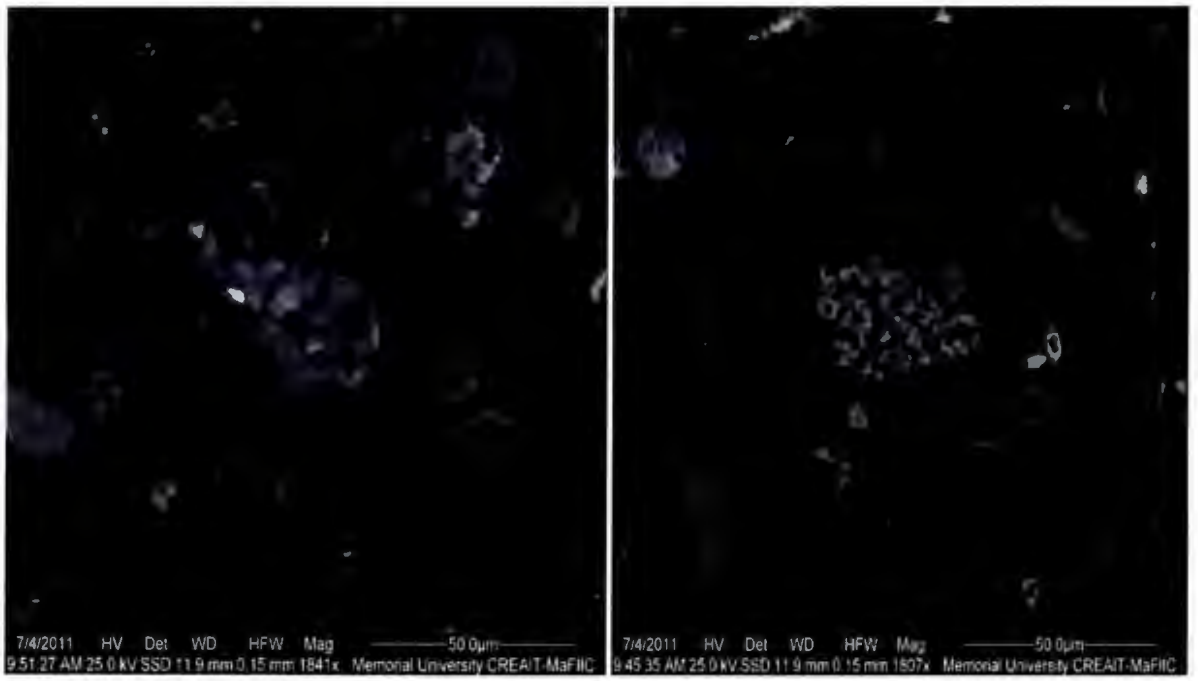

Figure C-3: MAP FA Morphology (50µm)

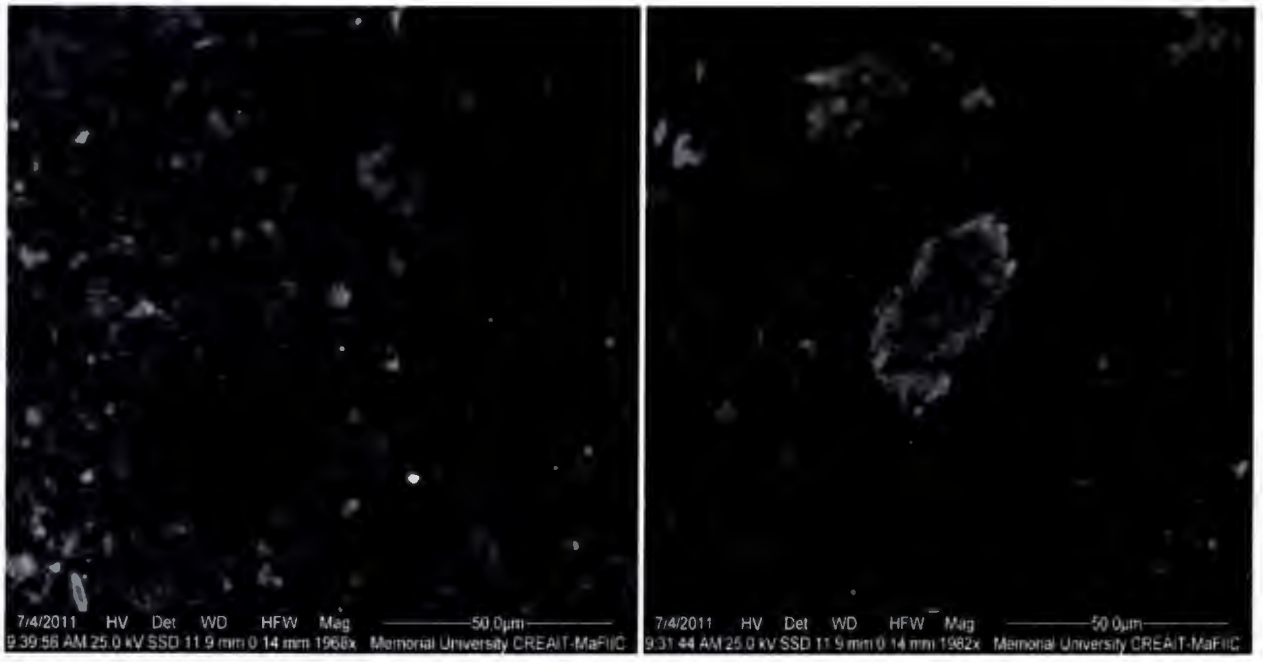

Figure C-4: MAP -Zeolite Morphology (50µm)

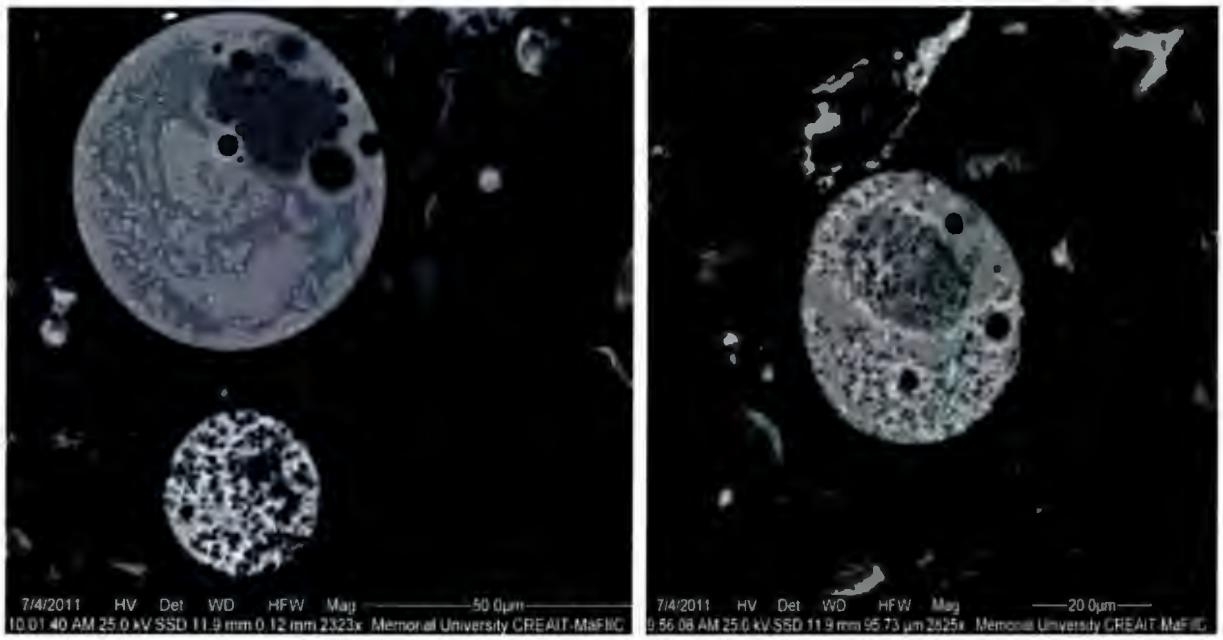

Figure C-5: HBP FA Morphology (20µm)

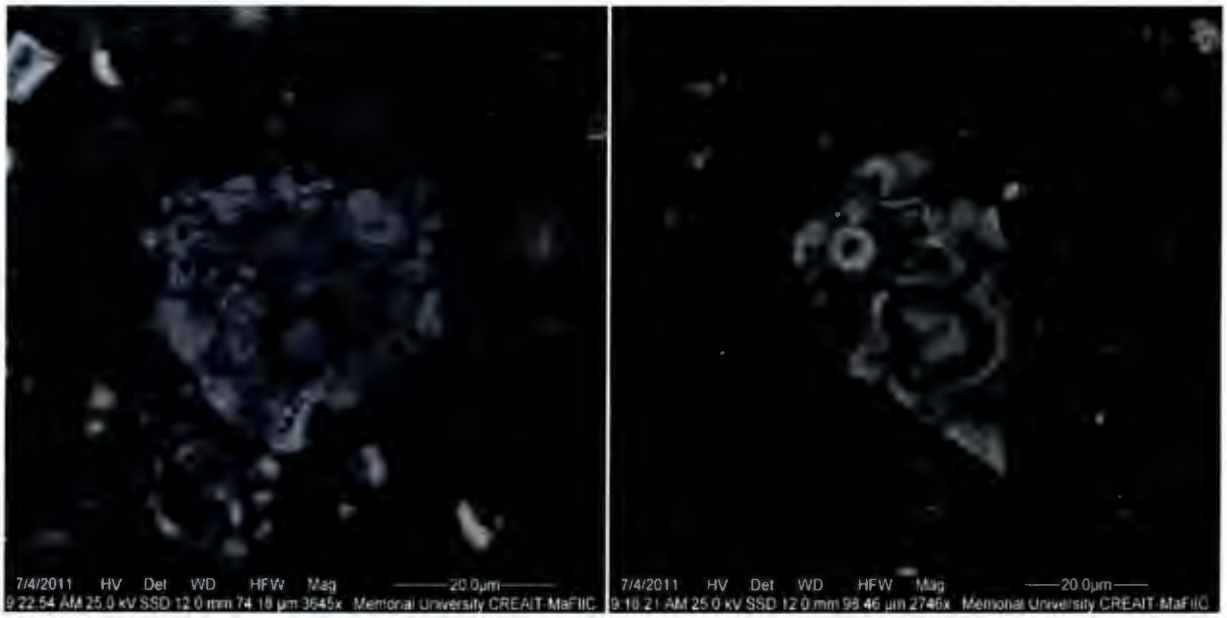

Figure C-6: HBP Zeolite Morphology (20µm)

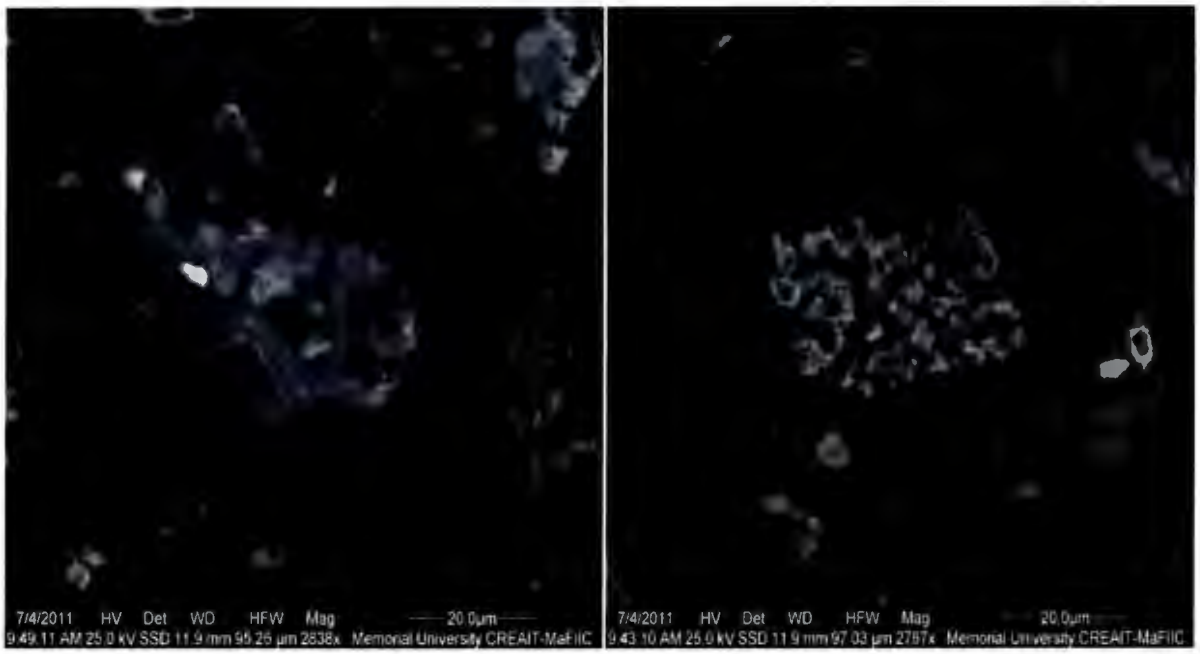

Figure C-7: MAP FA Morphology (20µm)

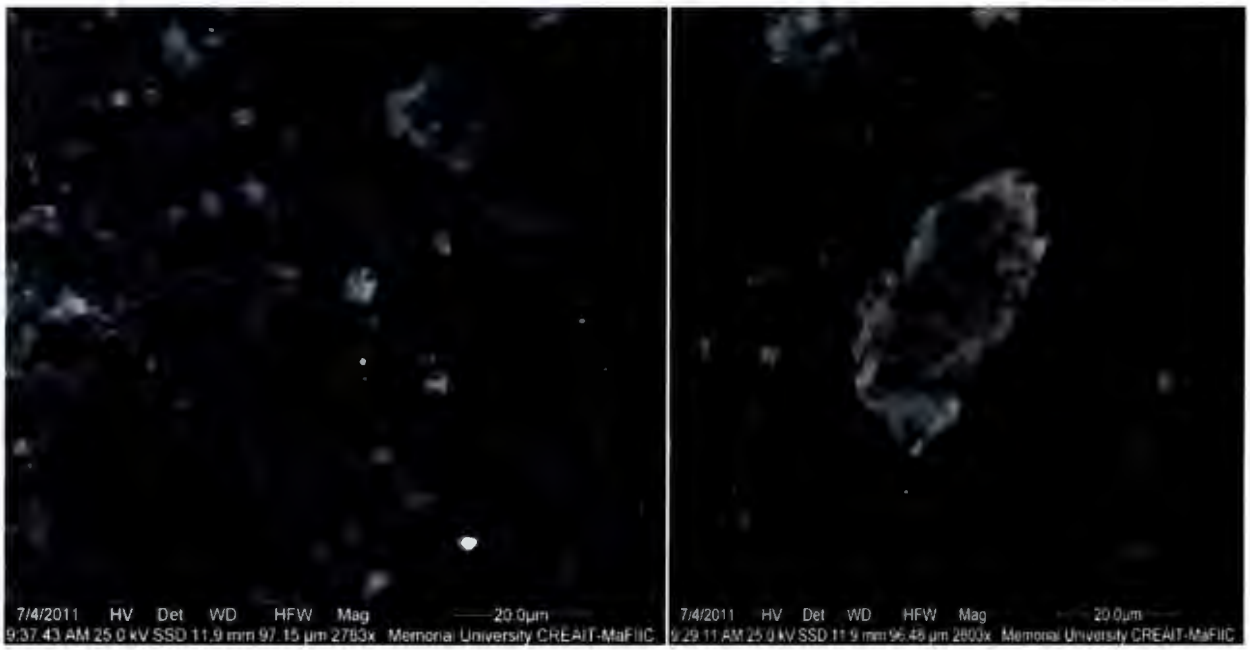

Figure C-8: MAP Zeolite Morphology (20µm)

APPENDIX D: TGA Thermogravimetric curve showing decomposition (%wt. change) of the ash sample with temperature and temperature derivative curve.

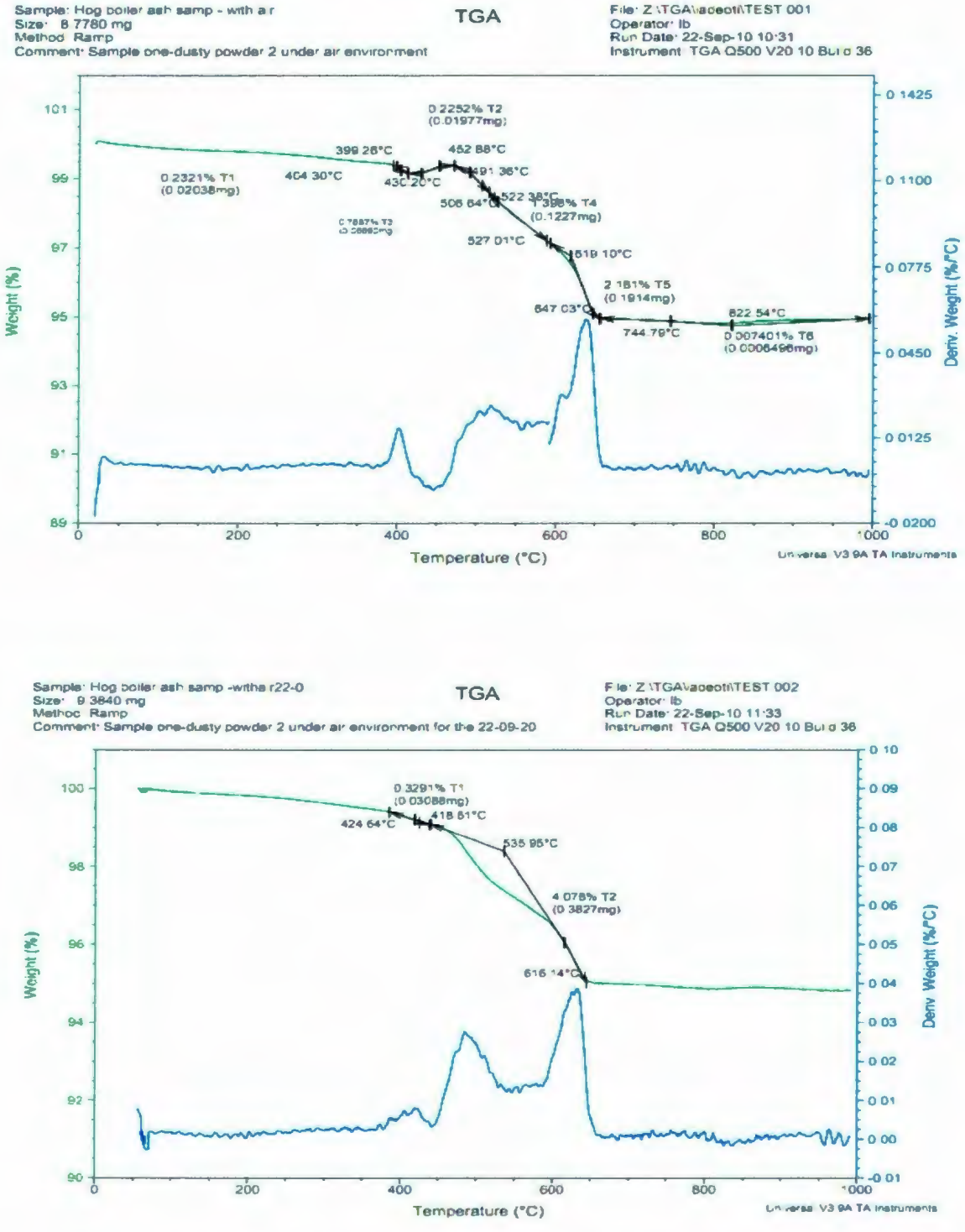

Figure D-1: Conventional TGA Method for HBP FA

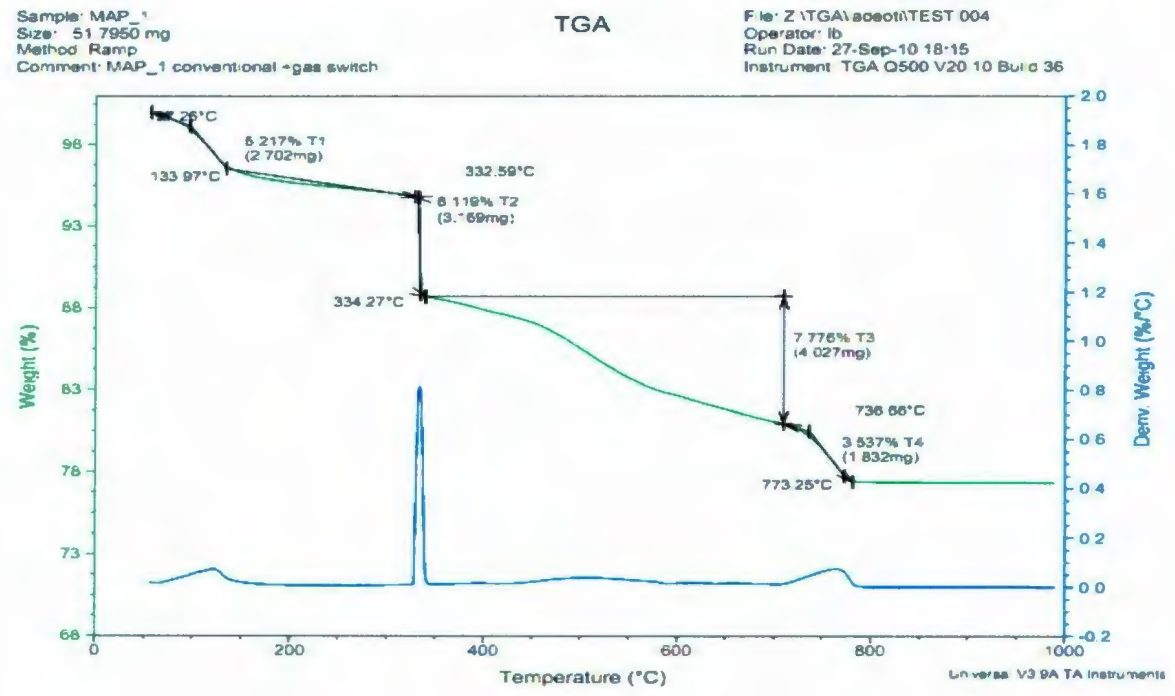

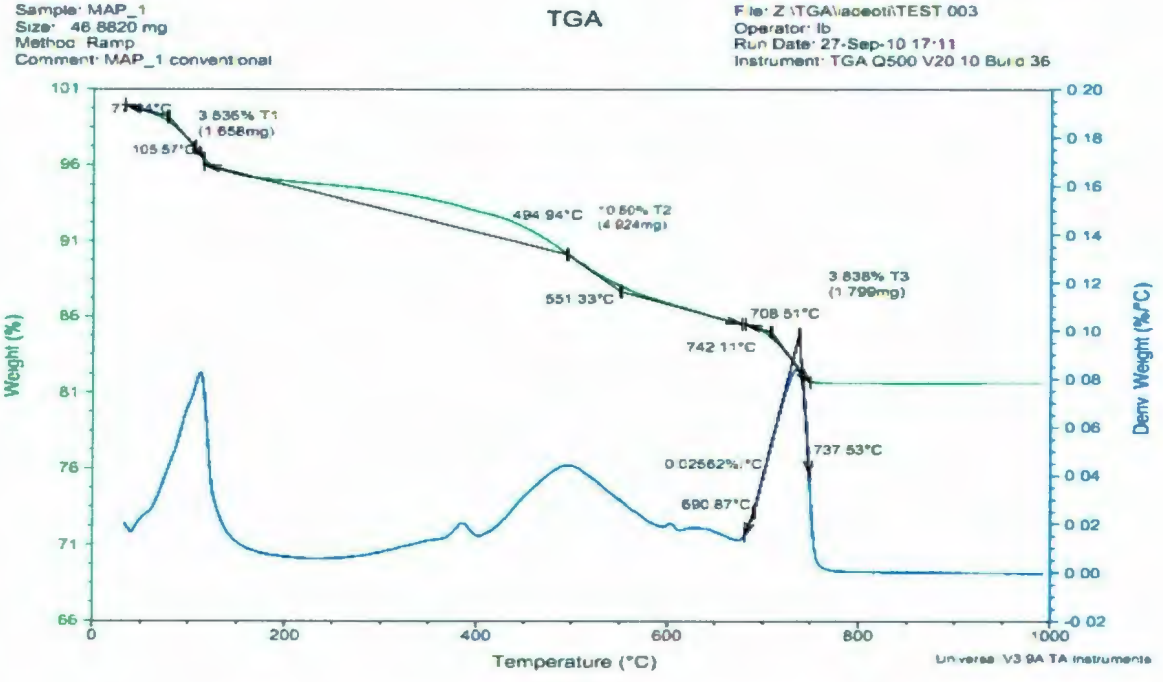

Figure D-2: Conventional TGA Method for MAP FA

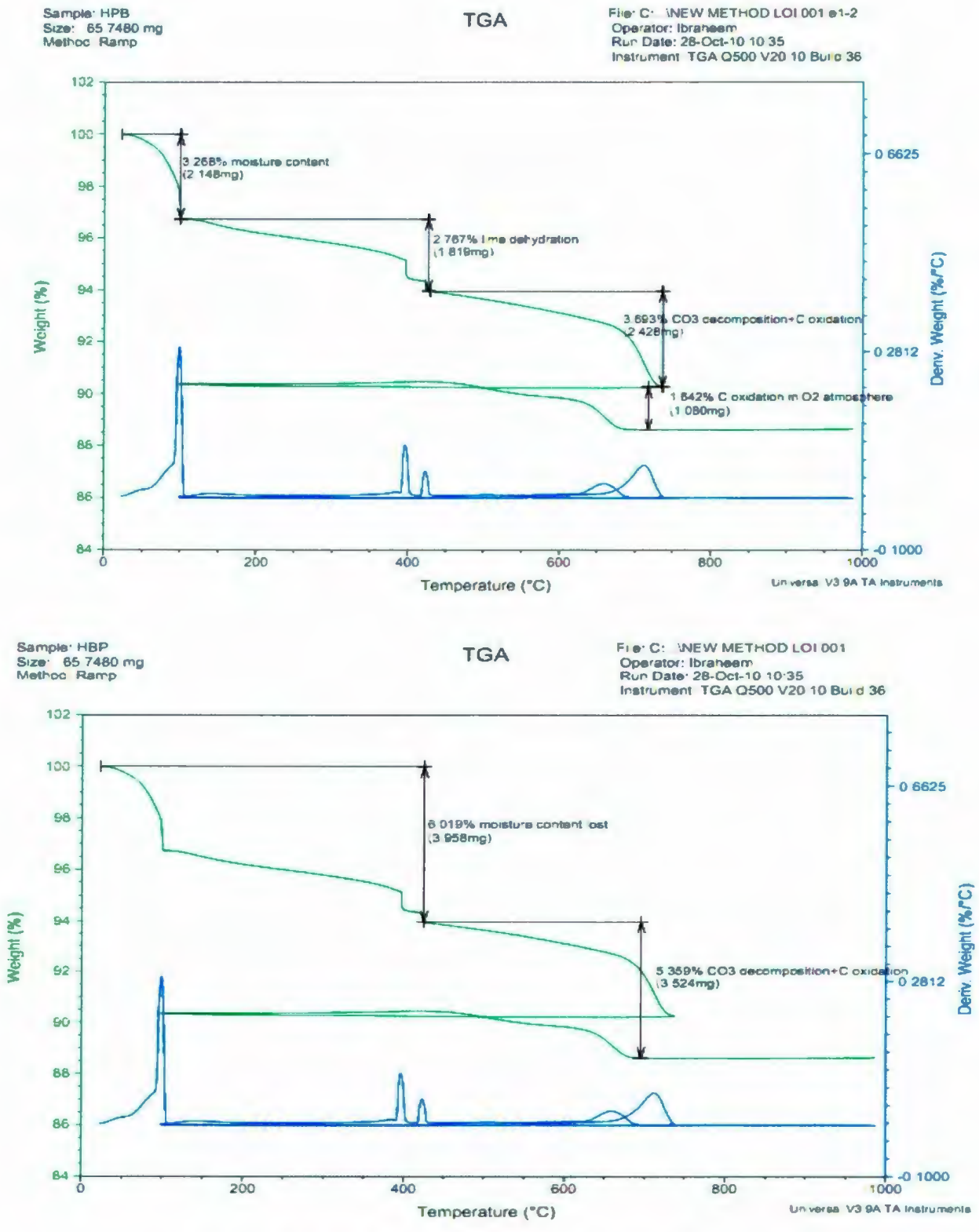

Figure D-3: Hi-Resolution TGA Method for HBP FA

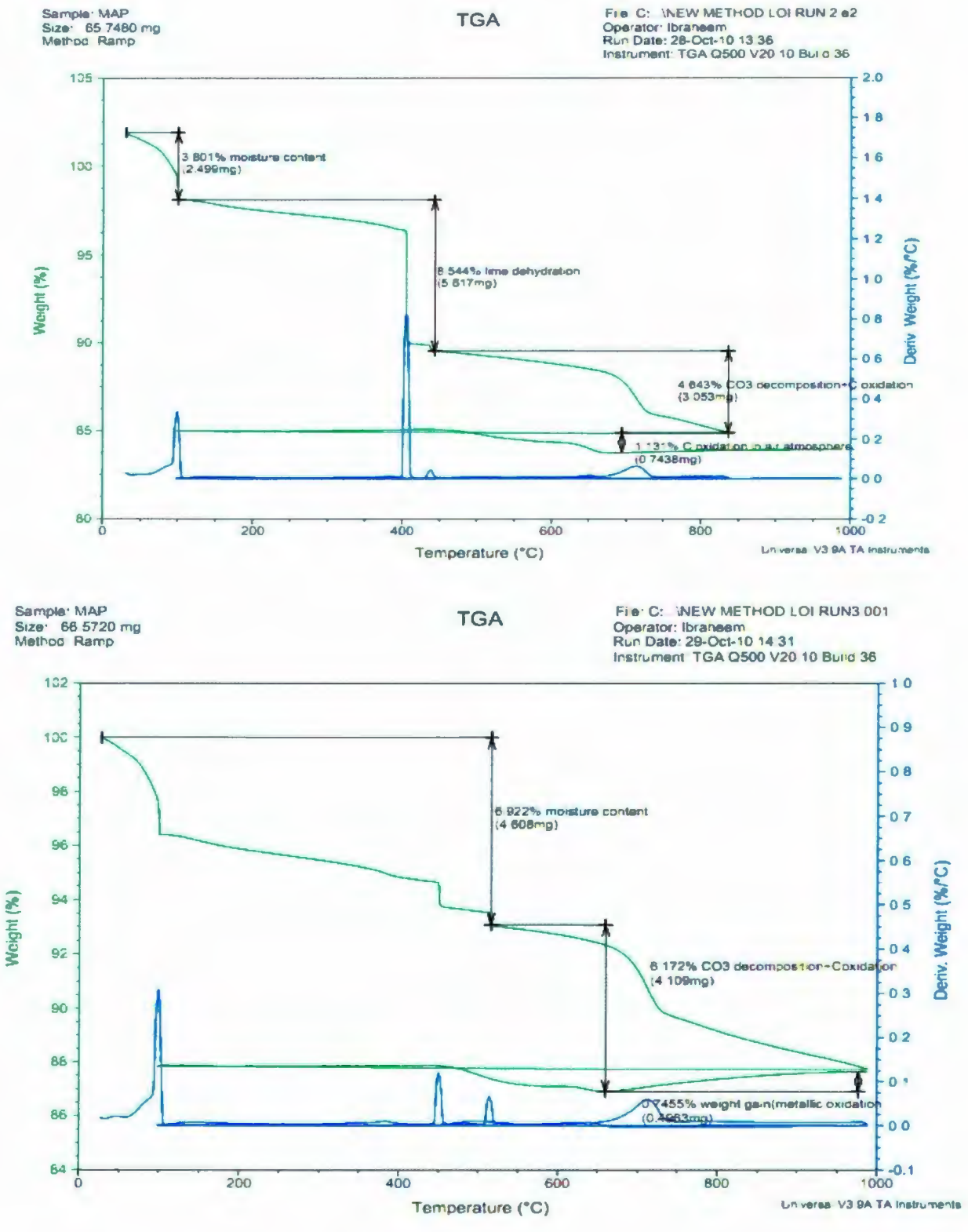

Figure D-4: Hi - Resolution TGA Method for MAP FA

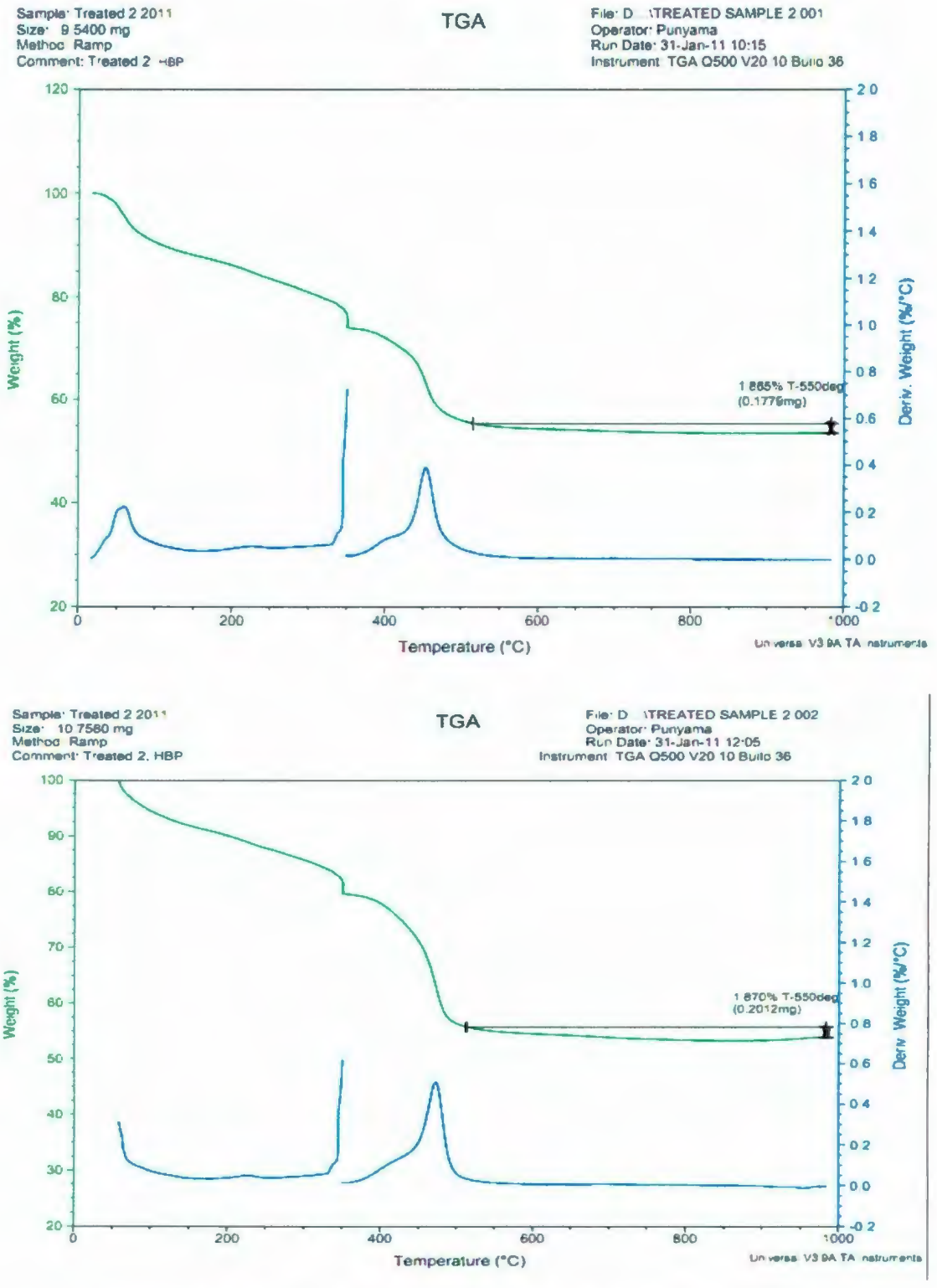

Figure D-5: Hi-Resolution TGA Method for Treated HBP FA

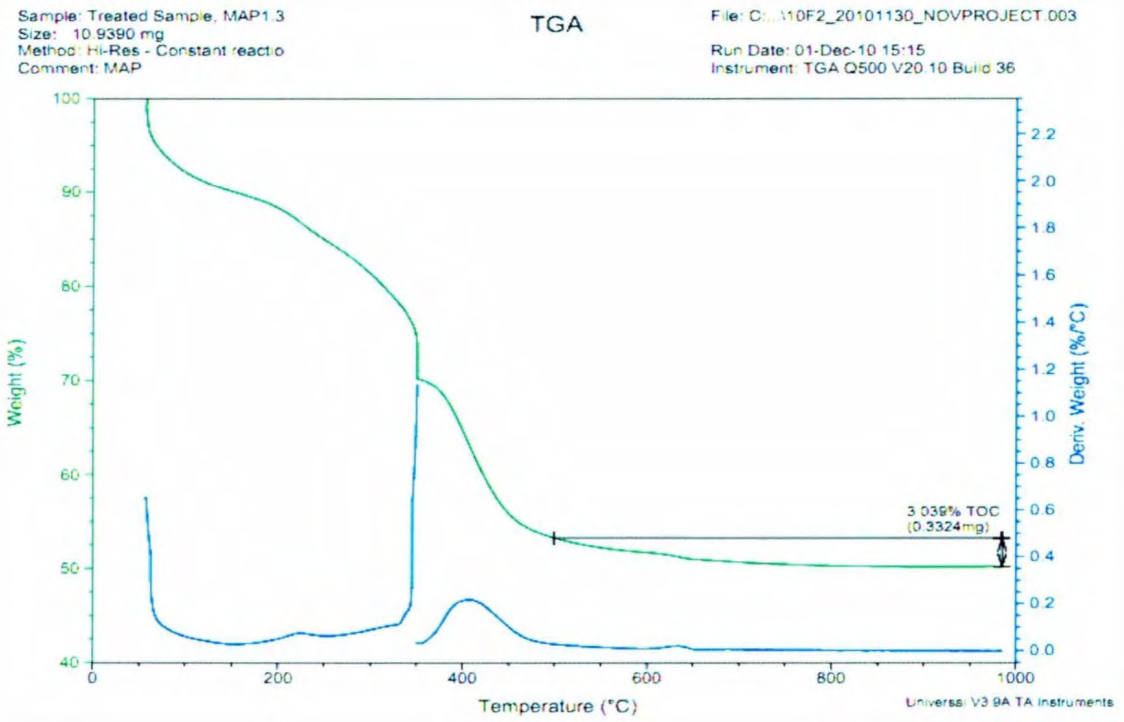

Figure D-6: Hi-Resolution TGA Method for Treated MAP FA